ESR STUDY OF THE DECAY OF METHYL AND ETHYL RADICALS ADSORBED ON POROUS *VYCOR* GLASS

By

Moses Olorunfunmi Adebajo

A Thesis

Submitted to the Faculty of Graduate Studies

in partial fulfillment of the requirements

for the degree of

MASTER OF SCIENCE

Department of Chemistry

The University of Manitoba

Winnipeg, Manitoba.

ISBN 0-315-86016-2

ESR STUDY OF THE DECAY OF METHYL AND ETHYL RADICALS ADSORBED ON POROUS VYCOR GLASS

BY

MOSES OLORUNFUNMI ADEBAJO

A Thesis submitted to the Faculty of Graduate Studies of the University of Manitoba in partial fulfillment of the requirements of the degree of

MASTER OF SCIENCE

DEDICATION

Dedicated to the Lord Jesus Christ,
the King of kings and Lord of lords

and

to my Sweetheart, Adedoyin.

TABLE OF CONTENTS

ABSTRACT

A study of the decay kinetics of methyl and ethyl radicals adsorbed on the surface of porous Vycor glass (PVG) pretreated at 750°C was investigated in this work at 77 K, 90 K, and 109 K by using the technique of electron spin resonance (ESR).

Methyl (or ethyl) radicals were obtained at 77 K by irradiation of azomethane (or azoethane) adsorbed on porous Vycor glass using the full UV spectrum of a medium pressure mercury arc. The results of the build-up of both radicals are discussed briefly. The ESR spectra of both radicals were all recorded at 77 K.

The decay of both methyl and ethyl radicals was found to be a cascade type but one surface adsorption site was postulated to be present for relatively short time decay. The cascade type of decay may, however, indicate the presence of a continuum of trapping potentials on the surface for relatively long time decay. It is therefore possible for the stabilization of both radicals to be achieved over a wide range of temperatures as previously observed for methyl radicals. The decay data obtained for both radicals gave the best fit to Dole's revised second order kinetics equation which was derived for the decay of free radicals in polymers from a second order equation modified on the assumption that a fraction of the radicals recombine by a second order mechanism while the remaining radicals are completely unreactive. The decay of methyl and ethyl radicals is therefore postulated in this work to be second order in mobile reactive radicals, consistent with a diffusion-controlled recombination process. Thus, two types of surface

adsorbed radicals are identified for each temperature namely, weakly, physically adsorbed mobile and immobile, unreactive radicals. The immobile, unreactive radicals are associated with siloxane bridge sites or stabilization by caging effects in pores while the mobile reactive radicals are identified with the large number of geminal hydroxyl groups as well as B-OH groups on the surface. Ethyl radicals were found to decay slightly faster on the PVG surface than methyl radicals and this behaviour is explained in terms of the orientation of the radicals in the adsorbed state and the possible additional interaction of ethyl radicals with both geminal hydroxyl and B-OH groups present on the surface. Values of the ratio of the concentration of mobile, reactive methyl and ethyl radicals to the concentration of the immobile, unreactive radicals were obtained from the Dole plots and their variation with temperature is discussed. The plots of this ratio against 1/T were obtained and the adsorption energies calculated from these plots are found to vary from 0.976 to 4.78 kJ mol^{-1} for methyl radicals and from 5.19 to 6.63 kJ mol^{-1} for ethyl radicals. The variations of adsorption energies with surface coverage are discussed.

Arrhenius plots for the decay of the radicals were obtained and and least squares values of activation energies for the decay between 77 K and 109 K were found to range from 3.23 to 7.31 kJ mol^{-1} for methyl radicals and from 3·77 to 5·52 kJ mol^{-1} for ethyl radicals. The variations of activation energies with both temperature and surface coverage are discussed. The effect of adsorbed water on the surface of a PVG sample pretreated at 500°C on the decay kinetics of the radicals is also discussed briefly.

ACKNOWLEDGEMENTS

All glory and thanks to the Almighty God for his faithfulness, guidance and protection throughout the period of this study.

I would like to express my sincere gratitude to my Supervisor, Dr H. D. Gesser, for his invaluable direction and advice and for the financial support received from his research funds.

I also gratefully acknowledge the financial assistance received from the Natural Sciences and Engineering Research Council of Canada and from the Department of Chemistry, University of Manitoba.

Finally, my heartfelt gratitude goes to my darling wife, Doyin, for her understanding, love and encouragement throughout the period of this work.

LIST OF FIGURES

LIST OF TABLES

CHAPTER 1
INTRODUCTION

1.1 Introductory remarks

Recently, a review of electron spin resonance studies of alkyl radicals adsorbed on porous Vycor glass was presented by Gesser.[1] The review indicates that various workers have been able to produce, stabilize and study the reactions of alkyl radicals on surfaces at low temperatures. These radicals were easily detected by using the technique of electron spin resonance which was found to be an effective tool in characterization of solid surfaces and in elucidation of active surface sites as well as surface reactions. However, consistency is lacking in the various reported studies of methyl radicals stabilized on porous Vycor glass or other surfaces while little work has been done on ethyl radicals. For instance, in the study of the decay of methyl radicals on surfaces, while Fujimoto et. al.[2] reported first order kinetics for the decay of methyl radicals on porous Vycor glass over the temperature range of 77 K to 132 K, Joppien and Willard[3] reported that the decay of methyl radicals on silica gel between 77 K and room temperature could be resolved into multiple first and second order processes and yet another worker, Garbutt,[4] showed that the decay of surface stabilized methyl radicals was complex and appear to follow second order kinetics more closely than first order and a slope of about 10 (7 to 12) was obtained for the order of the reaction from the plot of log Rate against log C (where C is the concentration of methyl radicals as determined by peak to peak amplitude). Hence, the decay kinetics of methyl and

ethyl radicals adsorbed on porous Vycor glass at 77 K was investigated more closely in this work by using ESR technique with the hope that the study would help to solve this problem of lack of consistency in the previous reported studies.

Gesser's review also reveals that various workers have observed that during the photolysis of adsorbed methyl iodide at 77 K, the concentration of methyl radicals formed usually approaches a constant value after a certain period of time of irradiation. This behaviour was attributed to possible back reaction of methyl radicals and iodine. It is therefore highly desirable to find some alternate sources of methyl radicals in order to prevent the inherent effect of iodine formed during the irradiation of methyl iodide which was commonly used. Azomethane, which is a suitable alternative suggested by Gesser[1], was therefore employed in this work as the source of methyl radicals. Azoethane, a higher homologue was similarly used as a source of ethyl radicals.

1.2 Porous Vycor glass

1.2.1 Manufacture and composition

Porous Vycor glass consists of 96% SiO_2, 3% B_2O_3 and 1% Al_2O_3, Na_2O, As_2O_5 etc.[5,6,7] The porous glass usually has a surface area of about 200 m^2/g with an average pore diameter of 40 Å.[5] It is manufactured by melting and fabricating a glass in the sodium borosilicate system at quite low temperatures. After fabrication, it is then heat treated to separate the glass into a boron-rich phase and a silica-rich phase. Weak acids may then be used to leach out the boron-rich phase. With this method, the undissociated boron remains

at the surface of the silicate skeleton, i.e. at the boundaries of the former separated phases. The boron is probably present as an "impurity" in silicon sites at the silicate surface. This manufacturing process and the possibility of the diffusion of internal boron to the surface during subsequent heat treatment has led various workers[8,9a] to speculate that B/Si ratio in the surface layer is probably about 1:3 (i.e. approximately 25% boron) rather than the 1:18 that might be expected from bulk analysis. The method of manufacture of porous Vycor glass results in a more rigid structure than silica gel and it is made into various sizes of tube, rod and plate i.e. it is easily cut and handled.

1.2.2 Nature of the surface

Basically, glass is a network of SiO_4 tetrahedra, with oxygen atoms shared by adjacent silicon atoms. The surface group of such a structure may be:

(1) A siloxane bridge represented as:

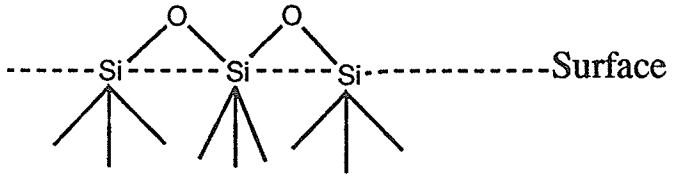

Figure 1-1

or (2) A $\geq$Si-O structure with the oxygen valence satisfied by hydrogen to form a silanol function $\geq$Si-O-H. Hydration of a siloxane bridge structure also results in this structure. These surface hydroxyls which can be relatively isolated from one another,

generally exist either vicinal or geminal to one another as illustrated in figure 1-2:

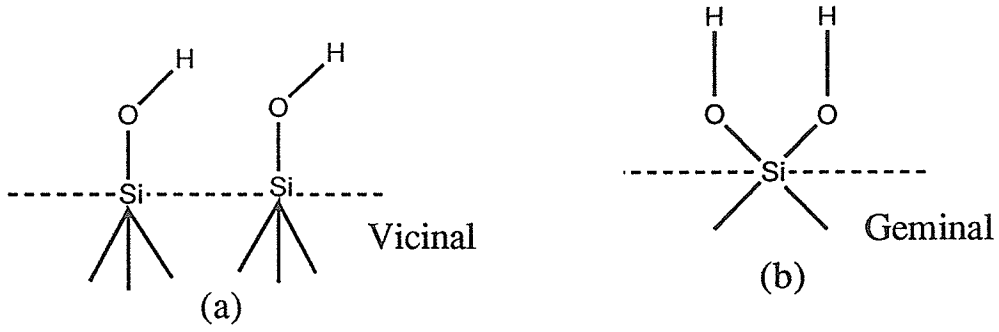

Figure 1-2

With these structures, there are unlimited opportunities for hydrogen bonding both among the surface hydroxyls and with adsorbed molecules. It is also possible to have structures such as ≡Si-H, ≻Si=O, ≡Si-X (where X=impurity) but these exist in relatively small numbers.

1.2.3 Infrared spectra of porous Vycor glass

Little's review[10] of various IR studies and especially the works of Low and Ramasubramanian[9] have established the existence of two sharp peaks at about 3748 cm^{-1} and 3703 cm^{-1} in the infrared spectrum of porous Vycor glass which has been dehydrated rigorously at high temperatures. From dehydroxylation, deuteration, flourination and adsorption experiments, Low and Ramasubramanian[9a] showed all absorptions to be due to surface hydroxyl species. They assigned the 3748 cm^{-1} absorption to free surface silanol (Si-OH) groups. From deuteration experiments and from impregnation of silica gel and porous glass with boric acid, Low

and Ramasubramanian assigned the 3703 cm^{-1} bond to a free hydroxyl attached to a surface boron atom. Many workers believe that high temperature treatment leads to the diffusion of boron atoms to the surface thereby leading to a higher concentration of hydroxyl groups on the surface. The leaching process may also be responsible for this high surface concentration of boron atoms. Slight shifts in the IR peaks to lower frequencies and general broadening and asymmetry of the peaks have also been attributed to hydrogen bonding of the surface hydroxyl species.

1.2.4 Heat treatment of porous Vycor glass

The work of Low and Ramasubramanian[9b] on the dehyration of porous Vycor glass indicates that:

(i) all of physically adsorbed water can be removed from the glass when evacuated at room temperature. However, in this work, IR spectra of porous Vycor glass evacuated at even 200 to 400°C for several hours still showed a broad absorption band at about 3600 cm^{-1} indicating the presence of some physically adsorbed water, though the intensity of this band decreases with increase in temperature of evacuation. The most efficient removal of adsorbed water could only be accomplished by evacuating and heating at 700 to 750°C for 4 to 6 hours. Thus, only some of the physically adsorbed water could actually be removed from the glass when evacuated below 200°C.

(ii) species which are more tightly bound than physically adsorbed water are removed by degassing at temperatures below 200°C and

more of such species continue to desorb at temperatures above 200°C.

(iii) the surface area decreases with increasing degassing temperature but significant decreases occurred only above 500°C.

(iv) fully hydroxylated surfaces exist below 600°C, some surface silicon atoms possibly carrying more than one hydroxyl group.

(v) above 600°C free hydroxyl groups which do not interact with their environment to any great extent, begin to appear.

(vi) degassing at 300°C leaves much of the surface covered with geminal hydroxyl groups.

(vii) degassing above 300°C may go by the mechanism:

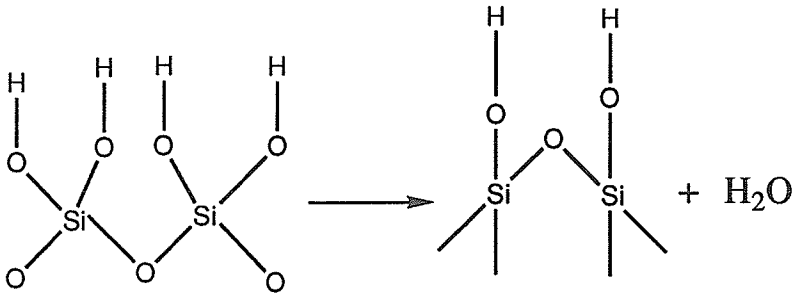

1-1

(viii) migration of boron to the glass surface occurs above 600°C.

Much information has also been given by Low and Ramasubramanian[9c] in their work on the sorption of water by porous glass. The infrared spectroscopic results indicated that the changes produced on well dehydroxylated porous glass surfaces by water sorption involved interaction with the 3703 cm^{-1} band of B-OH groups which increased markedly in intensity and shifted to lower

frequencies. The intensity increase of the silanol band was found to be much less pronounced than that of the B-OH band. These results indicated that water sorption produced a larger amount of B-OH groups than Si-OH groups. The imbalance in the numbers of Si-OH and B-OH groups was attributed to the distruption of B-O-B bridges to a greater extent than Si-O-Si or Si-O-B bridges thereby pointing to the existence of some B_2O_3 aggregates or "islands" on the glass surface. Water sorption may then occur on these islands. These workers showed that water adsorption at low relative pressures caused an absorption near 3600 cm^{-1} which was ascribed to molecular water adsorbed on boron on the glass surface. Their results indicated that the spectra of water adsorbed on fluorinated and untreated porous glass were the same. Hence, the same reaction centers (or adsorption sites) predominated in both cases and these were not surface silanol groups. Unlike pure silica which is quite hydrophobic when highly degassed, the siloxane bridges on porous glass were more readily attacked than those of pure silica. This greater siloxane-water reaction of porous glass than pure silica was then attributed to the presence of surface boron, molecular water adsorbed on B-OH groups and boria islands adjacent to the adsorption centres.

1.3 Electron spin resonance (ESR)

This work is not really an ESR study but the technique was rather used as an analytical tool to study the kinetics of the decay of methyl and ethyl radicals adsorbed on porous Vycor glass surface. A comprehensive description of ESR as a field of study is given in a

number of books.[11-13] The following discussion, therefore, considers only the basic principles of the technique.

Electron spin resonance (ESR) or electron paramagnetic resonance (EPR) is based on transitions between energy levels produced by the action of a magnetic field on an unpaired electron. The following substances can be studied by ESR spectroscopy due to their possession of unpaired electrons:

(i) Free radicals; these occur as transient intermediates in chemical reactions and as more-or-less stable species produced by chemical, photochemical, electrochemical or other means. They have one or more unpaired electrons.

(ii) Transition metal ions either in the solid state or in solution.

(iii) Triplet electronic states.

ESR signals also originate in structural defects in crystals and in electrons in semiconductors (cyclotron resonance).

1.3.1 Principles

The application of a magnetic field H to the unpaired spin of an electron causes a torque to act to align the magnetic dipole of the electron either parallel or antiparallel to the direction of the magnetic field; the only two allowable orientations. The electron dipole precesses about the axis of the applied field at a frequency, υ, which varies directly with the electron magnetic moment and the

applied magnetic field. When an electron is placed in a magnetic field, its energy will be changed by a definite amount given by:

$$E = \mu H = -g\beta sH = +1/2g\beta H \qquad 1\text{-}2$$

where H=magnetic field strength; μ=magetic moment; g=spectroscopic splitting factor (or the g-factor or gyromagnetic ratio) which is a function of the environment of the electron - for a free electron, g is approximately equal to 2 (or more precisely 2.00229 due to relativity effects);[14] β=magnitude of the magnetic dipole, the Bohr magneton=9.2732×10^{-28} joule/gauss; s=spin quantum number which is either +1/2 (spin aligned parallel to the direction of the magnetic field) or -1/2 (spin aligned antiparallel to the field).

In the presence of a magnetic field, electrons with spin +1/2 will decrease in energy by an amount 1/2gβH while those with spin -1/2 will increase in energy by a like amount. Hence, the difference in energy between the two levels is:

$$\Delta E = g\beta H = h\nu \qquad 1\text{-}3$$

This splitting of energy levels is shown in figure 1-3.

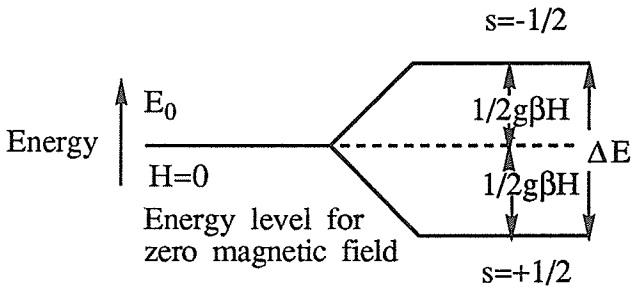

Figure 1-3: splitting of energy levels by a magnetic field.

For a free electron, the frequency of absorption, υ, is given by:

$$\upsilon = g\beta H/h = 2{\cdot}8026 \times 10^{6} \text{ cycles/sec/gauss} \qquad 1\text{-}4$$

(or 2·8026 Mc/sec/gauss)

At H=3400 G, $\Delta E = 6{\cdot}3 \times 10^{-24}$ joule/molecule or 3.8 J/mol. and υ=9500 Mc/sec. This frequency lies in the microwave region of the electromagnetic spectrum. Hence, instrumentation used will involve radar-type components: microwave cavities, klystrons and waveguides.

The relative population of the two energy levels separated by ΔE is governed by Boltzmann distribution given by:

$$n_{upper}/n_{lower} = e^{-\Delta E/kT} \qquad 1\text{-}5$$

where k=Boltzmann constant ($1{\cdot}38 \times 10^{-23}$ J/K), T=absolute temperature. At 300 K for a species for which g=2 and H=3400 G, the relative population of the two energy levels is 0·9984 so that for every 1000 electrons in the low energy state, 998 are in the high energy state. The net absorption and therefore, the sensitivity, depends on the difference in relative populations n_{upper} and n_{lower} so that working at H=3400 G will give a higher sensitivity than working at lower field strengths (other factors being assumed equal). A relatively high sensitivity can be obtained by working at low temperatures.

1.3.2 Saturation effects

Due to very small population difference, it is sometimes possible to produce sufficient rate of transitions to cause the

population of the higher energy state to be equal to that of the lower one so that the rate of absorption of energy, which depends on the population difference diminishes. This phenomenom is known as "saturation". When saturation occurs, the signal level decreases as the microwave power is increased and the signal broadens.

Saturation depends on the intensity of the microwave radiation and upon the time required for an unpaired spin in the upper level to fall to the lower level. This time is related to the spin-lattice relaxation time, T_1, which is a measure of the interaction of the unpaired elecron with the surrounding molecules (the lattice). Spin-lattice relaxation is one mechanism by which energy absorbed and stored in the upper state can be dissipated in such a manner as to allow return to the ground state. The process provides paths by which the excess spin energy finds its way into the vibrations and rotations of the surrounding molecules. The spin-lattice relaxation time is the time for the spin system to lose $1/e^{th}$ of its energy. Rapid dissipation of energy (i.e. short T_1) is required if the population difference of the spin states is to be maintained. Slow spin-lattice relaxation, which occurs frequently in systems containing free radicals, especially at low temperatures, can cause saturation of the spin system.

1.3.3 Hyperfine interactions

Well resolved ESR spectra of many substances contain additional splitting or "hyperfine structure". Hyperfine structure allows identification of the paramagnetic unpaired substance and

provides information on the chemical environment of the electron and distribution of electron density.

Hyperfine interaction is the effect of the magnetic moments of nuclei on the ESR spectrum leading to a splitting of the ESR line to give hyperfine structure. From the number and intensity distribution of the spectral lines, one can tell how many nuclei interact with the radical electron. The energies of a coupled level are given by:

$$E = g\beta M_S H + ahM_I \qquad 1\text{-}6$$

where a=hyperfine coupling (or splitting) constant, M_I=spin quantum number of the coupling nucleus and M_S=spin quantum number of the electron.

The selection rules for allowed ESR transitions are $\Delta M_I=0$ and $\Delta M_S=\pm 1$. A single nucleus of spin I=1/2 (e.g. ^{1}H, ^{19}F, ^{13}C, ^{15}N and ^{31}P) will cause a splitting into two lines of equal intensity (Figure 1-4). For hydrogen, the hyperfine splitting constant, a, is 508 gauss.

Interaction with a single deuterium or nitrogen nucleus (^{2}H or ^{14}N, I=1) will cause a splitting into three lines of equal intensity. In general, a single nucleus of spin I will cause a splitting into 2I+1 lines so that interactions in Mn(II) (I=5/2) give rise to a six-line spectrum, those in ^{14}N (I=1) give rise to a three-line spectrum and those in V(IV) (I=7/2) to an eight-line spectrum.

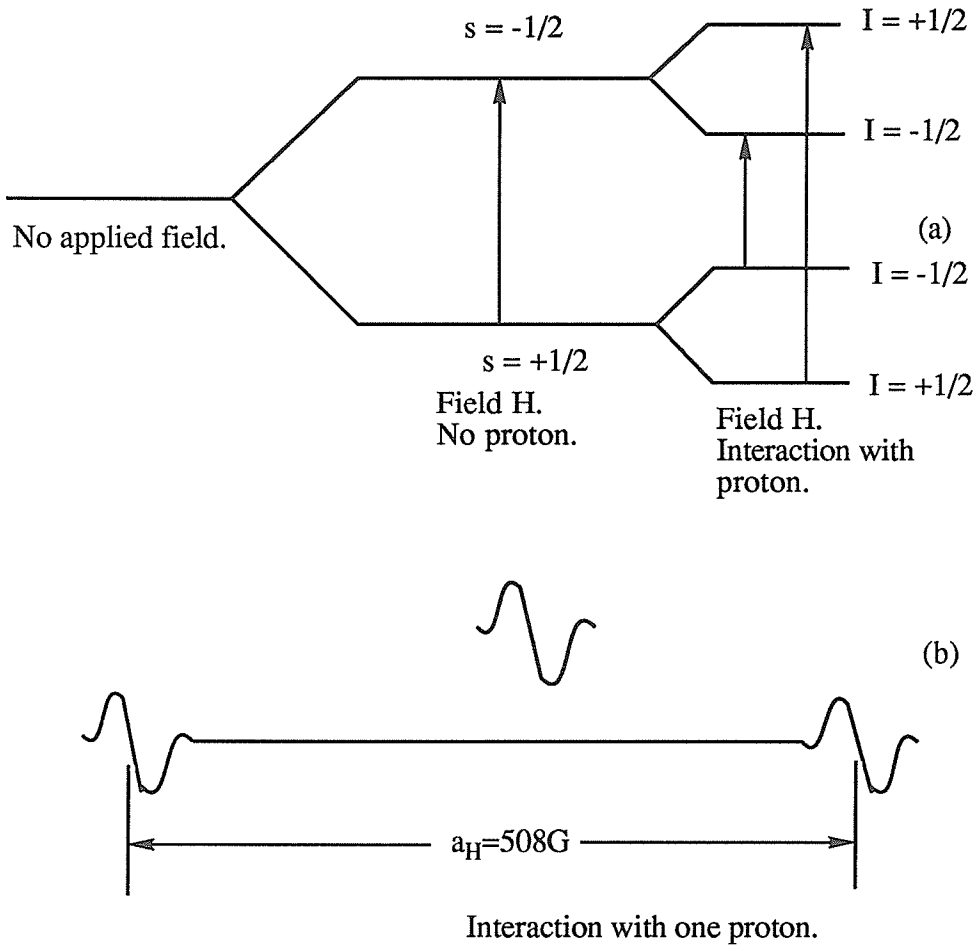

Figure 1-4: (a) splitting of energy levels by a magnetic field H and by interaction with one proton, (b) splitting of spectral line.

If several magnetic nuclei are present, the situation becomes more complicated. Generally, where there are n equivalent nuclei of spin I, the resulting spectrum involves (2nI+1) lines e.g. two equivalent ^{14}N nuclei produce a five-line spectrum. The relative intensities of the resulting lines follow the coefficients of the binomial expansion. In the case of methyl radicals, the unpaired electron interacts with three equivalent protons so that a quartet is produced with relative intensities 1:3:3:1. This has been experimentally observed.[1]

If an unpaired electron couples with non-equivalent protons, each proton will have its own coupling constant. In general, two sets of n and m equivalent protons in a molecule will produce a spectrum with (n+1)(m+1) maximum number of hyperfine lines.

1.3.4 Quantitative analysis

The integrated intensity is usually related to the concentration of the paramagnetic species by comparison with a standard. The area enclosed by either the unsaturated absorption or dispersion signal is proportional to the number of unpaired electron spins in the sample. Provided that the linewidth is kept constant, the peak heigths of the first derivative which are easier to measure than peak areas are also linearly propotional to concentration generally in the concentration range of 10^{-7} to 10^{-3} M.[15] At higher concentrations, the linewidth changes and linearity breaks down. To determine the concentration, comparison is made with a standard containing a known number of

unpaired electrons and having the same line shape as the unknown (Gaussian or Lorentzian). Suggested standards are:

(1) Standard solutions or mixtures of the substance being determined. When these are available, as in the determination of manganese(II) or vanadium(IV), they would represent the best kind of standards.

(2) Standards which contain a known number of unpaired spins. Examples are solid samples or solutions of stable free radicals such as 2,2-diphenyl-1-picrylhydrazyl (DPPH) or peroxylamine disulphonate. DPPH which is frequently used, has a molecular weight of 394 and contains $1{\cdot}53 \times 10^{21}$ unpaired spins per gram.[14] A crystal of $CuSO_4{\cdot}5H_2O$ has also been used.[12,14,16,17]

(3) Secondary standards such as powdered charcoal diluted in KCl, charred dextrose or synthetic ruby can be used.[14] Standards should generally be stable and have linewidths close to that of the sample. If the spin concentration of the standard is close to that of the sample, more accurate results will be obtained.

1.3.5 Matrix-isolated EPR

It was not until recently that the technique of electron paramagnetic resonance spectroscopy was extensively used for detecting surface-generated gas phase radicals during catalytic processes. The matrix-isolated EPR which involves the coupling of electron paramagnetic resonance spectroscopy with cryogenic trapping[18,19] has also proven very useful not only for detecting

surface-generated gas phase radicals but also for providing new insight into overall reaction mechanisms.[18] A brief review of early studies involving the use of matrix-isolation EPR has been given by Driscoll et. al.[18]

The full description of an efficient and versatile matrix-isolation EPR system which was recently designed and built by Martir and Lunsford[20] has been given. It is possible to use this system not only for detecting the formation of gas-phase radicals, but also for determining the amounts of radicals produced. The versatility of the system allows easy examination of a wide variety of different solids and gas reactants. Spin concentrations (or amounts of radicals) are obtained from double integration of the recorded EPR spectrum of the unknown and a standard. In all cases, the standard, which is also used to determine g values is a phosphorus-doped silicon chip. Although the system is primarily designed for the detection of surface generated gas-phase radicals, mass spectrometry or gas chromatography analysis can also be used to obtain stable product distributions.

1.3.6 EPR (or ESR) studies of surface stabilized alkyl radicals

Electron spin (or paramagnetic) resonance has been found to be very useful in the characterization of solid surfaces and in the elucidation of active surface sites as well as surface reactions. The alkyl radicals have been found to be primary intermediates in many reactions involving hydrocarbons. For instance, the alkyl radical is

usually the first product in the pyrolysis and combustion of hyrocarbons. Such radicals have been detected and stabilized in glasses at low temperatures and on surfaces at low and ambient temperatures. The technique of ESR has been widely used by various workers in this regard.

Gordy and McCormick[21] were the first to report an ESR study of the CH_3 and C_2H_5 radicals. They investigated the X-ray decmposition of CH_3 and C_2H_5 compounds of zinc, mercury and tin at 77 K. Irradiated $Zn(CH_3)_2$ was found to give a quartet having a total spread of 70 to 80 gauss which decayed over a period of ten days. The quartet was said to be due to the CH_3 radical trapped in a symmetrical cage and rapidly inverting (non-planar) at 77 K. $Hg(C_2H_5)_2$, on irradiation, produced a 6-line spectrum (1:5:10:10:5:1) which was attributed to C_2H_5 where the five protons were equally coupled to the spin vector of the odd electron. The review of other early ESR studies of alkyl radicals has been given by Garbutt.[4]

Gesser's review of ESR studies of alkyl radicals adsorbed on porous Vycor glass indicates that some of the earliest ESR studies of surface stabilized radicals were done by Russian workers. For example, the ESR of CH_3 radicals adsorbed on silica gel at low temperatures has been studied by Pariiskii et. al.[22] The CH_3 radicals were produced by first adsorbing methyl iodide at room temperature on silica gel having a specific area of 700 m^2/g, after outgassing the gel in a vacuum for six hours at 573 K. The silica gel samples were then irradiated at 77 K for 4 to 6 hours with a UV source. The ESR spectra, recorded at 77 K, consisted of four lines of 1-2 G width,

spaced 24·2±0·5 G apart, and the g-factor was 2·001±0·001. The relative intensities of the four lines were found to be 1:8·5:13:2·5 instead of the binomial values 1:3:3:1. However, the spectrum was still attributed to the CH_3 radical. Incomplete neutralization of the anisotropic hyperfine spin-orbital interactions were reported to be responsible for the unusual relative amplitudes. The CH_3 radical was thought to be bound to the surface by a one-electron bond due to attraction of the unpaired electron to the adsorbent. This makes only the rotation about the 3-fold symmetry axis to remain. However, the small linewidths of 1-2 gauss obtained indicates that there are still other motions of the stabilized CH_3 radicals. The CH_3 was found to be very stable on the silica gel surface. Gesser's review[1] also reports that Kazanskii and Pariiskii[23] have shown C_2H_5 radicals to be quite stable on silica gel surface especially at elevated temperatures by observation of the ESR spectra of the radicals after γ-irradiating ethane adsorbed on silica gel at 77 K. The reported values of proton hyperfine splitting constants are $|\alpha^H|$=20·5 G and $|\beta^H|$=27 G. These workers considered C_2H_5 radicals to be bound to the surface at one end only. They reported that the adsorbed radical resembles an entirely free one very closely and that its free electron should not participate to a considerable extent in forming a chemical bond with the surface.

Noble et. al.[24] have shown that CH_3 radicals may be stabilized for long periods in zeolites at temperatures below 90 K. These radicals were produced by γ-irradiation of methane sorbed on synthetic zeolite ($Na_{12}[(AlO_2)_{12}(SiO_2)_{12}]\cdot 27H_2O$, Linde Type A). Several unidentified species were detected besides the more stable

CH_3 radical. The CH_3 radical was reported to have the following parameters: g=2.0026; $|a^H|$=21·9 G; relative intensities 1·0:3·1:2·8:0·9. Turkevich and Fujita[25] were the first to report CH_3 radicals stabilized on porous Vycor glass, PVG (Corning glass No 7980). The CH_3 radicals were produced by UV photolysis of adsorbed methyl iodide.

Many other workers have reported various studies on alkyl radicals formed and stabilized on surfaces at low temperatures. An excellent review of all the studies done up to 1989 was recently given by Gesser.[1]

Production of radicals

Gesser[1] reported in his review that methyl radicals have been formed and stabilized on surfaces by (a) γ-irradiation of adsorbed CH_4, CH_3Cl or CH_3I at 77 K, (b) the UV photolysis of adsorbed CH_3I at 77 K, (c) the photosensitized decomposition of CH_4 on PVG coated with V_2O_5 or MoO_3 or on ZnO with $\lambda > 400$nm, (d) the triphenylamine photosensitized decomposition of adsorbed CH_3Br at 77 K and $\lambda <$ 300nm (e) the photolysis of adsorbed trimethylamine, dimethylamine and tetramethylurea and azomethane at 77 K. Ethyl radicals were surface stabilized by γ-radiolysis of ethane, ethylene and ethyl chloride adsorbed at 77 K. Methyl radicals were also detected at room temperature when $Al(CH_3)_3$ adsorbed on silica was exposed to air or oxygen. All the required references have been given by Gesser[1] in his review. Gesser's review also reported that no stabilized alkyl radicals were detected at 77 K when the following adsorbed substances were UV photolysed; methyl ethyl ketone, acetone, dimethylmercury, C_2H_5I, i-C_3H_7I, $C_6H_5CH_3$, $C_6H_5CH_2Cl$. It is

reported that it has also not been possible to produce and stabilize the methylene radical, CH_2, by photolysis of ketene on PVG.

Gesser's review indicates that consistency is lacking in the reported studies of CH_3 stabilized on PVG or other surfaces. It is hoped that this work and other future studies will help to solve this problem.

1.4 Reactions of alkyl radicals

1.4.1 General reactions of alkyl radicals in the gas phase

(A) Abstraction

Free radical abstraction reactions are those in which a free radical removes an atom from a stable molecule to produce a molecule and another free radical. The commonest type is one involving the transfer of an hydrogen atom.

Extensive studies have been conducted on abstraction reactions by methyl radical of the type:

$$CH_3^{\cdot} + RH \longrightarrow CH_4 + R^{\cdot} \qquad 1\text{-}7$$

where RH is any hydrogen-containing compound. It has been established[26,27] that the activation energy for the above reaction is greater when RH is an hydrocarbon containing primary hydrogen atoms than where RH is an hydrocarbon containing primary and secondary hydrogen atoms which in turn has greater activation energy than the reactions where RH has primary, secondary and tertiary hydrogen atoms.

Boddy and Steacie[28] have also studied the abstraction reactions by ethyl radicals. They produced deuterated ethyl radicals by photolysis of 3-pentanone-d_{10}. They then determined the activation

energies of their hydrogen abstraction reactions with neo-pentane, n-butane and iso-butane to be 52·7, 43·5 and 37 kJ mol^{-1} respectively. In each case, the ethyl radical abstraction reaction was found to have a higher activation energy than the methyl radical reaction.

(B) Addition

This involves the addition of a free radical to a stable molecule to form a bigger radical:

$$R_1 + A_1{=}{=}A_2 \longrightarrow RA_1{-}{-}A_2 \qquad 1\text{-}8$$

A typical example is:

$$CH_3^{\cdot} + C_2H_4 \longrightarrow C_3H_7^{\cdot} \qquad 1\text{-}9$$

It is very difficult to study this type of reaction due to the large numbers of other reactions which could occur at the same time. For example, in the above case, besides the addition reaction, one could also get methyl radical recombination, hydrogen atom abstraction, dimerization of propyl radicals, disproportionation to propylene and propane, decomposition to propylene and propane, or to a methyl radical and ethylene, or to an hydrogen atom and propylene. It is also possible for methyl radicals to abstract an hydrogen atom from ethylene to form vinyl radicals leading to a series of other reactions.

Mandelcorn and Steacie[29] did much work on the addition of methyl radicals to olefines. The activation energies for the addition of methyl radicals to ethylene, propylene, acetylene and butadiene were found to be 29, 25, 23 and approximately 10 kJ mol^{-1} respectively.

James and Steacie[30] have also studied the addition of ethyl radicals to unsaturated hyrocarbons. These workers were mainly

interested in correlating the structure of an olefine and the activation energy for the addition of the radical to that olefine. On selecting hydrocarbons as representatives of the classes: 1-alkyne, 1-alkene and 2-methyl 1-alkene, they obtained activation energies of 37±2, 29±1 and 24±4 kJ mol^{-1} respectively. The absolute value for the addition rate constant for 1-heptene was found to be:

$k = 1{\cdot}9 \times 10^{11} \exp(-33{\cdot}47 \pm 2{\cdot}93)/RT$ $cm^3\ mol^{-1}\ sec^{-1}$; energy is in kJ mol^{-1}.

(C) **Decomposition**

This involves the breakdown of a larger free radical into a molecule and a smaller radical, e.g.

$$RA_1{=}A_2 \longrightarrow R^{\cdot} + A_1{=}A_2 \qquad 1\text{-}10$$

The decomposition reactions of ethyl, propyl, n-butyl and isobutyl radicals have been investigated by Bywater and Steacie.[31] Their results indicated that the activation energies are quite high ranging from 165 kJ mol^{-1} for the ethyl:

$$C_2H_5 \longrightarrow C_2H_4 + H^{\cdot} \qquad 1\text{-}11$$

to 96 kJ mol^{-1} for the decomposition of n-butyl:

$$n\text{-}C_4H_9 \longrightarrow C_3H_6 + CH_3^{\cdot} \qquad 1\text{-}12$$

Trotman-Dickenson[32] has been able to classify the majority of unimolecular decompositions of free radicals into two, namely: (1) those in which the radicals lose methyl radicals (e.g. reaction 1-12) and have activation energies of 63-146 kJ mol^{-1} (2) those in which an hydrogen atom is lost and have activation energies around 167 kJ mol^{-1} (e.g. reaction 1-11). The difference in activation energy for these two classes of decomposition is of the same order of magnitude

as is the difference between the strengths of C-C and C-H bonds (i.e. 348 and 412 kJ mol^{-1} at 298 K, respectively[33]).

(D) Recombination and Disproportionation

This involves the combination of two free radicals to form molecules. For example, we have:

$$\text{(Recombination):} \quad CH_3^{\cdot} + C_2H_5^{\cdot} \longrightarrow C_3H_8 \qquad \text{1-13a}$$

$$\text{(Disproportionation):} \quad CH_3^{\cdot} + C_2H_5^{\cdot} \longrightarrow CH_4 + C_2H_4 \qquad \text{1-13b}$$

Only the recombination reaction is possible for the case of reaction of two methyl radicals:

$$CH_3^{\cdot} + CH_3^{\cdot} \longrightarrow C_2H_6 \qquad \text{1-14}$$

This reaction was found to have a rate constant of 4·5 x 10^{13} cm^3 mol^{-1} sec^{-1} at 125°C with an activation energy of 0±2·93 kJ mol^{-1} independent of the source of methyl radicals.[34] In 1980, Baulch and Duxbury[35] recommended a value of (2·4±0·4) x 10^{13} cm^3 mol^{-1} sec^{-1} as the best value for the rate constant for the recombination of methyl radicals in the temperature range 250-420 K. The recommendation of these workers was based on their evaluation of the literature data available until 1978. They reported that experimental points suggested an activation energy of 0±1·5 kJ mol^{-1} for the methyl radicals recombination in the temperature range 250-500 K. In a later work, Arthur[36] used molecular modulation spectrometry (m.m.s.) technique to determine the rate constant for CH_3 recombination at 302 K and 80-575 torr and obtained a value of (2·4±0·3) x 10^{13} cm^3 mol^{-1} sec^{-1} in excellent agreement with the value obtained earlier by Parkes et. al.[37] in their investigation using the same technique. The radicals were produced by periodic

photolysis of azomethane at ≈ 350 nm in a static system and were followed using their UV absorption at 216·4 nm. Arthur and Biordi[38] have also recently used the rotating sector technique to determine the rate constants for CH_3 recombination in the temperature range 373-463 K and a pressure of 30 torr. The radicals were produced by the photolysis of acetone. They obtained a value of (2·81±0·22) x 10^{13} cm^3 mol^{-1} sec^{-1}. These workers[38] also evaluated all the available data and then suggested a value of (2·8±0·4) x 10^{13} cm^3 mol^{-1} sec^{-1} as the best value for the rate constant for CH_3 radicals recombination in the temperature range 295-450 K.

In the case of ethyl radicals, both recombination (reaction 1-15) and disproportionation (reaction 1-16) reactions are possible:

$$C_2H_5^{\cdot} + C_2H_5^{\cdot} \longrightarrow C_4H_{10} \qquad 1\text{-}15$$

$$C_2H_5^{\cdot} + C_2H_5^{\cdot} \longrightarrow C_2H_4 + C_2H_6 \qquad 1\text{-}16$$

Shepp and Kutschke[39] have studied the recombination reaction 1-15. Using the rotating sector technique, they found the rate constant, $k_{1\text{-}15}$, for the recombination of ethyl radicals to be (1·5±1)x10^{13}, (2·0±0·5)x10^{13} and (4·2±0·8)x10^{13} cm^3 mol^{-1} sec^{-1} at 50°C, 100°C and 150°C respectively. An activation energy of 8·4±4 kJ mol^{-1} was obtained for the recombination reaction. The disproportionation reaction 1-16 has also been studied by Ivin and Steacie[40] who made an Arrhenius plot of $k_{1\text{-}16}/k_{1\text{-}15}$ and obtained $E_{1\text{-}16} - E_{1\text{-}15}$ to be equal to 3·3±0·8 kJ mol^{-1}. Taken with the value of 8·4±4 kJ mol^{-1} obtained by Shepp and Kutschke[39], one then obtains a value of 12±5 kJ mol^{-1} for the activation energy $E_{1\text{-}16}$ for the disproportionation reaction. The ratio of the rate of

disproportionation to the rate of recombination has been reported by Ausloos and Steacie[41] to be 0·125±0·01. Similarly, in the presence of both methyl and ethyl radicals, these workers showed that this ratio for the reactions 1-13b to 1-13a was only 0·04. However, it is now almost universally accepted that the ratio of the rate of disproportionation to the rate of recombination of ethyl radicals is 0·14 in the temperature range 300-500 K.[42,43] Recently, Arthur[42] used the molecular modulation spectrometry technique to measure the overall rate constants for the combination of ethyl radicals in the temperature range 301-373 K. The radicals were produced by the periodic photolysis of azoethane at $\lambda \approx 350$ nm and were monitored by means of their UV absorptions at $\lambda = 250$ nm. This worker reported that the rate constants obtained did not show any definite trend with temperature over the temperature range involved implying a zero activation energy in contrast with the value of 8·4±4 kJ mol^{-1} obtained by Shepp and Kutschke.[39] A value of (1·12±0·19) x 10^{13} cm^3 mol^{-1} sec^{-1} was obtained as the overall rate constant for the combination of ethyl radicals. On comparing his results with those available in the literature, Arthur[42] was then able to suggest the value of (11·0±1·8) x 10^{12} cm^3 mol^{-1} sec^{-1} as the best value for the overall rate constant for the ethyl radical combination reaction. Taking the disproportionation-recombination ratio to be 0·14, he obtained the values of (9·69±1·54) x 10^{12} cm^3 mol^{-1} sec^{-1} and (1·31±0·21) x 10^{12} cm^3 mol^{-1} sec^{-1} to be the corresponding recombination and disproportionation rate constants respectively. More recently, Dobis and Benson[43] have also reported that although a very small positive activation energy of about 0·29 kJ mol^{-1} could be

inferred from their data, the value of (1·20±0·04) x 10^{12} cm^3 mol^{-1} sec^{-1} which they obtained for the disproportionation rate constant could be regarded as essentially constant, within the precision of their data, over the temperature range 203-343 K involved. These workers[43] used their recently improved very low pressure reactor (VLPR) to generate ethyl radicals and study their combination reactions at very low pressures (3 mtorr). Using the value obtained for the disproportionation rate constant and the disproportionation-recombination ratio of 0·14, a value of (8·55±0·42) x 10^{12} cm^3 mol^{-1} sec^{-1} was obtained for the recombination rate constant of ethyl radicals within the temperature range 203-343 K. On comparing this value with those available in the literature, they were able to arrive at the conclusion that their result was the most accurate.

(E) Inversion or free radical displacement

In this reaction, a free radical adds on to a molecule and displaces another radical from the molecule. For example, in the study of the photolysis of biacetyl, Blacet and Bell[44] accounted for the large yields of acetone above 80°C by the following reaction:

$$CH_3^{\cdot} + CH_3COCOCH_3 \longrightarrow CH_3COCH_3 + CH_3CO^{\cdot} \qquad 1\text{-}17$$

in which the methyl radical displaced a larger free radical - the acetyl radical. An activation energy of 23 kJ mol^{-1} was estimated for this reaction. The reaction was reported not to take place below 80°C.

A direct proof for the occurrence of such reactions has been given by a more extensive study conducted by Pitts et. al.[45] Using acetone as a source of methyl radicals, they postulated the following reaction sequence when the methyl radicals were reacted with trans-methyl propenyl ketone:

$$CH_3CH{=}CHCOCH_3 + CH_3^{\cdot} \longrightarrow CH_3CH{=}CHCH_3 + CH_3CO^{\cdot} \quad 1\text{-}18$$

$$CH_3CO \longrightarrow CH_3^{\cdot} + CO \quad 1\text{-}19$$

These workers confirmed the above reaction sequence when they reacted deuterated methyls with $CH_3CH{=}CHCHO$ and on analysis of the products found $CD_3CH{=}CHCH_3$ to be the only C_4 olefine produced. It was therefore assumed that the mechanism is a free radical displacement one represented by:

$$CD_3^{\cdot} + CH_3CH{=}CHCHO \longrightarrow CD_3CH{=}CHCH_3 + HCO^{\cdot} \quad 1\text{-}20$$

Brinton[46] has also postulated a free radical displacement reaction:

$$CH_3^{\cdot} + (CH_3)_2CO \longrightarrow C_2H_6 + CH_3CO^{\cdot} \quad 1\text{-}21$$

to account for the large amount of ethane produced in the photolysis of acetone at high temperatures.

(F) Free radical chain reactions

The mechanism of many rapid gas-phase reactions involves the formation of free atoms and radicals as intermediates. These atoms and/or radicals then react with one of the original reactants to produce more atoms or radicals. This, so called "chain mechanism," is repeated many times until all the reactant is used up or the chain carriers recombine. A good example of such behaviour is the Rice-Herzfeld[47] reaction scheme which was postulated to account for the low activation energy involved in the thermal decomposition of saturated hydrocarbons. The mechanism can be represented as follows:

(1) $M \xrightleftharpoons{k_1} R_1 + R_1'$ 1-22

(2) $R_1 + M \xrightleftharpoons{k_2} RH + R_2$ 1-23

(3) $R_2 \xrightleftharpoons{k_3} R_1 + M'$ 1-24

(4) $R_1 + R_2 \xrightleftharpoons{k_4} M''$ 1-25a

(5) $R_1 + R_1 \xrightleftharpoons{k_5} M_x$ 1-25b

(6) $R_2 + R_2 \xrightleftharpoons{k_6} M_y$ 1-25c

In the first step, the reacting molecule M first dissociates into two radicals involving the rupture of a 348 kJ mol^{-1} carbon-carbon bond. The radical R_1' plays no part in further reactions. The steps 2 to 4 are then initiated by abstraction of an hydrogen atom to produce a stable compound RH and a new radical R_2. This radical dissociates to give R_1 again and an additional molecule M'. Steps 2 and 3 constitute a chain process which can only be broken when (i) the radicals R_1 and R_2 combine to form a third molecule M'' (reaction 1-25a) or (ii) the radicals R_1 combine with each other to form a fourth molecule M_x (reaction 1-25b) or (iii) the radicals R_2 combine with each other to form a fifth molecule M_y (reaction 1-25c).

1.4.2 Some reactions of alkyl radicals on surfaces

Alkyl radicals have been found to be involved in many surface reactions. A few of these reactions will now be discussed.

Turkevich and Fujita[25] have studied the reactivity of methyl radicals with several gases on porous Vycor glass at room temperature. Both hydrogen and deuterium were found to have a pronounced effect on the intensity of the methyl radical signal though the reactivity of deuterium was much lower than that of hydrogen. These workers reported that both oxygen and nitrogen

monoxide reacted readily but the rate of reaction was found to be lower than that with hydrogen. Methane was also observed to cause a slight decrease in signal intensity which they attributed to hydrogen impurity. Evacuation of the signal did not restore the loss in signal. Ethylene was found to show no appreciable decrease in the signal intensity. Methyl iodide showed some decrease in the signal of the methyl radicals but this loss in signal intensity was recovered on evacuation. These workers then attributed the disappearance of the signal to either the gradual diffusion of the methyl iodide into the pores containing CH_3 radical and broadening of the signal due to shortening of their lifetime as a result of the reaction:

$$CH_3^{\cdot} + CH_3I \longrightarrow CH_3I + CH_3^{\cdot} \qquad 1\text{-}26$$

or to the change in the Q of the cavity since the dielectric constant of CH_3I is 7. These workers also reported that methyl radicals did not react with ethane, n-butane and toluene.

The photolysis of azomethane has been investigated by (1) Jones and Steacie[48] in the temperature range 24 to 190°C, by (2) Toby[49] from -47 to +50°C and by (3) Toby and Weiss[50] in the temperature range 25 to 180°C. The following reactions have been proposed to be the main features of the photolysis:

$$(CH_3)N_2 + h\nu \longrightarrow 2CH_3^{\cdot} + N_2 \qquad 1\text{-}27$$

$$2CH_3^{\cdot} \xrightarrow{k_1} C_2H_6 \qquad 1\text{-}28$$

$$CH_3^{\cdot} + (CH_3)_2N_2 \xrightarrow{k_2} CH_4 + {}^{\cdot}CH_2N_2CH_3 \qquad 1\text{-}29$$

Hence, it follows that

$$R(CH_4)/\{R(C_2H_6)\}^{1/2}.[A] = k_2/k_1^{1/2} \qquad 1\text{-}30$$

where A = azomethane. The quantum yield of nitrogen formation at 366 nm was found to be unity and independent of temperature.[48] Jones and Steacie[48] obtained a value of 32 kJ mol^{-1} for the activation energy difference E_2-$^1/_2E_1$. These workers also gave evidence for the association reaction between methyl and azomethane and obtained an activation energy of 27 kJ mol^{-1} for this reaction. In a later work, Toby[49] studied the effects of wavelength, inert gas concentration and surface on the gas phase photolysis of azomethane and observed Arrhenius curvature below -10°C which increased when a photolysis cell of greater surface to volume ratio was used and decreased when the light beam was passed through the centre of the cell only. The curvature was attributed to a competing heterogenous reaction (reaction 1-31) between methyl radicals and azomethane adsorbed on the cell wall:

$$CH_3\cdot + (CH_3)_2N_2\text{-wall} \longrightarrow CH_4 + \cdot CH_2N_2CH_3 \qquad 1\text{-}31$$

In their study of the effects of third body on the combination of methyl radicals produced by photolysis of azomethane, Toby and Weiss[50] assumed that ethane was formed via a third body mechanism represented by:

$$2CH_3\cdot \underset{b}{\overset{a}{\rightleftharpoons}} C_2H_6^* \qquad 1\text{-}32$$

$$C_2H_6^* + M_1 \xrightarrow{c} C_2H_6 + M_1 \qquad 1\text{-}33$$

where M_1 represents an appropriate third body. The azomethane was also assumed to be the only third body. Their results indicated that there was a third body effect though this effect was only apparent at higher pressures than in the corresponding case of the photolysis of acetone. Acetone was then reported to be

approximately three times as efficient at deactivating the ethane complex as is azomethane.

Definitive evidence has been provided for hydrogen atom abstraction by thermal methyl radicals in crystalline acetonitrile[51] and methyl isocyanide[52] at 77 K and higher temperatures as represented by the reactions 1-34 and 1-35 respectively:

$$CH_3^{\cdot} + CH_3CN \longrightarrow CH_4 + {}^{\cdot}CH_2CN \qquad 1\text{-}34$$

$$CH_3^{\cdot} + CH_3NC \longrightarrow CH_4 + {}^{\cdot}CH_2NC \qquad 1\text{-}35$$

These reactions in the solid state were found to have apparent activation energies (ca. 5·8 kJ mol^{-1} at 77 K[51]) which are much lower than the value of 41·8±2·1 kJ mol^{-1} obtained for the corresponding reaction of CD_3 radicals with acetonitrile in the gas phase between 373 and 573 K.[53] However, it has been shown that these unusually low activation energies result from a very large contribution from quantum mechanical tunnelling at low temperatures.[54] In a later work, Campion and Williams[55] presented a convincing demonstration of a thermal hydrogen atom abstraction by CH_3 radicals in a methanol-d glass at 77 K. The reaction was found to proceed with the concomitant formation of the CH_2OD radical. They reported a first order kinetics for the reaction over 75% of its course and obtained good agreement between the rate constants as determined from the decay of CH_3 and the growth of CH_2OD. These workers also found that at 77 K, the rates of the hydrogen atom abstraction by CH_3 from CH_3OD and CH_3OH are comparable, but the rate of CH_3 decay in CD_3OD was found to be much slower by more than three orders of magnitude. This large deuterium isotope effect therefore comfirmed

that abstraction occurred mainly from the hydrogens of the methyl group. An activation energy of 4 kJ mol^{-1} which they obtained for the abstraction reaction in the glassy state between 67 and 77 K was much lower than the value of 34 ± 0·8 kJ mol^{-1} which was reported earlier for essentially the same reaction in the gas phase at 376 to 492 K.[56] Since all these observations are similar to the results obtained earlier for hydrogen atom abstraction by CH_3 radicals from acetonitrile and methyl isocyanide, it was concluded that the decay of methyl radicals by hydrogen atom abstraction in methanol glasses also occurred mainly by quantum mechanical tunnelling at low temperatures.

Oduwole and Wiseall[57] have also reported the results of their work on the reactivity of radiolytically produced methyl radicals stabilized at 300 K on basic and neutral alumina. In contrast with the observations of Turkevich and Fujita,[25] these workers reported that the stabilized methyl radical on Al_2O_3 did not show any reaction with oxygen and hydrogen and showed almost complete recovery of the signal with water vapour, methyl iodide, acetone and methanol upon evacuation. Linewidth of CH_3 radicals on Al_2O_3 were found to be two to four times wider than on PVG and this was interpreted to imply that the CH_3 radical is fixed and immobilized at an inaccessible site on the alumina surface.

Lunsford and co-wokers[58] have also used the technique of matrix isolation ESR to study the reactions of methyl radicals with certain members of the lanthanide oxide series. They reported that methyl radicals reacted extensively with the surfaces of CeO_2, Pr_6O_{11} and Tb_4O_7, all of which have multiple cationic oxidation states while

the oxides La_2O_3, Nd_2O_3, Sm_2O_3, Eu_2O_3 and Yb_2O_3 reacted with CH_3 radicals to only a small extent. Hence, the former group of oxides were reported to be ineffective in generating CH_3 radicals which emanate into the gas phase and it was suggested by these workers that it was likely that the Ln^{3+}/Ln^{4+} multivalency in these three oxides facilitated the electron transfer needed to generate methoxide species, according to the equation:

$$M^{(n+1)+}O^{2-} + CH_3^{\cdot} \longrightarrow M^{n+}(OCH_3)^{-} \qquad 1\text{-}36$$

Infrared and ESR evidence suggests that methyl radicals react with supported MoO_3 by a similar reaction.[59] Lunsford and his co-workers[58] also showed that the reaction of CeO_2 with CH_3 radicals was strongly inhibited by adding Na_2CO_3 thereby enhancing the production of radicals. This effect was manifested in the catalytic properties of CeO_2 which is a complete oxidation catalyst in its pure form but becomes a good catalyst for the oxidative coupling of methane on addition of Na_2CO_3.

In a later study by Tong and Lunsford,[60] the kinetics and mechanism of the reactions of CH_3 radicals with metal oxide surfaces were determined. The sticking coefficients for CH_3 radicals on ZnO, CeO_2 and MgO were reported to be $1{\cdot}8\times10^{-5}$, $2{\cdot}1\times10^{-6}$ and $1{\cdot}2\times10^{-7}$, respectively. A wide range of reactivities of the metal oxides with the CH_3 radicals was reported. These metal oxides in which the cations exhibit accessible multivalent oxidation states were found to be highly reactive. The order of reactivity of the radicals with metal oxides was found to be $ZnO > MoO_3 > NiO > CeO_2 > MgO \approx Li^+/MgO$. These workers determined first order rate constants for the reactions of CH_3 radicals with the metal oxides from the absolute sticking

coefficients and the relative reaction rates. They reported that methyl radicals reacted with MoO_3/SiO_2 by electron transfer which was apparent in the reduction of Mo^{6+} to Mo^{5+}. A similar reaction was believed to occur on CeO_2 at 100°C, but their results indicated that the electron was subsequently transferred to molecular oxygen, forming O_2^- on the surface:

$$O_2 + Ce^{3+} \longrightarrow Ce^{4+}O_2^- \qquad 1\text{-}37$$

Due to this reduction reaction, methoxide ions were produced and these were then eventually converted to formate ions. The resulting methoxide and formate ions are believed to be intermediates in the non-selective oxidation of CH_4 to CO, CO_2 and H_2O. These workers were then able to arrive at the following mechanism for the reaction of CH_3 radicals with metal oxides:

$$M^{(n+1)+}O^{2-} + CH_3^{\cdot} \longrightarrow M^{n+}(OCH_3)^- \qquad 1\text{-}38$$

$$M^{n+}(OCH_3)^- + O_2 \longrightarrow M^{n+}(O_2CH)^- + H_2O \qquad 1\text{-}39$$

$$M^{n+}(O_2CH)^- \longrightarrow M^{n+}(OH)^- + CO \qquad 1\text{-}40$$

$$2M^{n+}(OH)^- + 1/2O_2 \longrightarrow 2M^{(n+1)+}O^{2-} + H_2O \qquad 1\text{-}41$$

Tong and Lunsford[60] also reported that the methoxide ion may, in addition to these reactions, decompose to form formaldehyde which occurs during the catalytic oxidation of methanol, but that at the temperatures which they employed for the oxidative coupling of methane, there would be complete oxidation of the formaldehyde. Apart from the low sticking coefficients, low activation energies of 11 and 24 kJ mol^{-1} were also reported for the reactions of CH_3 radicals with ZnO and MgO respectively. Two mechanisms were then proposed to interpret these low activation energies and low sticking

coefficients. According to one of the mechanisms, the electrons on weakly adsorbed CH_3 radicals tunnel through the oxide ions and reduce the metal ions close to the surface:

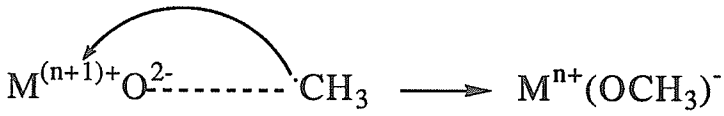

$$M^{(n+1)+}O^{2-} \cdots\cdots\cdots CH_3 \longrightarrow M^{n+}(OCH_3)^- \qquad 1\text{-}42$$

The other mechanism involves the initial adsorption of a CH_3 radical on a metal cation with a partial electron transfer. The adsorbed $CH_3{\cdot}^{\delta+}$ species then moves to a neighbouring oxide ion through a 3-centre transition state complex, as a result of a coulombic interaction between the positively charged CH_3 radical and the oxide ion:

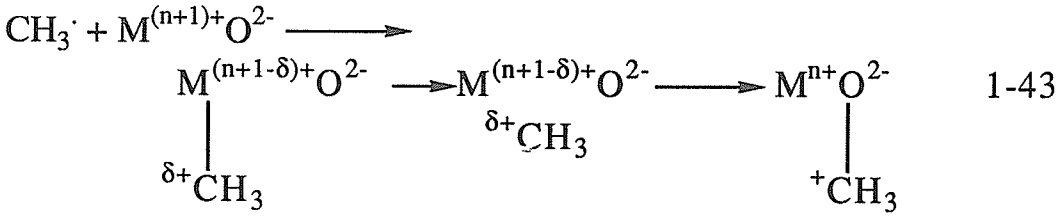

$$CH_3^{\cdot} + M^{(n+1)+}O^{2-} \longrightarrow M^{(n+1-\delta)+}O^{2-} \longrightarrow M^{(n+1-\delta)+}O^{2-} \longrightarrow M^{n+}O^{2-} \qquad 1\text{-}43$$

$$\delta+CH_3 \qquad\qquad \delta+CH_3 \qquad\qquad +CH_3$$

Since a small sticking coefficient is required for the selective oxidative dimerization of CH_4 so that a CH_3 radical may reflect off a catalyst surface many times before colliding and reacting with another CH_3 radical, these workers were able to conclude that ZnO, MoO_3, NiO and CeO_2 are non-selective oxidation catalysts whereas Li^+/MgO is a reasonably active and selective catalyst for the oxidative dimerization reaction.

In their study of the decay kinetics of methyl radicals on porous Vycor glass, Fujimoto et. al.[2] reported that the gas chromatographic analysis of the products of the surface photolysis of CH_3I at 77 K showed the presence of both CH_4 and C_2H_6 with the ratio C_2H_6/CH_4 being larger at lower surface coverage. The CH_4 was

believed to be formed by hydrogen atom abstraction by hot CH_3 radicals. They reported a cascade type of decay as the temperature was raised from 77 K to 132 K. Gesser's review[1] of ESR studies of alkyl radicals adsorbed on porous Vycor glass has shown that other workers have obtained similar results of the decay kinetics of CH_3 radicals.

Recent studies[61] of the photolysis of alkyl ketones adsorbed on Vycor glass by hydrogen bonding have also demonstrated that the photochemical reactions in the adsorbed layer indicated some deviations in the reaction yields and selectivity as compared with those in the gas phase. These studies have shown that these deviations were generally caused by the high reactivity and high polarity of the surface OH groups on Vycor glass which seemed to play a significant role in the reactivity and stabilization of intermediate species in the chemical reactions. Evidence was provided for the fact that hydrogen atom abstraction reaction from the surface OH groups by methyl radicals occurred on the surface of Vycor glass:

1-44

The activation energy for this abstraction reaction was found to be less than 38 kJ mol^{-1} being smaller than the corresponding value for the hydrogen atom abstraction from acetone molecules.[62] Hence, the hydrogen atom abstraction from surface OH groups on Vycor glass is expected to occur more easily.

CHAPTER 2
EXPERIMENTAL

2.1 Chemicals and Equipment

2.1.1 Chemicals

Yellow mercury (II) oxide (99+% purity), 1,2-dimethylhydrazine dihydrochloride (99+% purity) and 1,2-diethylhydrazine dihydrochloride which were used in the preparation of azomethane and azoethane were all reagent grade chemicals obtained from Aldrich Chemical Company, Inc. They were all used without further purification. Analytical reagent sodium hydroxide (98·7% purity) which was used to neutralize the 1,2-dimethylhydrazine dihydrochloride and 1,2-diethylhydrazine dihydrochloride in the synthesis of azomethane and azoethane, was obtained from Mallinckrodt Company Inc.

Hydrogen peroxide (30%) used in the treatment of porous Vycor glass was analytical reagent grade. It was obtained from Mallinckrodt Company.

2.1.2 Electron Spin Resonance Spectrometer

The ESR observations and study of the decay kinetics of methyl and ethyl radicals adsorbed on PVG were conducted with a Varian E-3 Electron Spin Resonance Spectrometer (Varian Associates Ltd., Palo Alto, California) employing 100kHz modulation.

The Varian E-3 is an X-band ESR spectrometer with the following specifications:

Operating frequency:	8·8 to 9·6 GHz
Microwave power to cavity:	0·2 to 200 milliwatts
Field Modulation frequency:	100 kHz

Modulation field intensity: $5x10^{-3}$ to 40 gauss

Magnetic field strength: 0-6000 gauss

Scan time: 0·5 min. to 16 hours.

Scan range: $\pm 0{\cdot}025$ to $\pm 10^4$ gauss

Recorder Filter time constants: 0·1 to 100 sec.

ESR spectra were recorded on the flat-bed recorder of the instrument.

2.1.3 Measurement of Infrared Spectra

A Perkin-Elmer 881 Infrared Spectrophotometer was used to observe the condition of the Vycor glass during its heat-vacuum pre-treatment. A special sample holder was used to simultaneously support, position and mask the sample in the light path of the instrument. The same quartz sample tubes used for ESR measurements were used for IR measurements. The IR spectra of the empty sample tubes were taken prior to taking the spectra of the samples to make sure that the sample tubes were IR transmitting and did not absorb in the OH region ($\approx 2{\cdot}7\ \mu$ or 3700 cm^{-1}). During each IR measurement, a neutral density comb was placed in the reference beam for optimum spectral presentation when necessary.

2.1.4 Temperature control and measurements

Studies on samples in the ESR cavity at -196°C were done by using a dewar flask having a dewar "finger" extending into the resonance cavity. The dewar flask was filled with liquid nitrogen coolant to maintain the temperature. Studies at -183°C and -164°C were done by keeping the sample tube containing the sample in liquid oxygen and liquid natural gas (methane, mainly) respectively, for a specified period of time and then transferring it quickly to the

cavity dewar containing liquid nitrogen for ESR measurements. Hence, all ESR measurements were done at liquid nitrogen temperature (-196°C). However, some ESR measurements were also taken at -164°C as follows. The sample tube was quickly transferred from the cavity dewar containing liquid nitrogen to a nearby dewar containing liquid natural gas and, without much loss of time, the cavity dewar was removed, emptied of liquid nitrogen, warmed slightly with a heat gun, filled with liquid natural gas and then replaced. The sample tube was then re-inserted into the cavity dewar now containing liquid natural gas and the decay at -164°C observed. Measurements at -164°C were done in this way in order to compare the results of the decay kinetics with those obtained at the same temperature by keeping the sample in liquid natural gas for a specified period of time and then transferring it quickly to the cavity dewar containing liquid nitrogen for ESR measurements at -196°C. Liquid oxygen and liquid natural gas were made by liquefying oxygen and natural gas in liquid nitrogen. It should be mentioned that care was taken to ensure that the liquid natural gas had warmed up to its boiling point before transfer to the cavity dewar (also warmed) so as to obtain an invariant temperature in the cavity. During all operations of the spectrometer, dry compressed air was kept flowing continuously through the cavity so as to prevent water from condensing in the cavity.

In his ESR study of the decay of hydrogen atoms adsorbed on glass surfaces, Bader[63] observed that the signal intensity varied with the hydrostatic head of the coolant in the dewar, and an artifact decay could be observed as the coolant evaporated. Hence, during

each kinetic run on the sample, care was taken to maintain the liquid nitrogen at approximately constant level by manual additions of the coolant. This level was chosen arbitrarily but was constant for all runs.

Temperature measurements for the heat treatment of the Vycor glass were made with a chromel-alumel thermocouple connected to a pyrometer whose scale was calibrated directly in temperature units (0°-1100°C). The measuring junction of the thermocouple was placed in the furnace in such a way as to be in the same position as the sample in the sample tube.

The furnace used for the heat treatment of the Vycor glass was made of nichrome wire (≈13 ohms total resistance) wound on a ceramic tube (≈2 cm I.D.) and insulated with an asbestos paste. The temperature of the furnace was controlled with an Ohmite variable transformer.

2.1.5 Vacuum system

The schematic diagram of the vacuum system used for the purification and handling of gases as well as the evacuation, heat treatment and loading of Vycor glass samples is shown in Figure 2-1.

The vacuum was provided by a mercury diffusion pump along with a mechanical, rotary oil pump.

Pressure measurements were made with a mercury manometer mounted on the vacuum apparatus. The pressure of the vacuum was monitored using a Veeco thermocouple vacuum gauge.

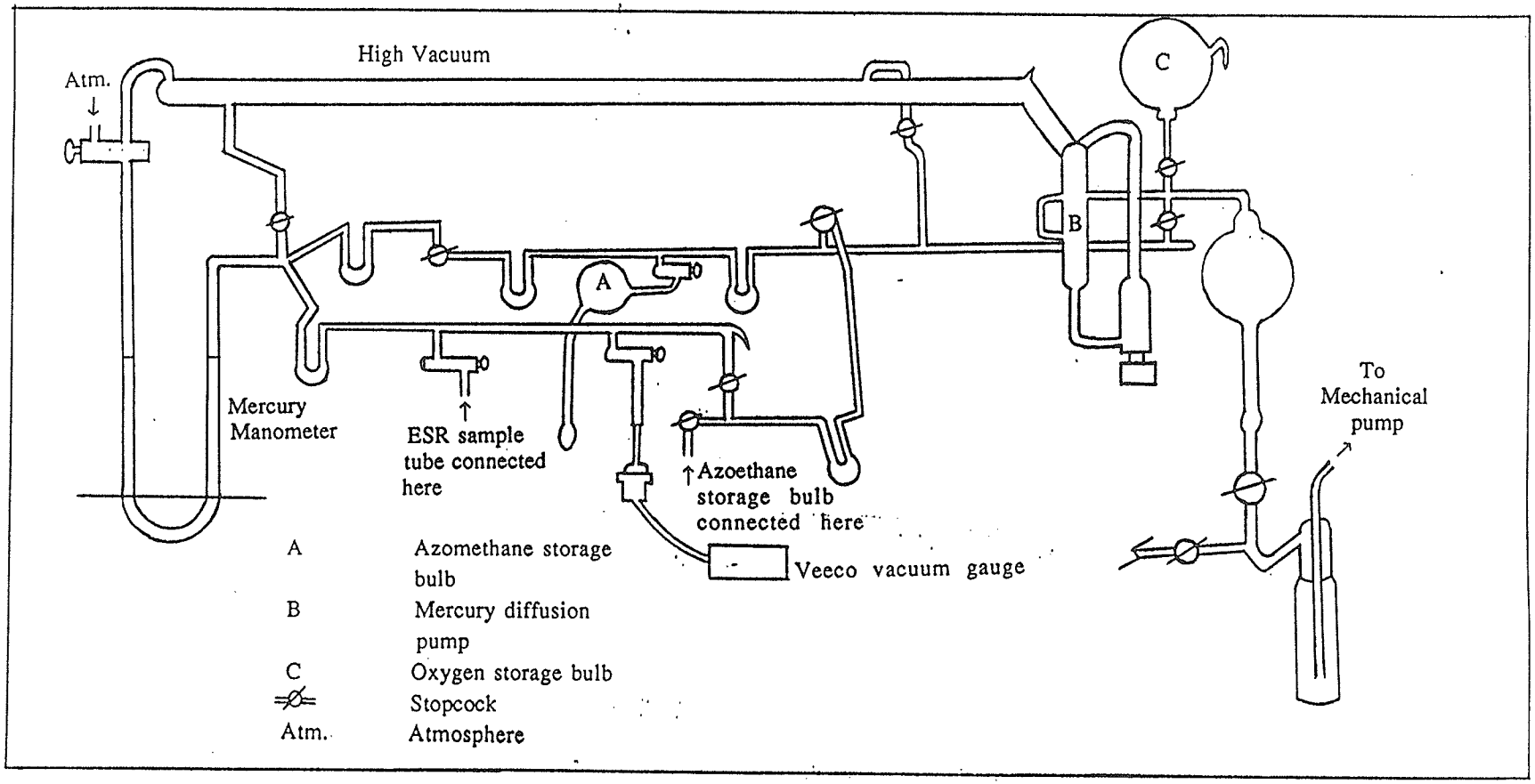

Figure 2-1: Schematic diagram of the vacuum system.

The stopcock grease used throughout the apparatus was Dow Corning high vacuum silicone grease (Dow Corning Corporation, Midland, Mich. U.S.A.).

2.1.6 Production of methyl and ethyl radicals

Methyl radicals were obtained in this work by photolysing a known amount of azomethane adsorbed on PVG. The azomethane-loaded PVG samples were immersed in liquid nitrogen in an unsilvered quartz dewar flask and the photolysis was achieved at the liquid nitrogen temperature (77 K) with an S-500 Hanovia mercury lamp without any filter. Ethyl radicals were obtained in a similar manner by photolysing azoethane adsorbed on PVG.

2.2 Preparation of azomethane

Azomethane used in this work was prepared using the method of Renaud and Leitch.[64]

A mass of 13·2930 g of 1,2-dimethylhydrazine dihydrochloride was first dissolved in about 33 mL water and neutralised with 8·0079 g NaOH dissolved in about 33 mL water. The neutralised 1,2-dimethylhydrazine dihydrochloride was then added slowly, through a dropping funnel, to a suspension of 25·1386 g of yellow mercury(II) oxide in 40 mL of water. An additional 6·0027 g of mercury(II) oxide was added and the reaction mixture was then stirred continuously at room temperature for two hours. When the reaction mixture was heated, azomethane distilled over and was collected in a liquid nitrogen trap. The azomethane was dried by slow distillation through a U-tube containing calcium sulphate (Drierite) on a vacuum line and introduced into the storage bulb on the

vacuum apparatus by using trap to trap distillation. Figure 2-2 shows the set-up of the apparatus used for the preparation.

2.3 Preparation of azoethane

Azoethane was also synthesized using the method of Renaud and Leitch.[64] A mass of 9·7294 g of 1,2-diethylhydrazine dihydrochloride was first dissolved in about 13·5 mL water and neutralised with 4·9728 g NaOH in 13·5 mL water. The neutralised 1,2-diethylhydrazine dihydrochloride was then added dropwise, with the aid of a dropping funnel, to a stirred suspension of 17·3018 g of yellow mercury(II) oxide in about 27 mL water in a 3-necked round bottom flask with a short fractionating column (packed with stainless steel) and still head. The reaction mixture was quickly brought to a boil. After an azeotrope of azoethane and water had been collected between 52 and 60°C, the temperature rapidly rose to about 95°C, and the distillation was stopped. The product was then dried over anhydrous calcium sulphate (Drierite) and introduced into the storage bulb on the vacuum line by using trap to trap distillation method. The set-up of the apparatus used for the preparation is shown in Figure 2-3. The gas chromatography-mass spectrometric analysis of the liquid obtained showed it to contain mainly azoethane and just a little amount of another substance of mass 64.

2.4 Experimental procedures

2.4.1 Porous Vycor glass

(a) Cutting and cleaning of PVG

The porous Vycor glass used in this work was obtained from the Corning Glass Co., Corning, New York (Corning Code No. 7930). The glass was in form of a plate. The glass was cut into small pieces in

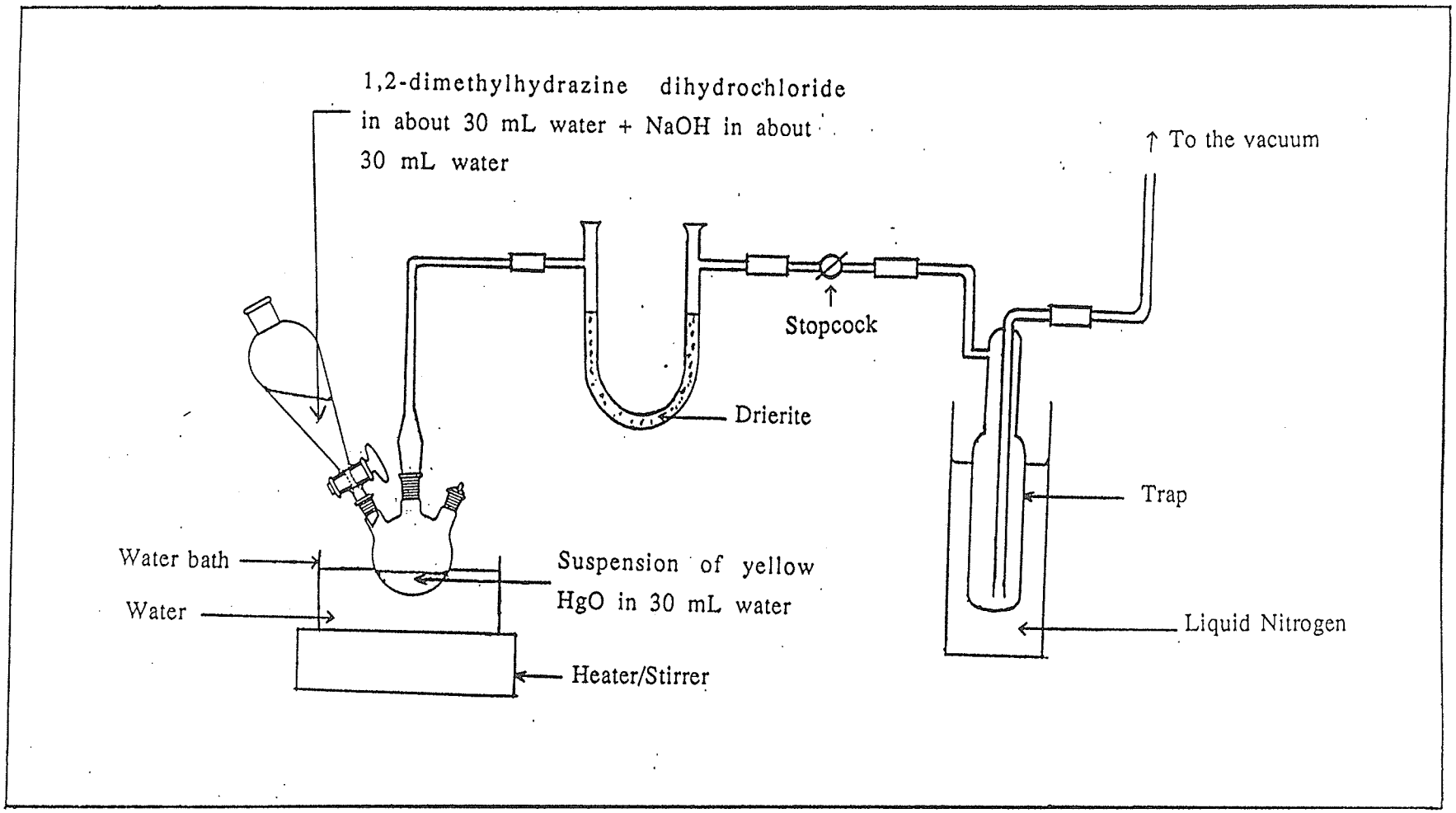

Figure 2-2: Apparatus for the preparation of azomethane.

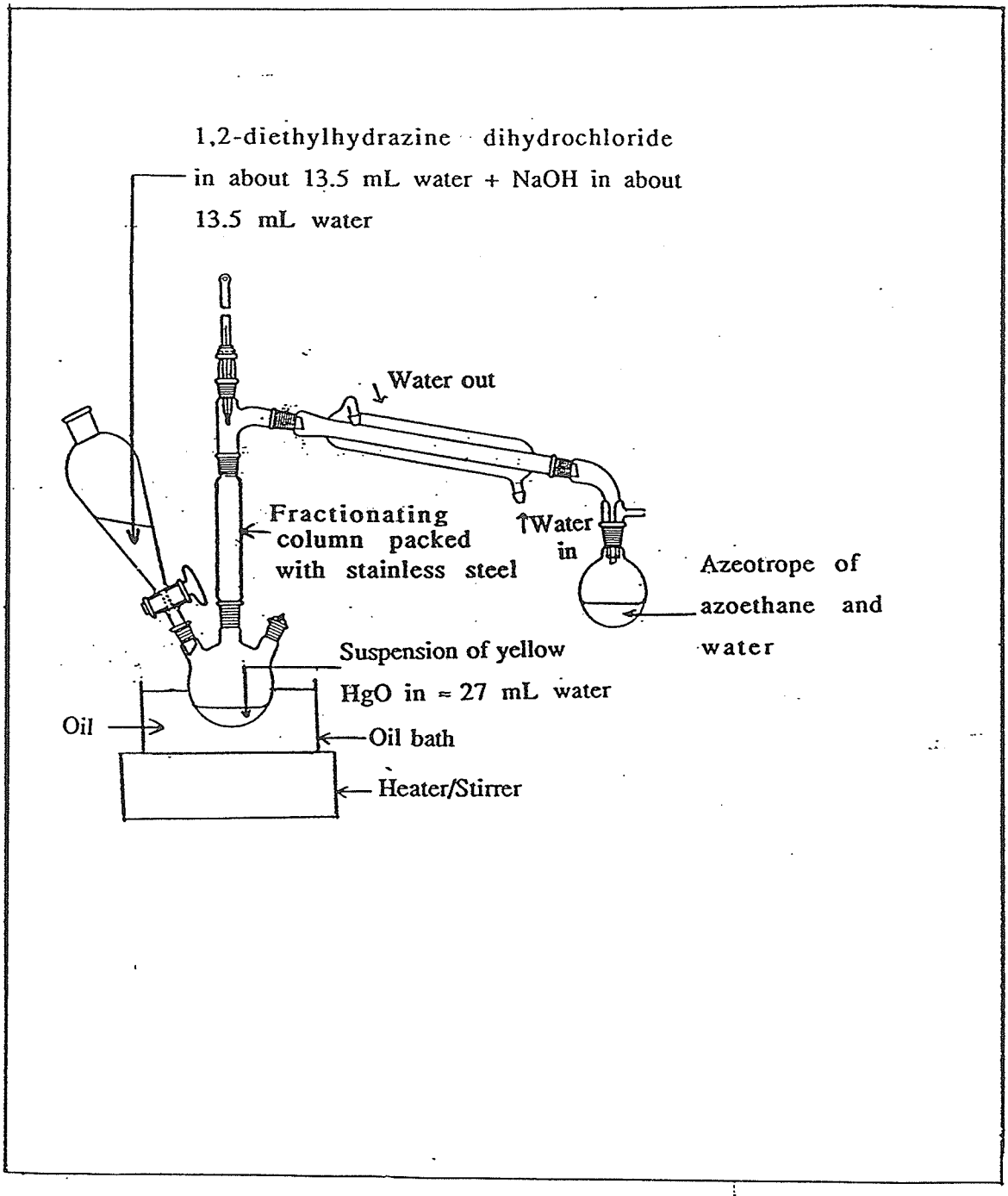

Figure 2-3: Apparatus for the preparation of azoethane.

such a way that each piece could fit into the ESR sample tube. The pieces were approximately 20 x 2 x 1 mm and weighed 50 to 100 mg after cleaning. The Vycor glass was assumed to have a surface area of 200 m^2/g.[5,63]

The cut glass pieces were cleaned by boiling in 30% hydrogen peroxide[65] for $2^1/_2$ hours until they became transparent. The pieces were then rinsed in boiling deionised water, dried in the oven at 110°C for 48-72 hours and weighed.

Each weighed PVG piece was then introduced into an ESR sample tube (Figure 2-4) for further treatment.

(b) Evacuation and heat treatment

The Infrared spectra of Vycor glass samples that were evacuated at 500°C or temperatures below 500°C for several hours showed a broad absorption band at about 3600 cm^{-1} indicating the presence of some physically adsorbed water, though the intensity of the band decreases with increase in temperature of evacuation as can be seen in Figures 2-5 to 2-7. The adsorbed water was most efficiently removed by heating and evacuation at 700-750°C for several hours. Hence, in this work, the ESR sample in which each Vycor glass was placed was connected to the vacuum system and then subjected to heating and evacuation at about 750°C for 7-9 hours. The vacuum was better than 10^{-3} torr. However, after such a treatment, the sample usually blackened due to charring of organic contaminants from packaging and handling. So, after each treatment at 750°C, the sample was usually thermoleached in 100-200 torr of oxygen at 500°C for 5 hours after which the black colour disappeared

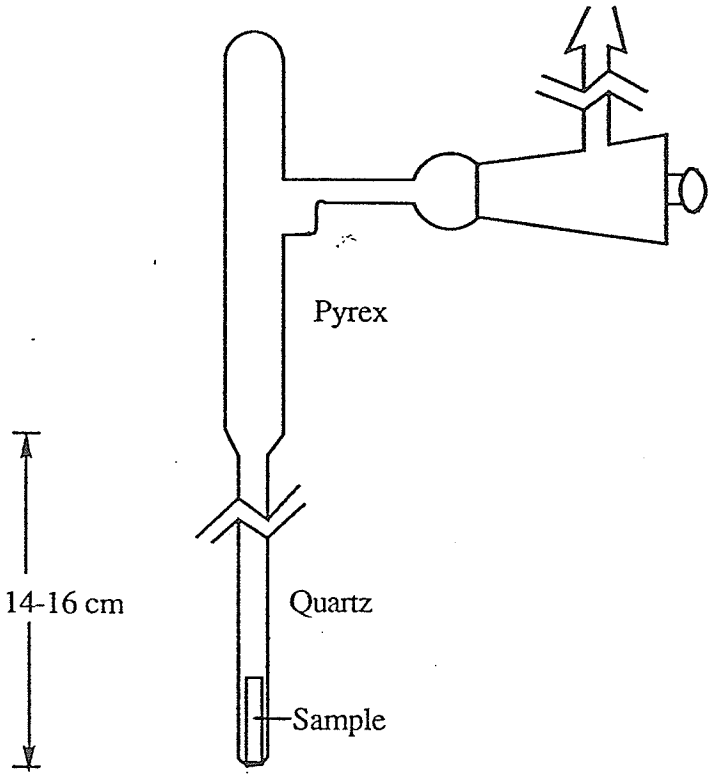

Figure 2-4: ESR sample tube.

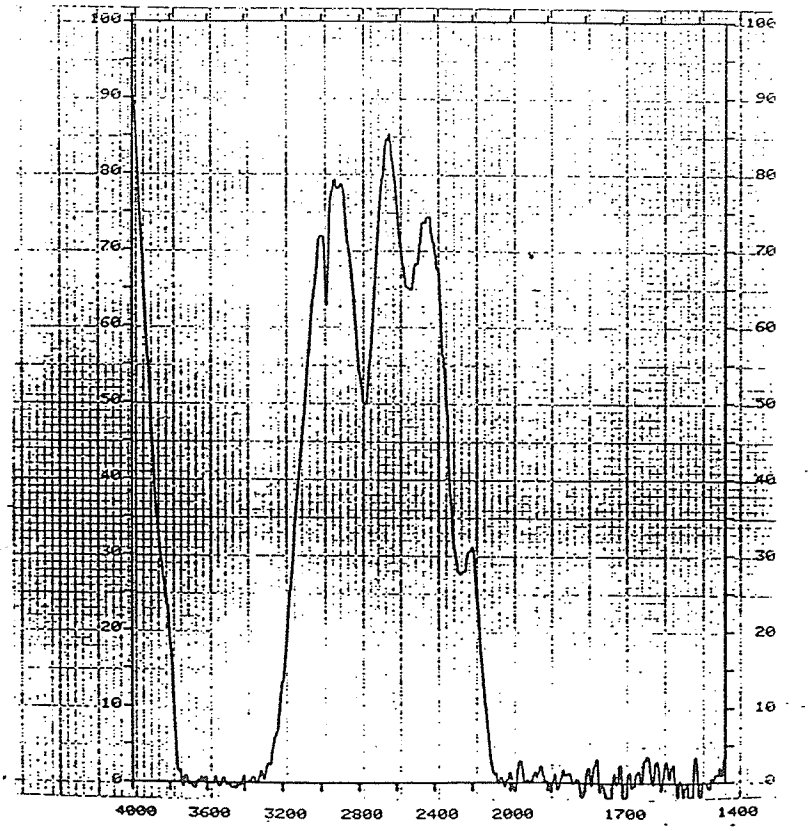

Figure 2-5: IR spectrum of porous Vycor glass heated and evacuated at 200°C for 5 hours.

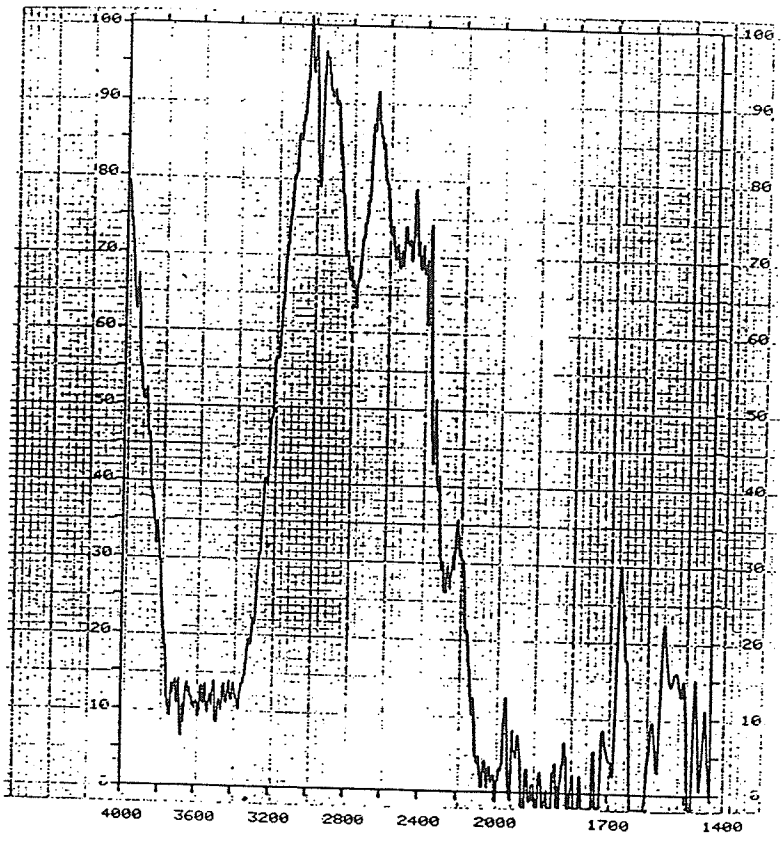

Figure 2-6: IR spectrum of PVG heated and evacuated at 400°C for 8 hours.

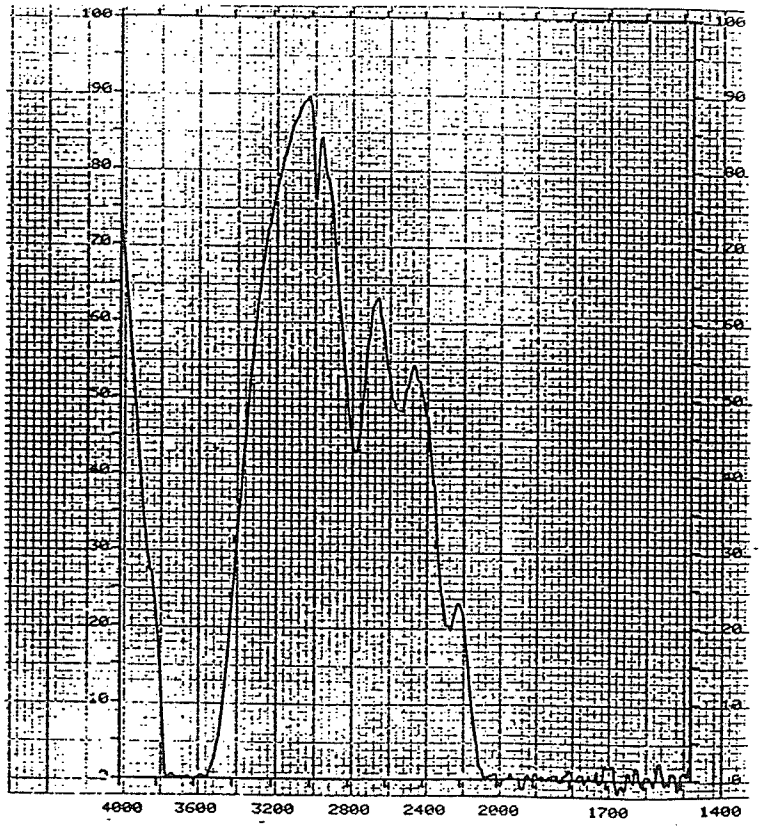

Figure 2-7: IR spectrum of PVG thermoleached in 141 torr of O_2 for 5 hours followed by evacuation at 500°C for 1 hour.

as the char was converted slowly to CO_2, H_2O, etc. in the hot oxygen atmosphere. After thermoleaching, the sample was then evacuated at 500°C for 1 hour and following this, the sample became colorless but slightly frosted. The IR spectra taken after each treatment at 750°C and subsequent thermoleaching usually showed clearly resolved Si-OH and B-OH peaks as shown in Figure 2-8.

In the study of the effect of surface adsorbed water on the decay of the radicals, a sample was evacuated at 300°C followed by thermoleaching at 500°C so as to leave some adsorbed water on the surface.

2.4.2 Generation of methyl and ethyl radicals

After all necessary degassing as discussed in section 2.4.1, azomethane (or azoethane) was introduced into the ESR sample tube containing the PVG piece in such an amount as to have the desired surface coverage; the molecular areas of azomethane and azoethane were calculated to be $27{\cdot}9 \times 10^{-20}$ and $39{\cdot}3 \times 10^{-20}$ m^2 respectively, using the equation of Young and Crowell[66]. The azomethane- (or azoethane-) loaded PVG sample was then irradiated at 77 K with the S-500 Hanovia mercury lamp without any filter to generate methyl (or ethyl) radicals. ESR spectra were taken at intervals during irradiation to follow the build-up of the radicals until signals large enough for decay studies were obtained.

2.4.3 Machine parameters of the ESR spectrometer

The machine parameters for the ESR observation of the line chosen for study were maximized by trial and error for both methyl

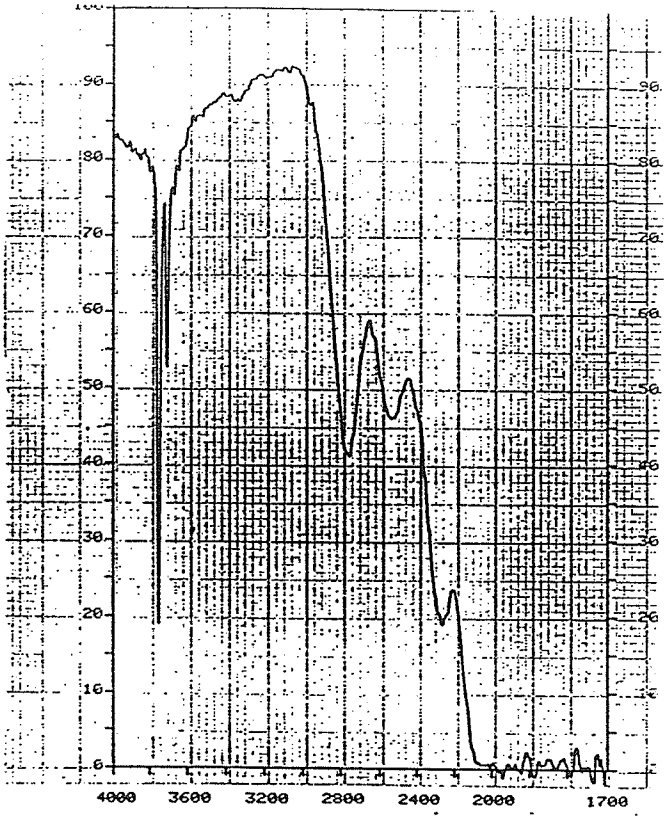

Figure 2-8: IR spectrum of PVG heated and evacuated at 750°C for 9 hours.

and ethyl radicals and these were then retained throughout the study.

The standard instrument settings are shown in Table 2-1. All intensity measurements were standardized to the same receiver gain setting of $4{\cdot}0 \times 10^4$ for methyl radicals and $8{\cdot}0 \times 10^4$ for ethyl radicals.

Prior to studying the decay kinetics of the radicals, the effect of microwave power on the peak intensity was studied. For methyl radicals, the peak intensity was found to increase with increasing microwave power input to the resonant cavity up to 2·0 milliwatts, and then decreased with increasing power as shown in Figure 2-9. This effect is due to saturation of the signal as discussed in section 1.3.2. Hence, a microwave power input of 1·6 mW was chosen for the decay study. Saturation effect was also observed in the case ethyl radicals but the ESR signal was found to saturate at about 4·0 mW power as shown in Figure 2-10. A microwave power input of 4·0 mW was therefore chosen for decay study of ethyl radicals.

2.4.4 Measurement of the g values and absolute concentrations of the radicals

The g values of the ESR spectra of methyl and ethyl radicals were obtained by comparison with the value for the spectrum of 2,2-diphenyl-1-picrylhydrazyl (DPPH; g=2·0036).

Table 2-1: Standard instrument settings for the observation of ESR signals.

	Methyl Radicals	Ethyl Radicals
Magnetic field set	3235 G	3235 G
Magnetic field scan range	$\pm 0{\cdot}5 \times 10^2$ G	$\pm 1 \times 10^2$ G
Modulation amplitude	0·5 G	1·0 G
Time constant	1·0 sec	1·0 sec
Scan time	8 min	8 min
Microwave power	1·6 mW	4·0 mW
Microwave frequency	Tuned	Tuned

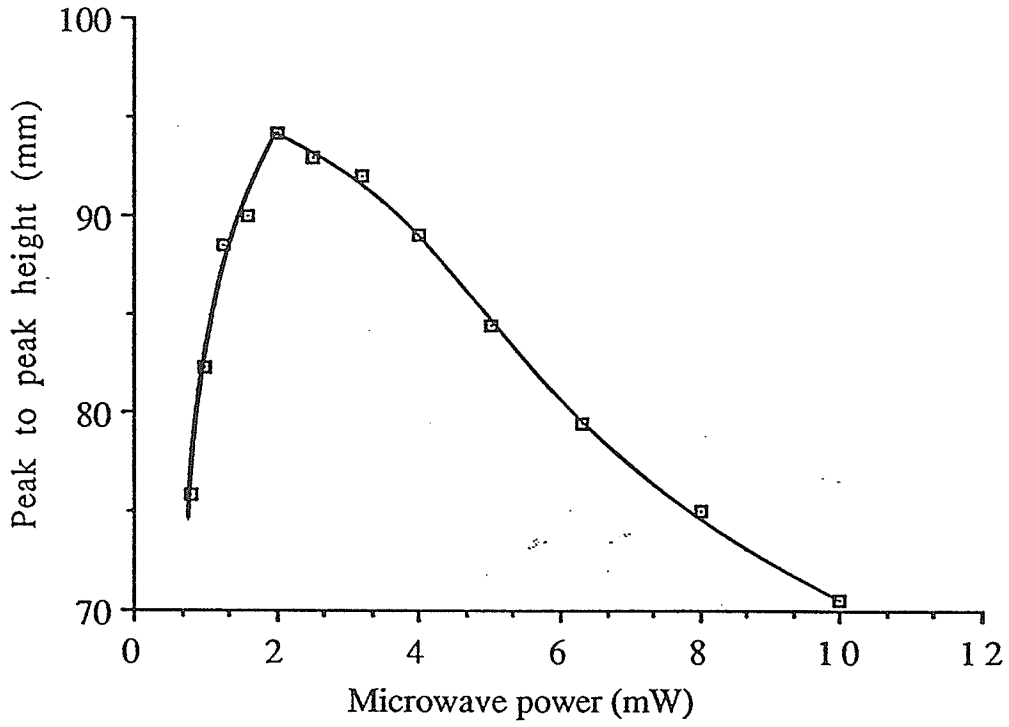

Figure 2-9: Plot of peak to peak height against microwave power at 77 K for line 3 (second line from the low field side) of the ESR spectrum of methyl radicals on PVGM containing 1.03 monolayer (1.23×10^{-3} mmole/mg) azomethane.

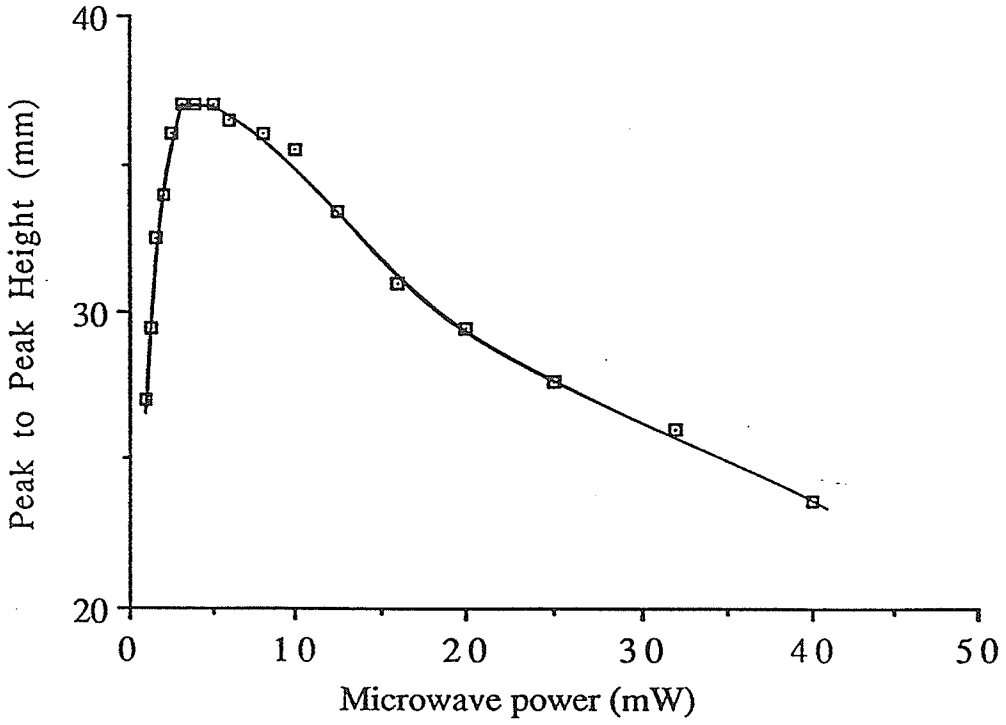

Figure 2-10: Plot of peak to peak height against microwave power at 77 K for the upfield most intense line of the ESR spectrum of ethyl radicals on PVGE1 containing 2.10 monolayers (1.78×10^{-3} mmole/mg) azoethane.

The surface concentrations of both methyl and ethyl radicals in spins/m^2 were determined by using the numerical method of Wyard[67] to obtain the double integration of the first derivative signals of the radicals which were normally obtained. For each radical, the area obtained using this method was then compared with that obtained with a known concentration of DPPH in benzene. During kinetic measurements, absolute radical concentrations were then obtained from the peak heights of the first derivative signals using peak height and area correlations. The error in the spin concentrations was estimated to be ±2%. All the required details about the measurement of the absolute spin concentrations as well the raw data are given in Appendix I.

The intensity ratio of the 4-line spectrum of methyl radicals was found in this work to be 1:3·7:3·5:1·1 which is quite close to the theoretical binomial value of 1:3:3:1. Hence, in the calculation of the spin concentration of methyl radicals, the spectrum of the radicals was assumed to have the binomial intensity ratio. The values of the spin concentrations of the radicals calculated on this assumption were only about 6% higher than the values obtained when the spectrum was assumed to have the experimental intensity ratio. In the case of ethyl radicals, an intensity ratio of 1·0:9·8:5·1:1·3:38:5·9:5·2:38:1·2:4·0:10:0·94, quite different from the literature value[68,69] of 1:2:3:1:6:3:3:6:1:3:2:1, was obtained because the 12 lines obtained in this work were not completely resolved. Consequently, the spin concentrations of the radicals calculated using the literature value of the intensity ratio were found to be about 68%

higher than the value obtained using the intensity ratio obtained in this work. Nevertheless, the literature value of the intensity ratio was used in the calculation of the spin concentrations of the radicals.

2.4.5 Decay kinetics of the radicals

Following treatment of the PVG sample at 750°C and subsequent thermoleaching at 500°C as described in section 2.4.1, the sample was loaded at room temperature with a specific amount of azomethane (or azoethane) and then irradiated at 77 K to generate signals of methyl (or ethyl) radicals large enough to study the decay kinetics. ESR spectra were then taken to follow the decay of the radicals at -196°C, -183°C and -164°C using liquid nitrogen, liquid oxygen and liquid methane respectively as described in section 2.1.4. The studies were done at different surface coverages in order to study the effect of surface coverage on the activation energies for the decay of the radicals.

CHAPTER 3

RESULTS AND DISCUSSION

3.1 Electron Spin Resonance Spectra

3.1.1 ESR spectra of methyl radicals

As mentioned earlier in section 2.4.4, the observed ESR spectrum of methyl radicals adsorbed on PVG shown in Figure 3-1 was a quartet with relative intensities of 1:3·7:3·5:1·1 which are quite close to the binomial values of 1:3:3:1. The hyperfine splitting constant a^H=24·5 G and the g-factor, g_m, was determined to be 2·0021±0·0001 by comparison with that of a standard spectrum of 2,2-diphenyl-1-picrylhydrazyl (DPPH; g=2·0036). The peak to peak linewidth was found to be about 1·5 G indicating a rapid tumbling motion of the radical.[2] The hyperfine splitting constant, a^H, and the g-factor, g_m, for the methyl radicals have been reported[1] to be 23·4 G and 2·0024, respectively. All the results reported here therefore indicate that methyl radicals are formed by the irradiation of azomethane adsorbed on porous Vycor glass using the full UV spectrum of a medium pressure mercury arc. It should be noted that many attempts which proved abortive were also made to generate abnormal methyl radicals on porous Vycor glass samples. Unsuccessful efforts were made too to generate methylperoxy radicals by addition of oxygen to adsorbed methyl radicals.

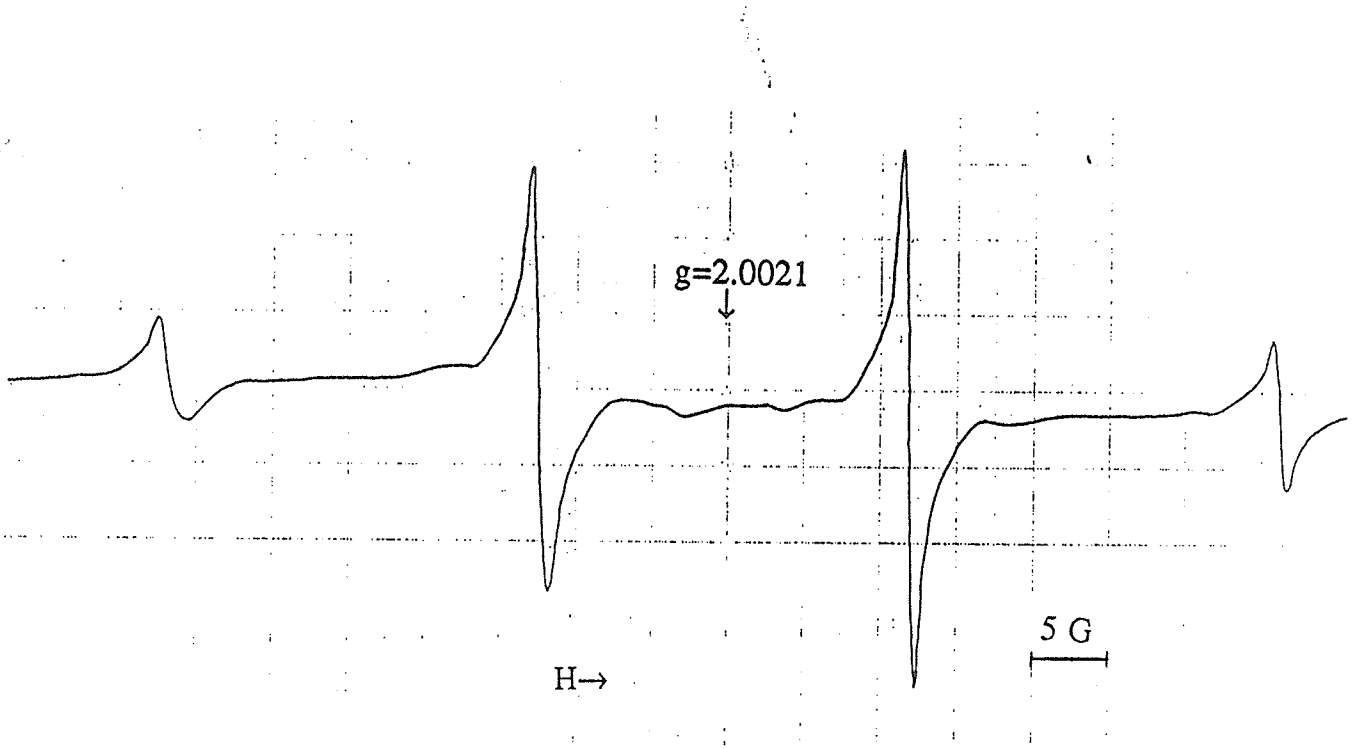

Figure 3-1: ESR spectrum of methyl radicals adsorbed on porous Vycor glass at 77 K.

3.1.2 ESR spectra of ethyl radicals

Figure 3.2 shows the observed ESR spectrum of ethyl radicals obtained by irradiation of azoethane adsorbed on PVG. The spectrum consisted of 12 lines similar to the 12-line spectrum of ethyl radicals having non-equivalent α and β protons which has been reported[68,69] as giving an intensity ratio of 1:2:3:1:6:3:3:6:1:3:2:1 and hyperfine splitting constants of a_α^H=21 G and a_β^H=26·2 G. The hyperfine splitting constants obtained in this work are a_α^H=21·5 G and a_β^H=28·5 G which are in good agreement with the values reported in the literature. However, as mentioned in section 2.4.4, the intensity ratio of the lines was found to be 1·0:9·8:5·1:1·3:38:5·9:5·2:38:1·2:4·0:10:0·94 quite different from the ratio reported in the literature because the 12 lines obtained in this work were not completely resolved. The linewidth was found to be about 3·71 G and the g-factor, g_e, was determined to be 2·0027. The g-factor obtained in this work is in good agreement with the value of 2·003 reported by Katsu et. al.[70] The agreement of the hyperfine splitting constants and the g-factor with the published spectra of ethyl radicals therefore indicates that ethyl radicals are produced by irradiation of porous Vycor glass containing adsorbed azoethane employed in this work. It should be mentioned that some unfruitful attempts were also made to produce ethylperoxy radicals by addition of oxygen to ethyl radicals adsorbed on PVG surfaces.

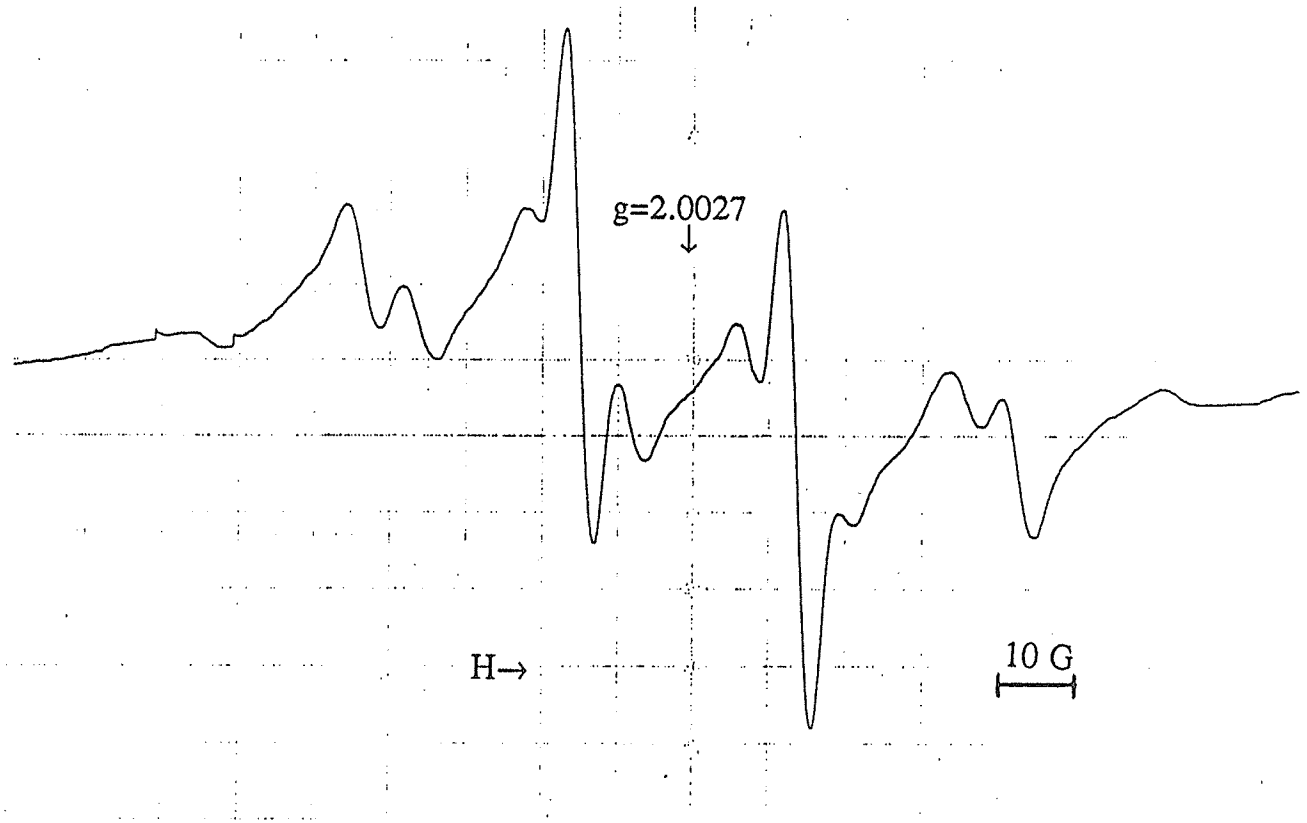

Figure 3-2: ESR spectrum of ethyl radicals adsorbed on porous Vycor glass at 77 K.

3.1.3 Absolute concentrations of the radicals

By comparison of the ESR signals of methyl and ethyl radicals to that of a standard DPPH sample, it was established (as clearly shown in Appendix I) that the concentration of the radicals in the ESR cavity was about 10^{14}-10^{15} spins/m^2 (or 10^{10}-10^{11} spins/cm^2) in good agreement with the value of 10^{17} for methyl radicals on a PVG sample having a surface area of 35 m^2 as reported by Fujimoto et. al.[2] and the value of 10^{10} atoms/cm^2 as calculated by Bader and Gesser[71] for hydrogen atoms. This quantity of methyl and ethyl radicals was large enough to study their decay kinetics in detail. The raw data for the spin concentrations of the radicals obtained during kinetic measurements are tabulated in Appendix I.

3.2 Build-up studies

3.2.1 Build-up of methyl radicals

Figures 3.3 and 3.4 illustrate the build-up of methyl radicals as a function of UV irradiation at 77 K on two PVG samples labelled PVGM and PVGM1, respectively. The two PVG samples were loaded with approximately 1 monolayer azomethane prior to UV irradiation to generate the radicals. These build-up curves show that the concentrations of the radicals do not approach a constant value during their formation by photolysis of adsorbed azomethane at 77 K. This is in contrast to what was observed previously[2,4,25] for the build-up of methyl radicals formed by photolysis of adsorbed CH_3I at 77 K. The approach to saturation in these previous studies was

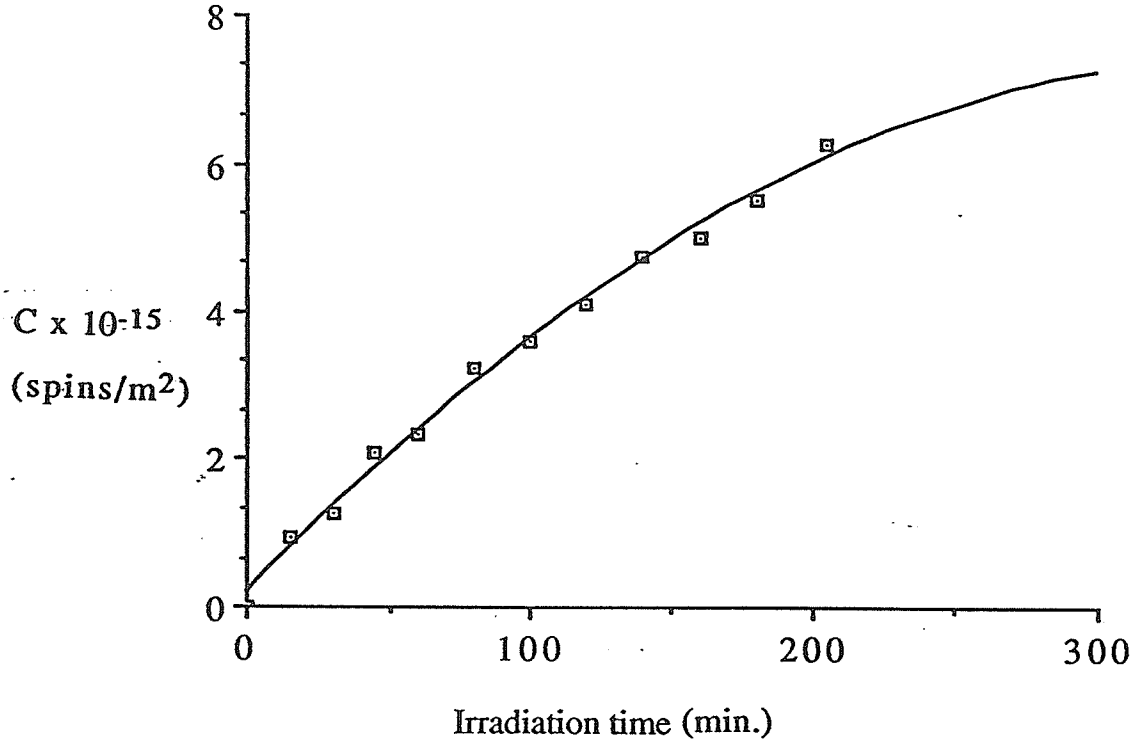

Figure 3-3: Build-up of methyl radicals at 77 K on PVGM loaded with 1.03 monolayers (1.23×10^{-3} mmole/mg) azomethane.

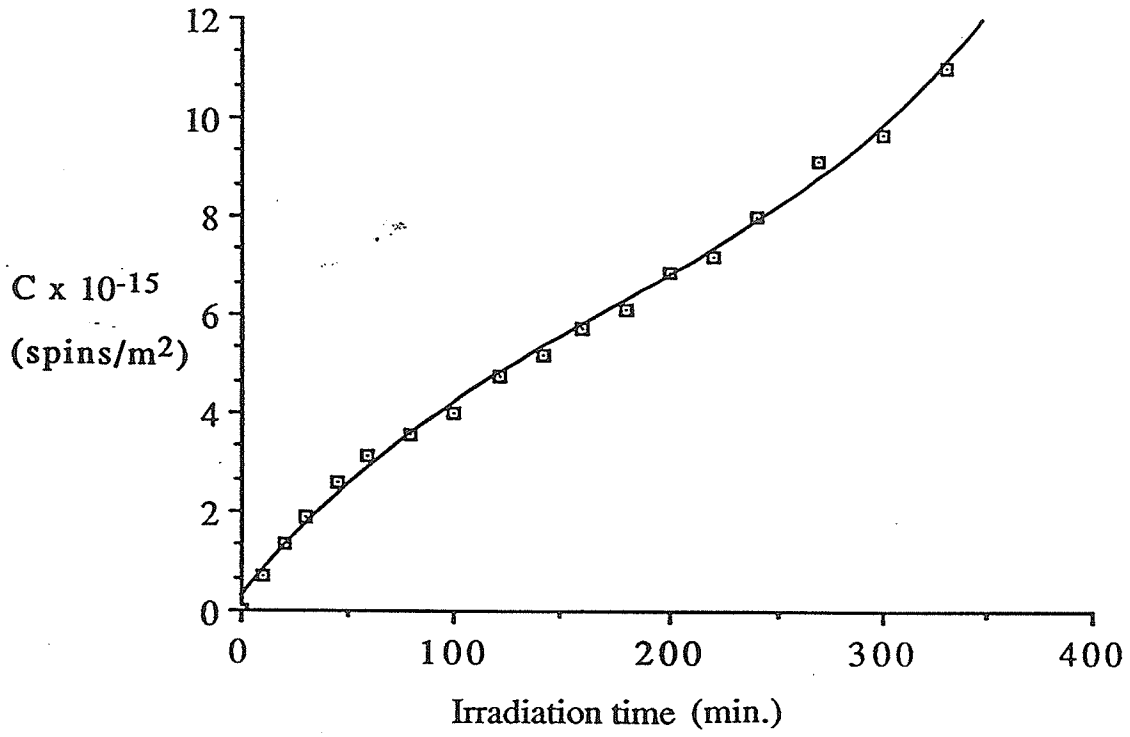

Figure 3-4: Build-up of methyl radicals at 77 K on PVGM1 loaded with 1.00 monolayer (1.19 x10^{-3} mmole/mg) azomethane.

attributed to recombination of the CH_3 radicals and to the possible back reaction of the radicals and iodine. In the present study, the percentage of azomethane molecules that decomposed during the $3\,1/2$ to $5\,1/2$ hours of irradiation to produce methyl radicals was estimated to be about 1·41 to 1·71% for PVG surfaces covered with about 0.1 monolayer azomethane, 0·0615 to 0·153% for surfaces covered with approximately 1 monolayer azomethane and 0·0182 to 0·0255% for surfaces covered with about 2 monolayer azomethane i.e. there is a gradual decrease in percentage decomposition with increase in surface coverage (see Appendix II). Thus, the non-approach to saturation observed in this work may be attributed to the fact that only a very small fraction of the azomethane molecules actually decomposed to produce methyl radicals during the period of photolysis. The approach might probably have been observed if the irradiation had been carried out for a much longer time to allow a much larger fraction of the azomethane molecules to decompose to produce methyl radicals as this might increase the probability of recombination of the radicals during photolysis.

Figures 3-5 and 3-6 also indicate that there is no significant change in the rate of formation of methyl radicals when they are left to decay for several hours at 77 K after previous irradiation for a certain period of time. This implies that during each re-irradiation, the radicals are probably still generated from the azomethane molecules rather than from tetramethylhydrazine, the product of the possible addition reaction of the radicals with azomethane.

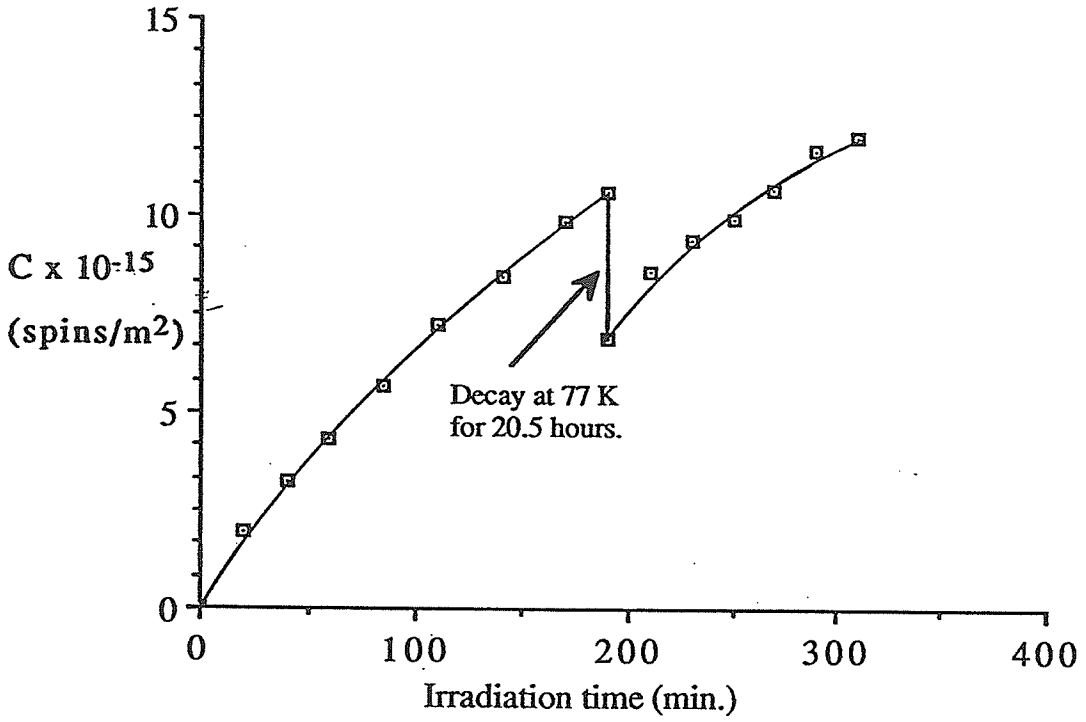

Figure 3-5: Build-up of methyl radicals at 77 K on PVGM5 containing 0.104 monolayer azomethane.

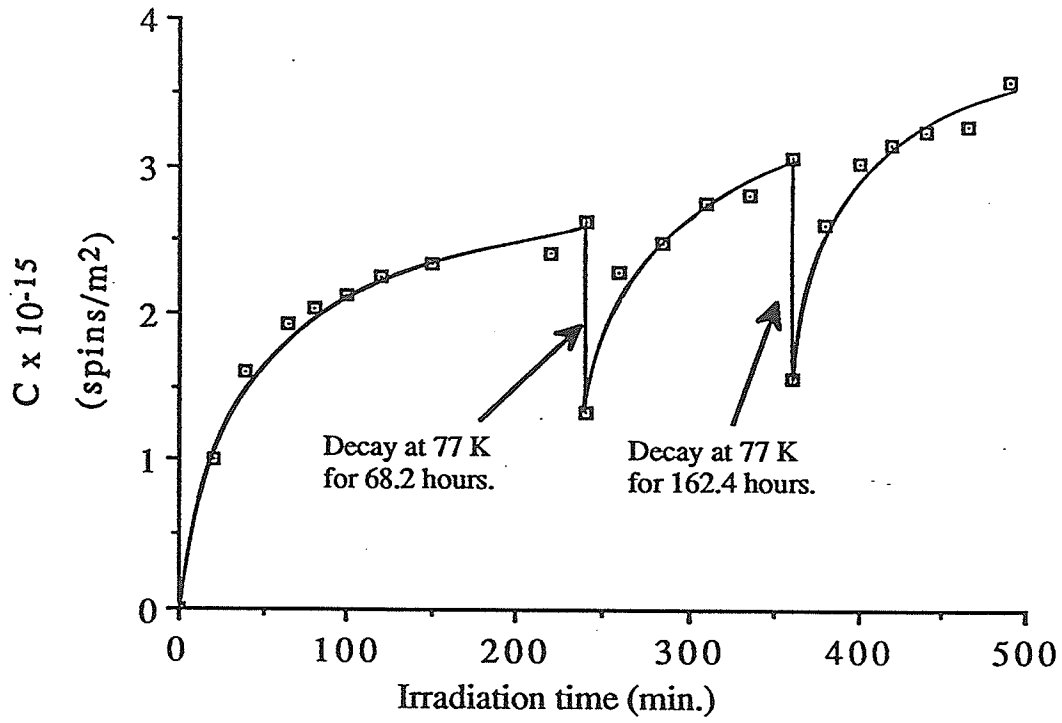

Figure 3-6: Build-up of methyl radicals at 77 K on PVGM4 containing 2.01 monolayers (2.38×10^{-3}mmole/mg) azomethane.

It was observed too that methyl radicals are generated much faster and in larger quantity on a PVG surface with low surface coverage of azomethane (about 0·1 monolayer) than on a surface containing about 2 monolayers of azomethane. This is illustrated in Figure 3-7. This behaviour may be attributed to the possibility of the radicals decaying by recombination at a much slower rate during irradiation on the low-coverage surface than on the high-coverage surface. The results of the decay kinetics presented later in section 3.3.1 have actually shown this to be the case. The observed gradual increase in the percentage of azomethane molecules that decomposed during irradiation with decrease in surface coverage probably also contributed to the higher rate of formation of the radicals on the surface loaded with 0·1 monolayer azomethane than on the surface containing 2 monolayers azomethane.

3.2.2 Build-up of ethyl radicals

It was observed that ethyl radicals were slightly more difficult to produce by UV irradiation of azoethane adsorbed on PVG surface; relatively small signals of the radicals could only be observed by ESR even after several hours of photolysis. This is illustrated in the curves for the build-up of ethyl radicals at 77 K on two PVG samples, PVGE and PVGE2, shown in Figures 3-8 and 3-9. PVGE and PVGE2 were loaded with 1·54 monolayers and 2·01 monolayers azoethane, respectively, prior to photolysis to generate ethyl radicals. It has been demonstrated[72] that the quantum yield for the photolysis of gaseous azomethane is independent of pressure and remains

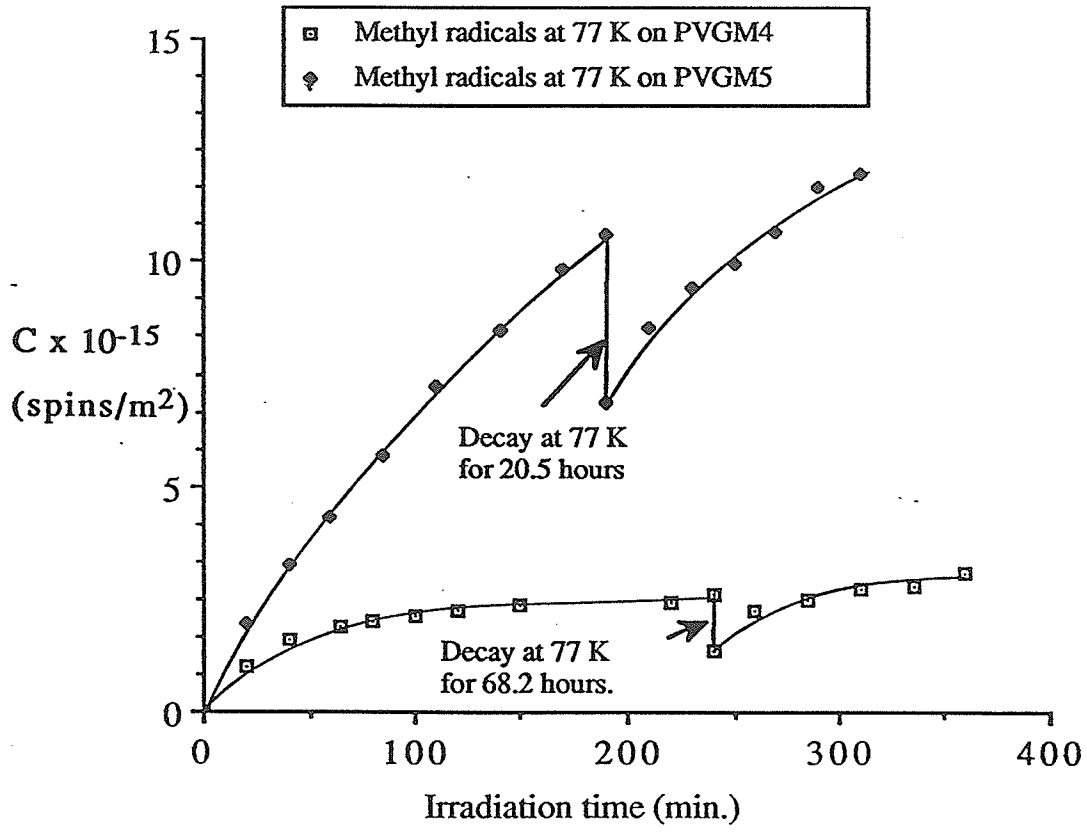

Figure 3-7: Build-up of methyl radicals at 77 K on PVGM4 and PVGM5 containing 2.01 and 0.104 monolayers azomethane, respectively.

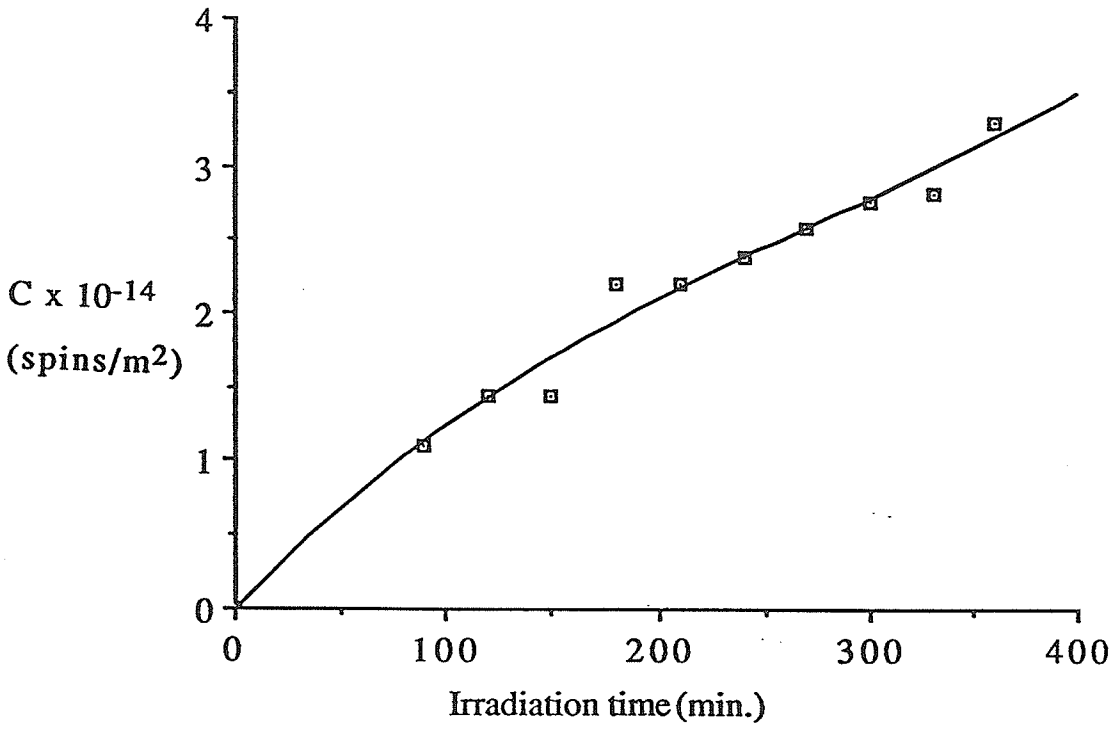

Figure 3-8: Build-up of ethyl radicals at 77 K on PVGE loaded with 1.54 monolayers (1.31×10^{-3} mmole/mg) azoethane.

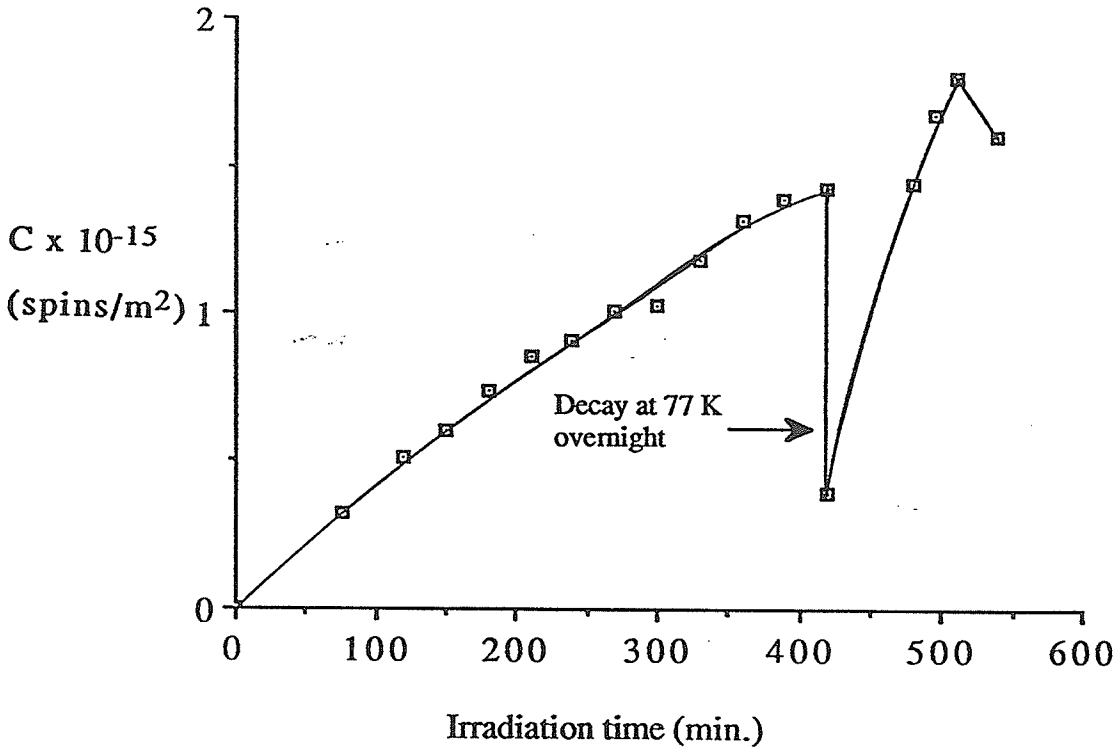

Figure 3-9: Build-up of ethyl radicals at 77 K on PVGE2 loaded with 2.01 monolayers (1.71×10^{-3} mmole/mg) azoethane.

approximately unity up to a pressure of 630 torr at 3660 Å; it has, however, been observed in this laboratory[73] that methyl radicals could only be produced on the surface of porous Vycor glass at 77 K when the full UV spectrum of the Hg lamp rather than light of $\lambda >$ 3600 Å was used to photolyse azomethane adsorbed on the glass. In contrast to the result obtained for the photolysis of azomethane, it has been shown[74] that the quantum yield at 3660 Å for the photodecomposition of azoethane is unity at low pressure but decreases with increase in pressure of the azoethane molecules. This implies that an excited azoethane molecule is probably present as an intermediate during the photolysis and that, in the gas phase, this photo-excited state can be pressure-quenched. This in accordance with the results obtained by Kozak and Gesser[75] in the photolysis of triethylamine which showed that the rates of formation of products, with the exception of hydrogen and ethylene, increased with decrease in pressure of reactant under constant irradiation intensity indicating that the products, except hydrogen, were formed by dissociation of an excited triethylamine molecule which was said to be capable of being pressure-quenched. Analogous results had earlier been obtained by Gesser et. al.[76] for the photolysis of trimethylamine. In this work, the azoethane molecules are adsorbed on to the surface of PVG samples corresponding to a condition of high pressure. Thus, in this study, the PVG surface is capable of quenching the excited state and the quantum yield for the production of ethyl radicals by the photodecomposition of azoethane adsorbed on PVG is therefore expected to be far less than unity. Hence, the reason for the slightly greater difficulty in generating ethyl radicals than

methyl radicals can be attributed to a much lower quantum yield for the photodecomposition of azoethane than the value for the photodecomposition of azomethane. However, Figure 3-9 shows further that ethyl radicals were formed much faster and in larger quantity when they were left to decay overnight at 77 K after previous 7 hours (420 minutes) irradiation. This may be due to the possible addition reaction of the ethyl radicals with azoethane molecules during the decay at 77 K to form tetraethylhydrazine (Equation 3-1) so that during subsequent re-irradiation, ethyl radicals are probably formed from tetraethylhydrazine molecules rather than from azoethane molecules.

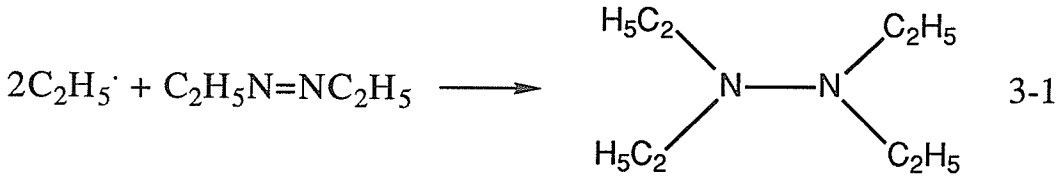

3-1

Furthermore, it is also clear from Figures 3-8 and 3-9 that the build-up curves obtained for ethyl radicals at 77 K are similar to the results obtained for methyl radicals in that they do not show any plateau. The percentage of azoethane molecules that decomposed during the 5-7 hours irradiation to produce ethyl radicals was estimated to be 0·00648 to 0·0279% (Appendix II). The non-approach to plateau may therefore be attributed to the same reason given earlier in section 3.2.1 for the case of methyl radicals. The much lower percentage decomposition estimated for azoethane molecules also confirms further that the quantum yield for the photodecomposition of azoethane is much lower than that for the photodecomposition of azomethane thereby making it slightly more

difficult to produce ethyl radicals from azoethane than methyl radicals from azomethane.

3.3 Results and Discussion of the decay kinetics

3.3.1 Methyl radicals decay kinetics

(a) Results

Figure 3-10 shows a typical curve for the decay of methyl radicals at -164°C after a previous decay first at -196°C and subsequently at -183°C while Figure 3-8 presents a plot of the decay of the radicals at the three temperatures employed in this study. Figure 3-11 shows that the decay of methyl radicals is a cascade type as previously shown[2,3] indicating the presence of a continuum of trapping potentials on the surface. However, as will be shown later, only one trapping site on the surface is postulated in this work for relatively short time decay. The existence of multiple sites on the surface is only possible when the decay is carried out for a period of time long enough for the concentrations of the radicals to reach a constant value.

The simple first and second order plots of the decay data shown in Figures 3-12 and 3-13 respectively indicate that the decay is not a simple first or second order reaction. However, all the kinetics data were found to give the best fit to the revised second order kinetics equation derived by Dole[77,78] for the decay of free radicals in polymers. The simple second order equation,

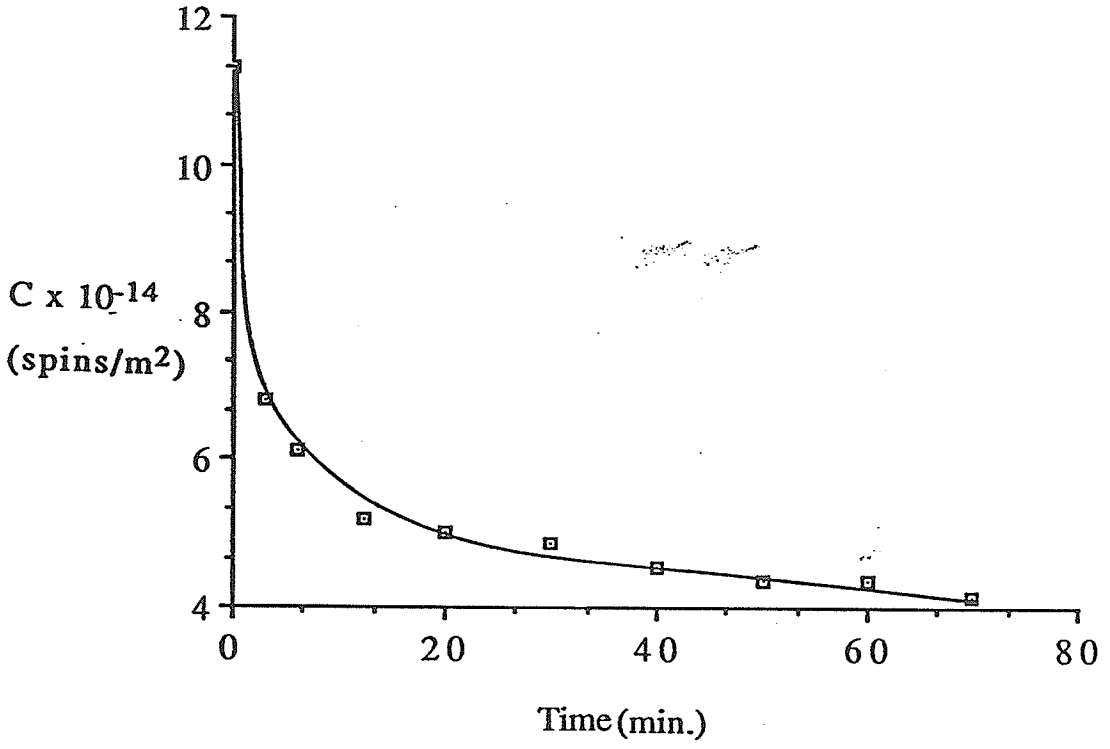

Figure 3-10: Decay of methyl radicals at -164°C (109 K) on PVGM1 loaded with 1.00 monolayer (1.19×10^{-3} mmole/mg) azomethane.

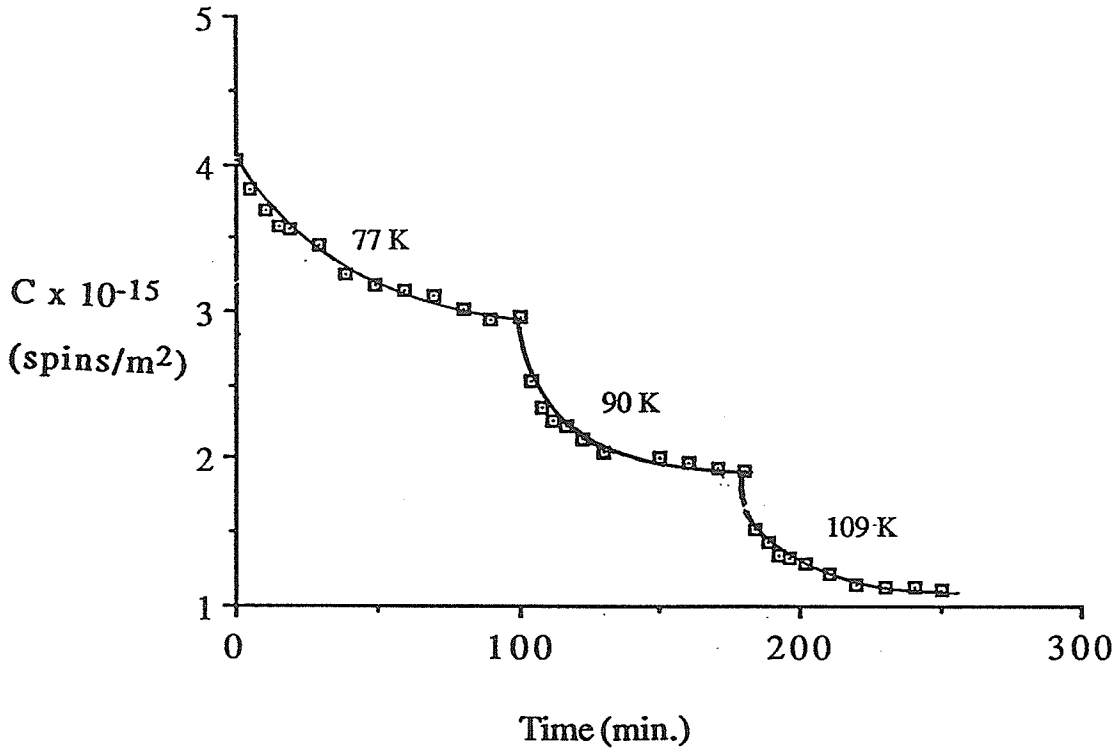

Figure 3-11: Decay of methyl radicals on PVGM3 loaded with 3.19 monolayers (3.80 x 10^{-3} mmole/mg) azomethane at various temperatures.

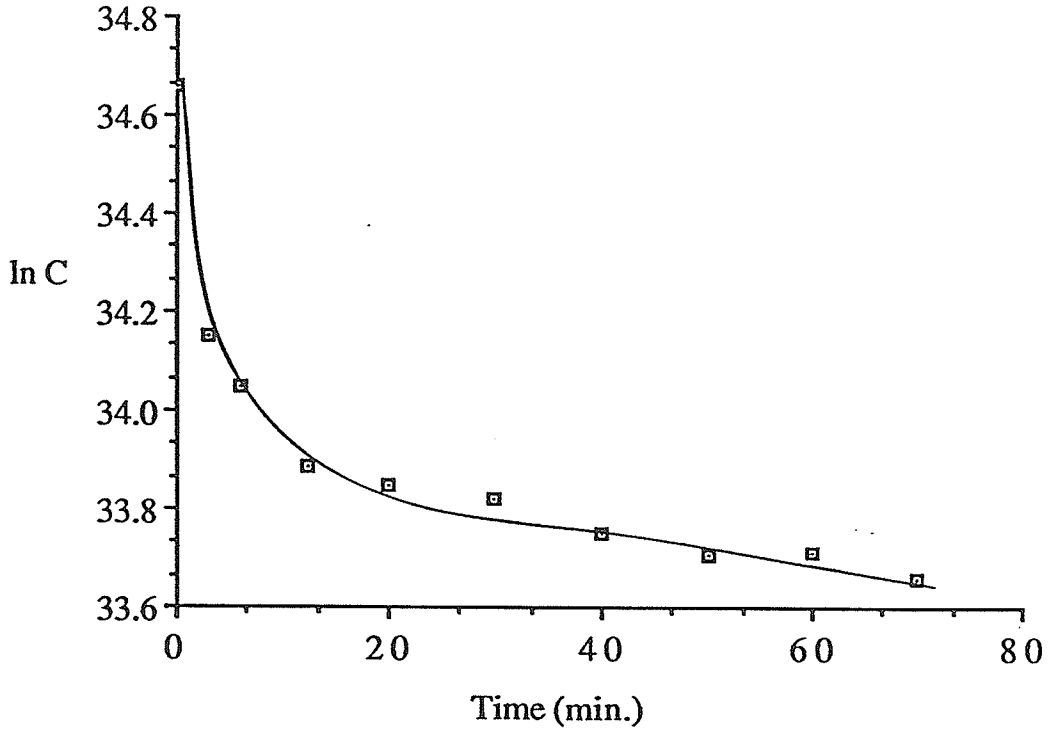

Figure 3-12: First order plot for the decay of methyl radicals on PVGM1 loaded with 1.00 monolayer (1.19 $x10^{-3}$ mmole/mg) azomethane at -164°C (109 K).

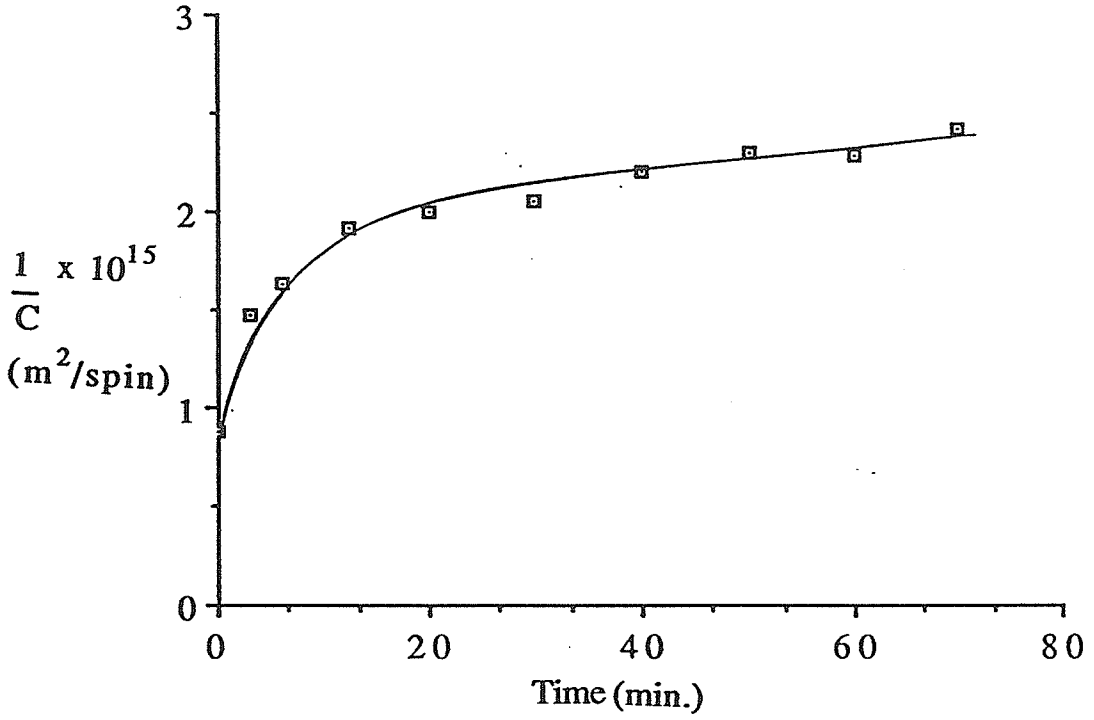

Figure 3-13: Second order plot for the decay of methyl radicals on PVGM1 loaded with 1.00 monolayer (1.19 x 10^{-3} mmole/mg) azomethane at -164°C (109 K).

$$\frac{1}{C} - \frac{1}{C_0} = k_2 t \qquad 3\text{-}2$$

can be re-written in the form

$$\frac{C_0 - C}{CC_0} = k_2 t \qquad 3\text{-}3$$

so that

$$\frac{CC_0}{C_0 - C} = \frac{1}{k_2 t} \qquad 3\text{-}4$$

or

$$\frac{t}{C_0 - C} = \frac{1}{CC_0 k_2} \qquad 3\text{-}5$$

From Equation 3-2, C is simply given by

$$C = \frac{C_0}{C_0 k_2 t + 1} \qquad 3\text{-}6$$

Substitution of Equation 3-6 for C in the right-hand side of Equation 3-5 then simply gives the revised Dole's second order kinetics equation given by

$$\frac{t}{C_0 - C} = \frac{t}{C_0} + \frac{1}{C_0^2 k_2} \qquad 3\text{-}7$$

where C_0 and C are the concentration of the reacting species at zero time and time t, respectively and k_2 is the second order rate constant. Dole[77,78] then assumed that a fraction of the radicals were recombined by second order mechanism according to Equation 3-2 while the remaining radicals were completely unreactive. Hence, if

the concentration of the unreactive free radicals is A, then the concentration of the reacting radicals is (C_0-A) at zero time and (C-A) at time t. Putting these values into Equation 3-2 gives

$$\frac{1}{C-A} - \frac{1}{C_0-A} = k_2 t \qquad 3\text{-}8$$

so that

$$\frac{C_0-A-C+A}{(C-A)(C_0-A)} = \frac{C_0-C}{(C-A)(C_0-A)} = k_2 t \qquad 3\text{-}9$$

or

$$\frac{t}{C_0-C} = \frac{1}{(C-A)(C_0-A)k_2} \qquad 3\text{-}10$$

Replacing 1/(C-A) by its value given in equation 3-8 simply gives

$$\frac{t}{C_0-C} = \frac{t}{C_0-A} + \frac{1}{(C_0-A)^2 k_2} \qquad 3\text{-}11$$

Hence, A can be calculated from the slope of the plots of $t/C_0 - C$ versus t if C_0 is known, and k_2 can be determined from the intercept. The Dole plots for the decay of methyl radicals on three PVG samples at the three temperatures employed in this study are shown in Figures 3-14 to 3-16. The Arrhenius plots for the data in Figures 3-14 to 3-16 are shown in Figures 3-17 to 3-19, respectively. Activation energies, E_a, for the decay of the radicals are obtained from least squares analysis of the Arrhenius plots. The values of E_a, k_2, (C_0-A), A, and (C_0-A)/A at different temperatures for the PVG samples loaded with different amounts of azomethane prior to irradiation are presented in Tables 3-1 to 3-3. All the PVG samples,

Table 3-1: Dole plot and non-linear least squares fit* data for the decay of methyl radicals on PVGM1 loaded with 1·00 monolayer ($1{\cdot}19 \times 10^{-3}$ mmole/mg) azomethane

Expt. No.	Temp. (K)	$(C_0\text{-}A)$ $\times 10^{-15}$ (spins/ m^2)	A $\times 10^{-15}$ (spins/ m^2)	$(C_0\text{-}A)/A$	k_2 $\times 10^{17}$ (m^2 $spin^{-1}$ min^{-1})	E_a (kJ mol^{-1}) (Fig. 3-17)	
						Calculated	Least squares value
1	77	0.808 ± 0.057 (0.825 ± 0.077)	2.02 ± 0.06 (1.99 ± 0.09)	0.400 ± 0.040 (0.415 ± 0.057)	2.82 ± 0.67 (2.44 ± 0.85)	1.26 (1.67)	6.19 ± 2.84 (7.32 ± 3.26)
2	90	1.31 ± 0.03 (1.30 ± 0.03)	0.910 ± 0.029 (0.901 ± 0.032)	1.44 ± 0.08 (1.44 ± 0.08)	3.75 ± 0.37 (3.56 ± 0.37)		
3	109	0.732 ± 0.009 (0.708 ± 0.020)	0.398 ± 0.009 (0.420 ± 0.097)	1.84 ± 0.06 (1.69 ± 0.44)	49.0 ± 10.2 (71.1 ± 8.2)	11.0 (12.8)	

*The values written in parentheses are the values obtained from non-linear least squares analysis.

Table 3-2: Dole plot and non-linear least squares fit* data for the decay of methyl radicals on PVGM2 loaded with 2·06 monolayers ($2{\cdot}45 \times 10^{-3}$ mmole/mg) azomethane

Expt. No.	Temp. (K)	$(C_0\text{-}A)$ x 10^{-15} (spins/m^2)	A x 10^{-15} (spins/m^2)	$(C_0\text{-}A)/A$	k_2** x 10^{17} (m^2 $spin^{-1}$ min^{-1})	E_a (kJ mol^{-1}) (Fig. 3-18)	
						Calculated	Least squares value
9, 11 & 13	77	-	-	-	1.82 ±0.38	3.61	3.23 ± 0.19
4	90	1.48 ± 0.08 (1.52 ± 0.10)	3.38 ± 0.08 (3.30 ± 0.11)	0.438 ± 0.034 (0.461 ± 0.046)	4.11 ± 0.95 (3.26 ± 0.92)		
5	109	1.76 ± 0.04 (1.67 ± 0.09)	1.92 ± 0.04 (1.96 ± 0.07)	0.917 ± 0.040 (0.852 ± 0.076)	8.07 ± 1.43 (9.09 ± 2.02)	2.90 (4.39)	

*The values written in parentheses are the values obtained from non-linear least squares analysis.

**The value of k_2 at 77 K given in this table is average of the values obtained for experiments 9, 11 and 13 presented later in Table 3-6.

Table 3-3: Dole plot and non-linear least squares fit* data for the decay of methyl radicals on PVGM3 loaded with 3·19 monolayers ($3{\cdot}80 \times 10^{-3}$ mmole/mg) azomethane

Expt. No.	Temp. (K)	$(C_0\text{-}A)$ $\times 10^{-15}$ (spins/ m^2)	A $\times 10^{-15}$ (spins/ m^2)	$(C_0\text{-}A)/A$	k_2 $\times 10^{17}$ (m^2 $spin^{-1}$ min^{-1})	E_a (kJ mol^{-1}) (Fig. 3-19)	
						Calculated	Least squares value
6	77	1.43 ± 0.05 (1.47 ± 0.06)	2.59 ± 0.05 (2.53 ± 0.07)	0.552 ± 0.030 (0.581 ± 0.040)	1.97 ± 0.27 (1.64 ± 0.29)	7.99 (9.12)	4.56 ± 1.91 (5.23 ± 2.13)
7	90	1.14 ± 0.01 (1.11 ± 0.02)	1.83 ± 0.01 (1.85 ± 0.02)	0.623 ± 0.009 (0.600 ± 0.017)	12.0 ± 1.2 (12.9 ± 1.1)		
8	109	0.891 ± 0.015 (0.855 ± 0.034)	1.03 ± 0.02 (1.05 ± 0.02)	0.865 ± 0.031 (0.814 ± 0.048)	16.1 ± 2.1 (18.5 ± 2.7)	1.26 (1.55)	

*The values written in parentheses are the values obtained from non-linear least squares analysis.

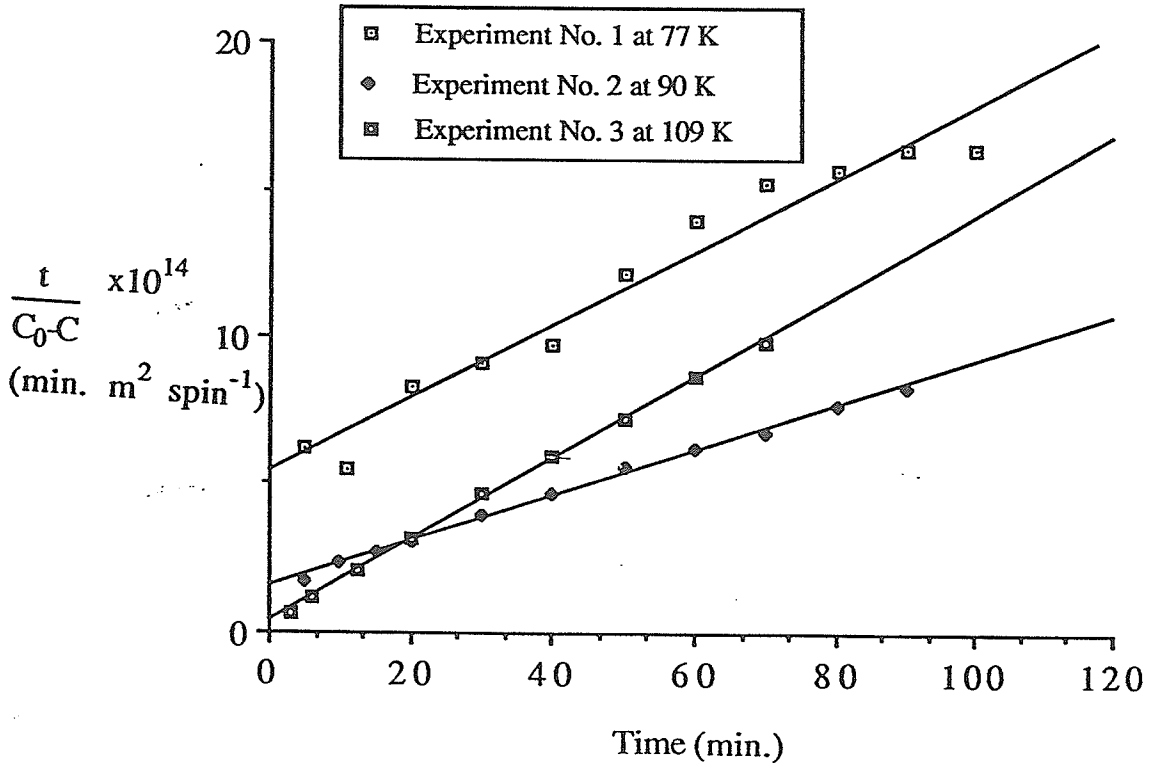

Figure 3-14: Second order Dole plots for the decay of methyl radicals on PVGM1 loaded with 1.00 monolayers (1.19×10^{-3} mmole/mg) azomethane at different temperatures.

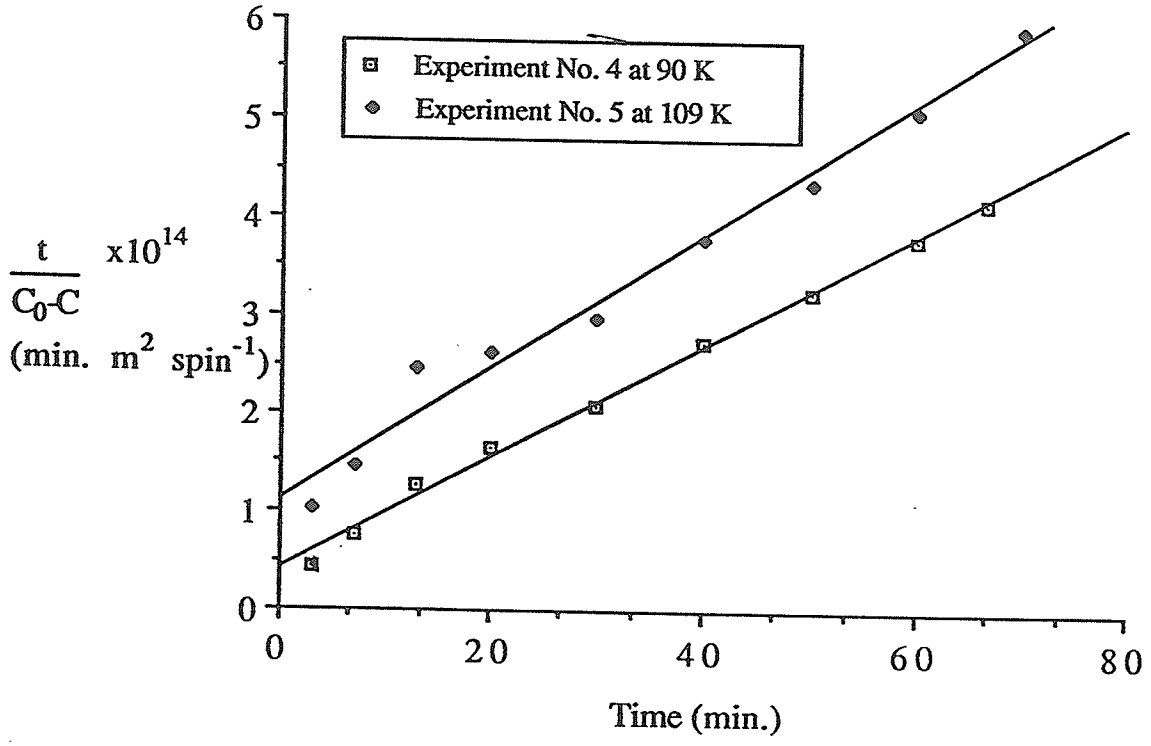

Figure 3-15: Second order Dole plots for the decay of methyl radicals on PVGM2 loaded with 2.06 monolayers (2.45×10^{-3} mmole/mg) azomethane at different temperatures.

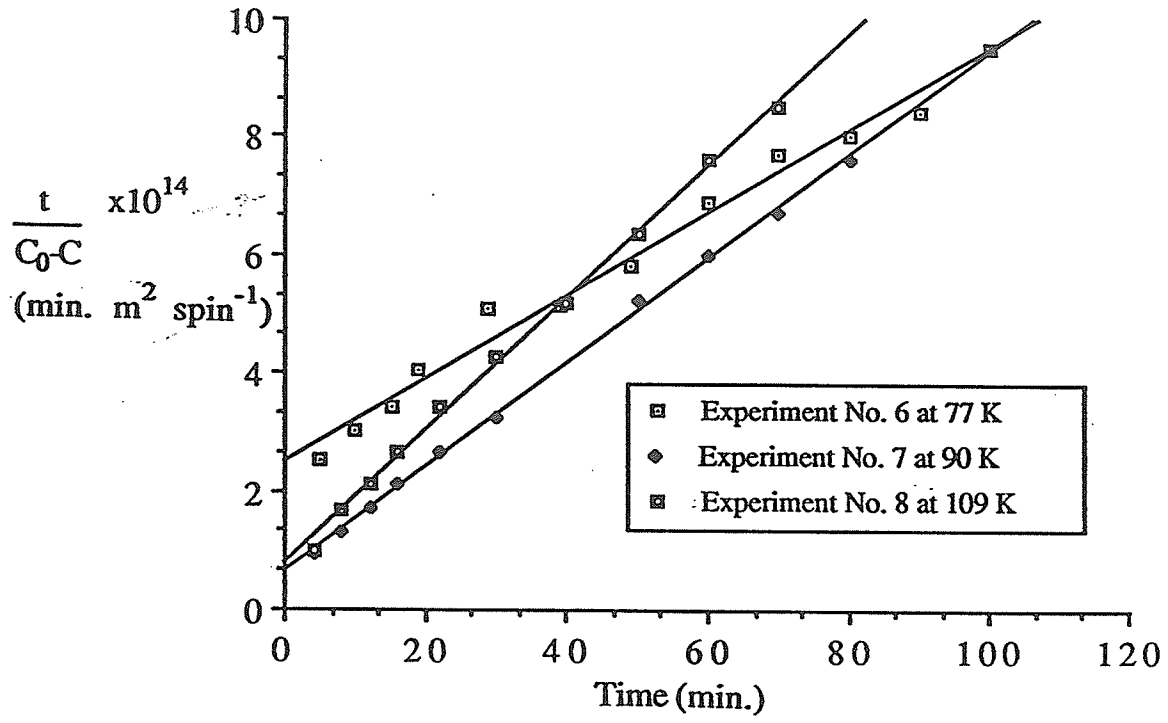

Figure 3-16: Second order Dole plots for the decay of methyl radicals on PVGM3 loaded with 3.19 monolayers (3.80 x 10^{-3} mmole/mg) azomethane at different temperatures.

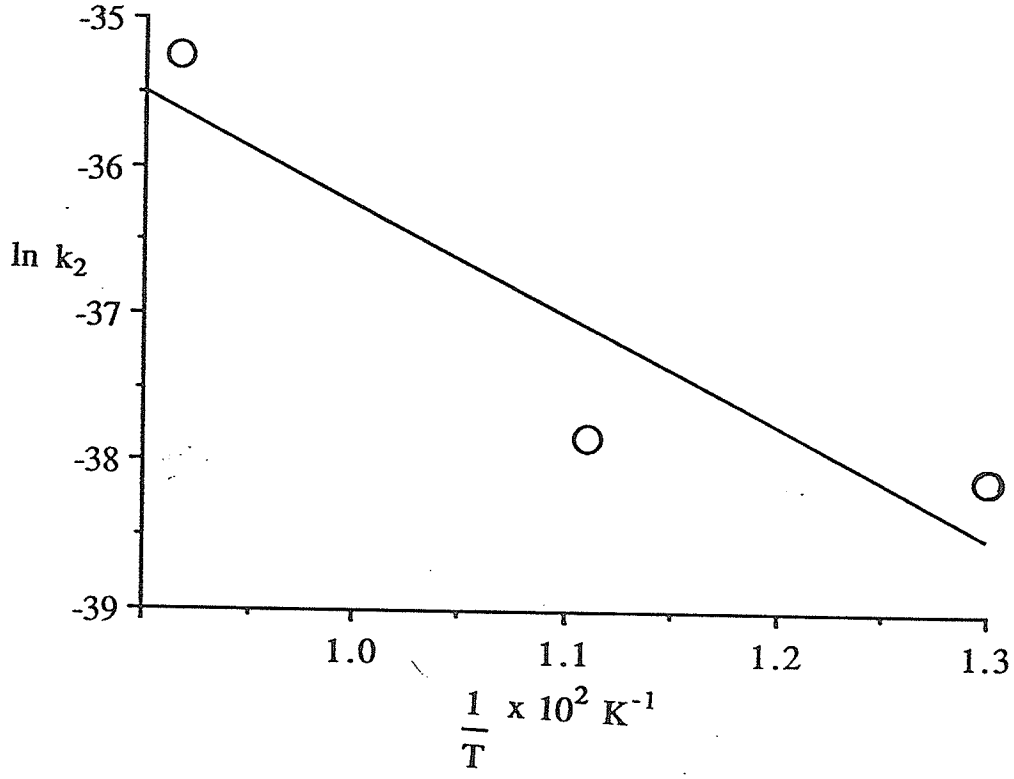

Fig. 3-17: Arrhenius plot for the decay of methyl radicals on PVGM1 loaded with 1.00 monolayer (1.19 x 10^{-3} mmole/mg) azomethane.

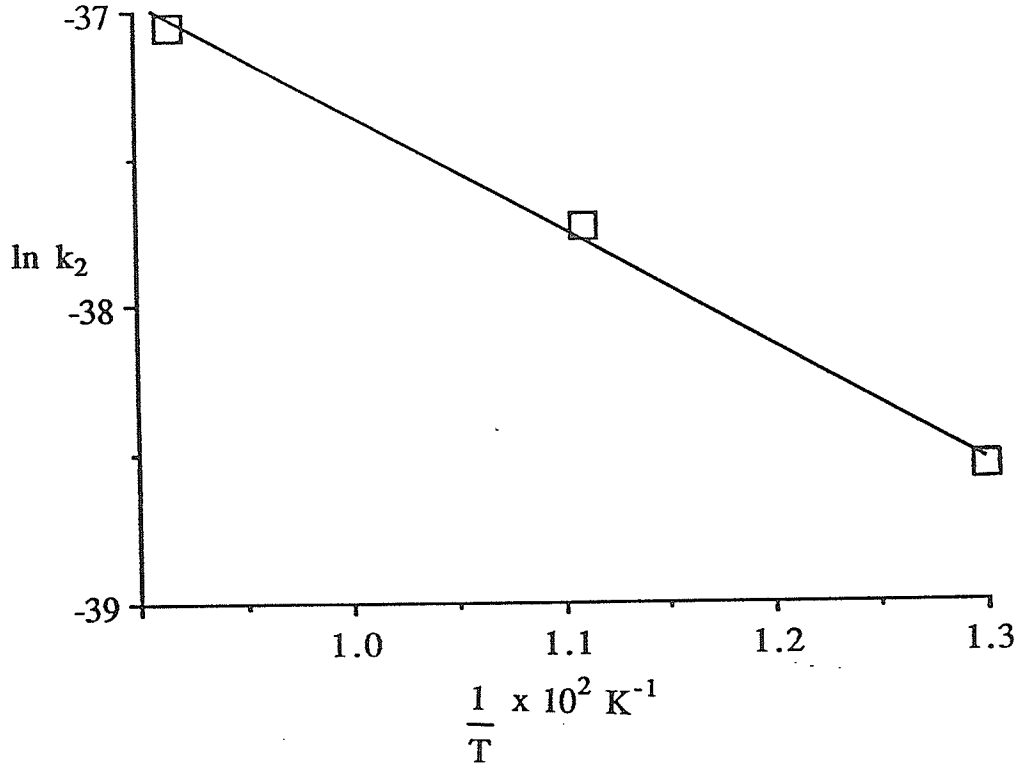

Figure 3-18: Arrhenius plot for the decay of methyl radicals on PVGM2 loaded with 2.06 monolayers (2.45 x 10^{-3} mmole/mg) azomethane. (Note that the value of k_2 at 77 K used for the plot is the average of the values obtained for experiments 9, 11 and 13 given in Table 3-6).

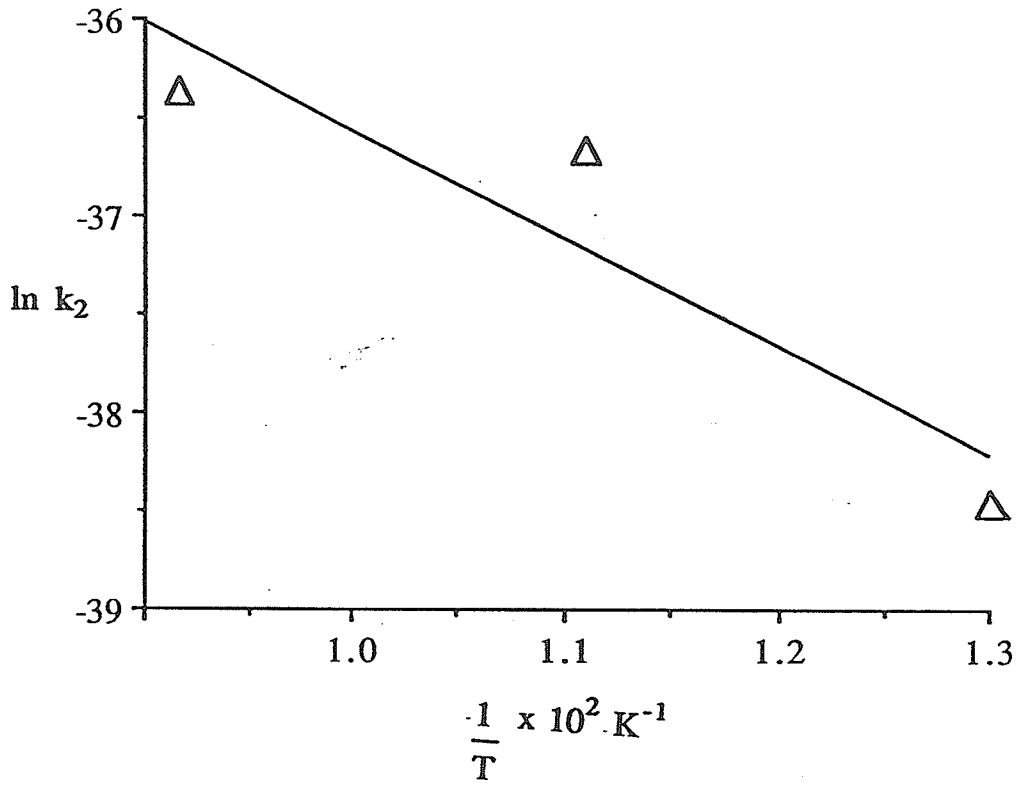

Figure 3-19: Arrhenius plot for the decay of methyl radicals on PVGM3 loaded with 3.19 monolayers (3.80×10^{-3} mmole/mg) azomethane.

labelled PVGM1, PVGM2 and PVGM3 were all pretreated at 750°C followed by thermoleaching in 100-200 torr O_2 at 500°C and subsequent evacuation at 500°C prior to loading with 1·00, 2·06 and 3·19 monolayers of azomethane, respectively.

It should be noted that equation 3-11 can be rearranged to give the following expression for C;

$$C = A + \frac{(C_0-A)}{1 + (C_0-A)k_2t} \qquad 3\text{-}12$$

Hence, non-linear least squares analysis of the decay data presented in Tables AI-1 to AI-3 was done using equation 3-12 and values of (C_0-A), A and k_2 were obtained accordingly. The values of E_a, k_2, (C_0-A), A and $(C_0-A)/A$ obtained from the non-linear least squares fits are written in parentheses in Tables 3-1 to 3-3. Typical decay curves obtained from non-linear least squares analysis along with experimental points are shown in Figures 3-20 to 3-22. Tables 3-1 to 3-3 clearly show a close agreement between the Dole plot data and non-linear least squares fit data. The non-linear least squares curves for the decay of the radicals are also found to agree well with experimental points as illustrated in Figures 3-20 to 3-22.

The typical decay curves shown in Figures 3-10 and 3-23 for experiment numbers 3 and 8, respectively, show that the signal of the methyl radicals does not disappear completely in each case, but rather decays to some specific "steady state" value. This value actually represents A, the concentration of the unreactive methyl radicals; the steady state does not imply the existence of a

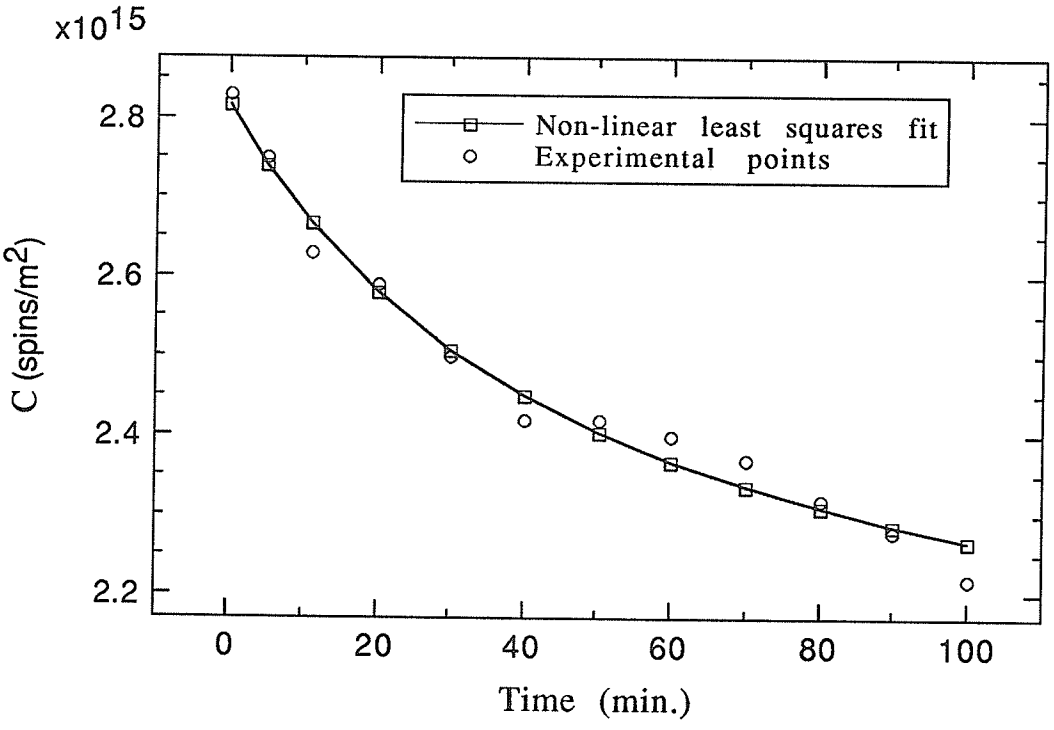

Figure 3-20: Non-linear least squares fit for the Decay of methyl radicals at 77K on PVGM1 containing 1.00 monolayer (1.19×10^{-3} mmole/mg) azomethane.

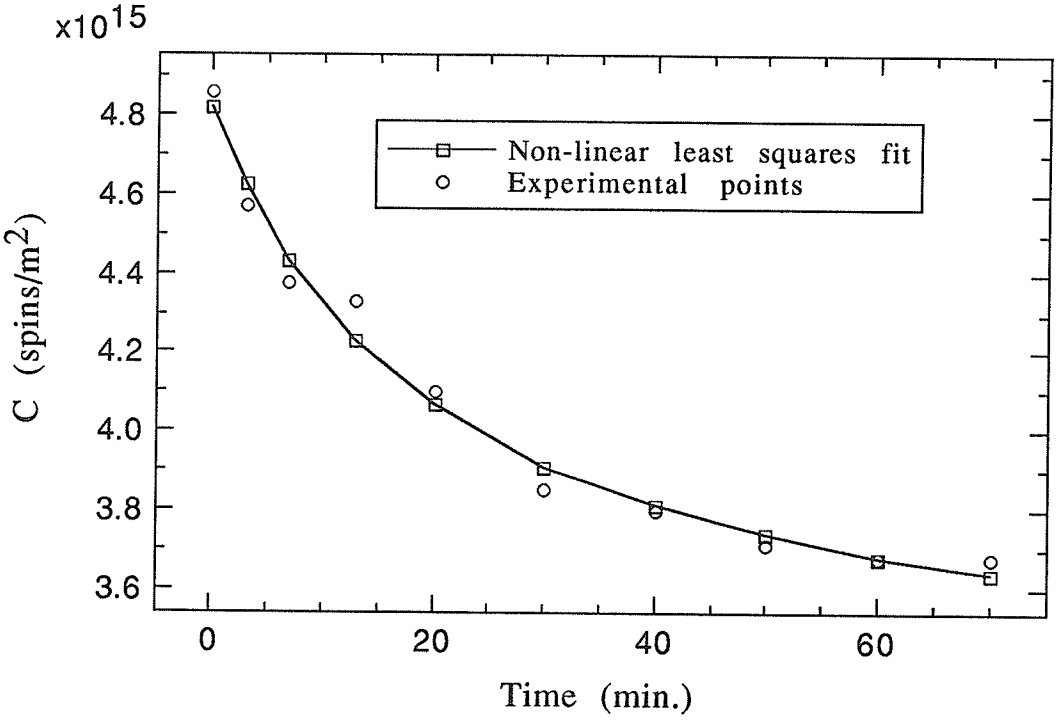

Figure 3-21: Non-linear least squares fit for the decay of methyl radicals at 90 K on PVGM2 containing 2.06 monolayer (2.45 x 10^{-3} mmole/mg) azomethane.

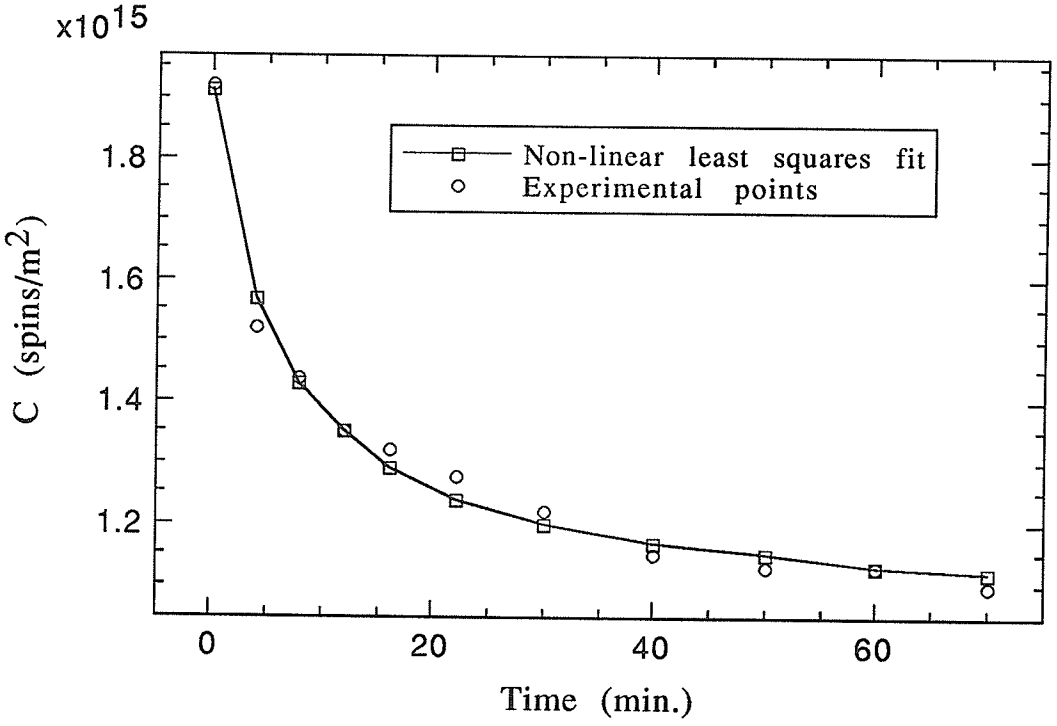

Figure 3-22: Non-linear least squares fit for the decay of methyl radicals at 109 K on PVGM3 containing 3.19 monolayers (3.80×10^{-3} mmole/mg) azomethane.

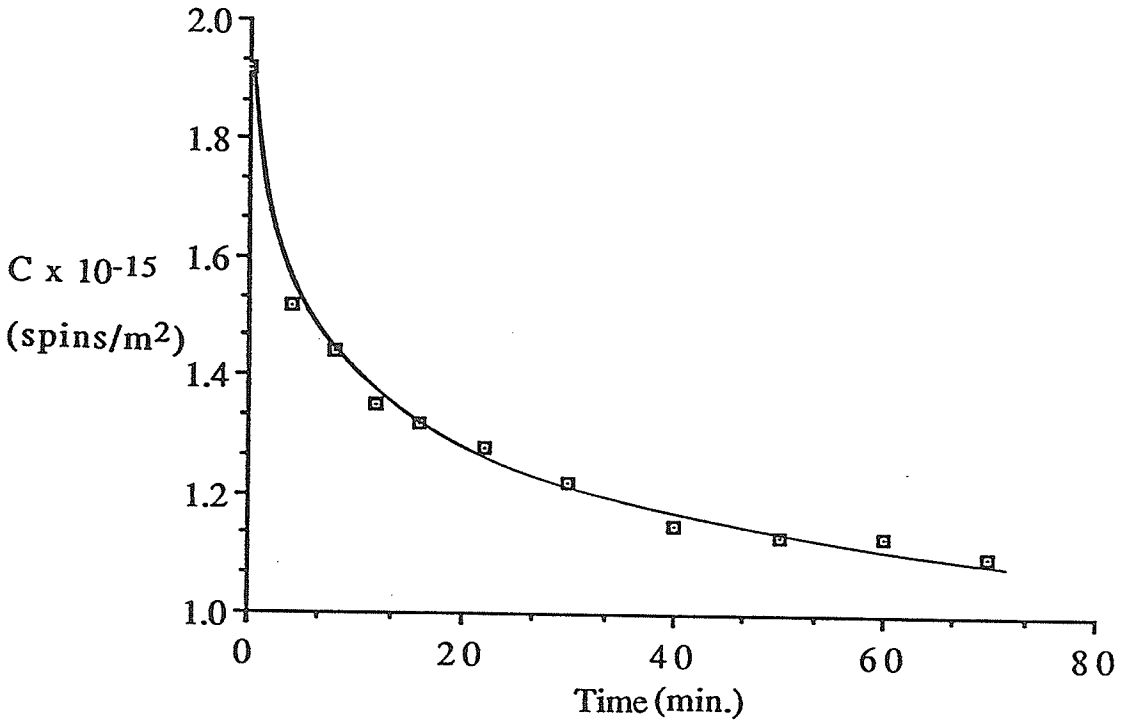

Figure 3-23: Experimental curve for the decay of methyl radicals at -164°C (109 K) on PVGM3 loaded with 3.19 monolayers (3.80 x 10^{-3} mmole/mg) azomethane.

simultaneous radical decay and production. Hence, A can actually be measured directly from the decay curve if the decay study is carried out for a relatively long period of time thereby making it possible to apply Equation 3-8 to the kinetics data in addition to Equation 3-11. When the values of A measured from the decay curves 3-10 and 3-23 are substituted into Equation 3-8, straight line graphs are obtained on plotting 1/(C-A) against t as shown in Figures 3-24 and 3-25, respectively. Values of k_2, (C_0-A), A and $(C_0-A)/A$ obtained from Figures 3-24 and 3-25 together with the corresponding values obtained from the Dole plots of $t/(C_0-C)$ against t in accordance with Equation 3-11 are presented in Table 3-4.

It is clearly observed from Tables 3-1 to 3-3 and from Table 3-7 presented later that A decreases gradually with increase in temperature. This temperature dependence of A can be related to the decreased adsorption of unreactive methyl radicals A at higher temperatures as previously observed for hydrogen atoms.[71] Figure 3-26 shows the plots of ln $(C_0-A)/A$ against 1/T for the data in Tables 3-1, 3-3 and 3-7 from which the heats of adsorption presented in Table 3-5 as ΔH_A, were determined. The fact that these plots do not show any curvature indicates that there is only one trapping site on the surface rather than a continuum of trapping potentials. ΔH_A for the data in Table 3-2 was calculated to be -3.17 kJ mol^{-1}.

The decay of methyl radicals on PVG samples was also found not to follow a modified first order plot of ln (C-A) against time as

Table 3-4: Rate constants and concentration values obtained from both modified second order and Dole plots for the decay of methyl radicals on PVGM1 and PVGM3 at -164°C (109K)

	PVGM1 containing 1·00 monolayer ($1·19 \times 10^{-3}$ mmole/mg) azomethane		PVGM3 containing 3·19 monolayers ($3·80 \times 10^{-3}$ mmole/mg) azomethane	
	Modified 2nd order plot (Fig. 3-24) value	Dole plot (Eqn. 3-11) value	Modified 2nd order plot (Fig. 3-25) value	Dole plot (Eqn. 3-11) value
$k_2 \times 10^{16}$ (m^2 $spin^{-1}$ min^{-1})	5·55	4·90	2·16	1·61
$(C_0\text{-}A) \times 10^{-14}$ ($spins/m^2$)	5·12	7·32	6·98	8·91
$A \times 10^{-14}$ ($spins/m^2$)	4·20	3·98	11·2	10·3
$(C_0\text{-}A)/A$	1·22	1·84	0·623	0·865

Table 3-5: Decay and adsorption energies for adsorbed methyl radicals on PVG samples

PVG sample	Surface coverage (monolayer)	Decay Activation energy, E_a (kJ mol^{-1})	Adsorption energy, $-\Delta H_A$ (kJ mol^{-1})	k_2 at 77 K (m^2 $spins^{-1}$ min^{-1})
PVGM5d & $PVGM5d_2$	0.103	7.31	4.78	1.40×10^{-18}
PVGM1	1.00	6.19	3.31	2.82×10^{-17}
PVGM2	2.06	3.23	3.17	1.82×10^{-17}
PVGM3	3.19	4.56	0.976	1.97×10^{-17}

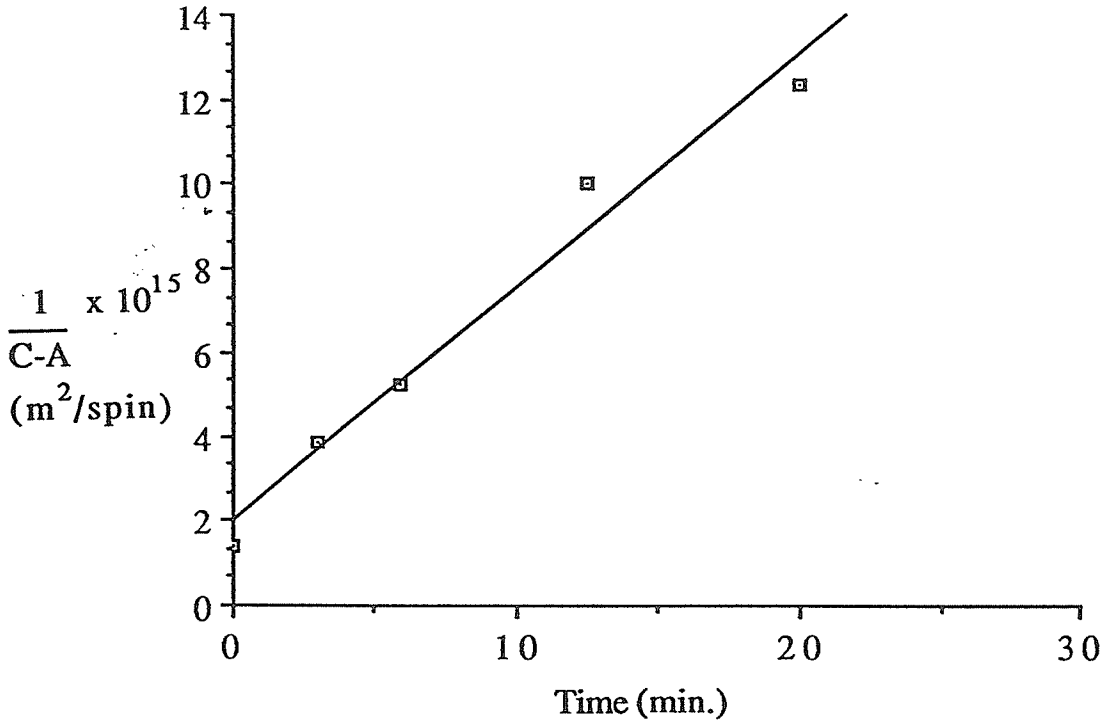

Figure 3-24: Modified second order plot for the decay of methyl radicals at -164°C (109 K) on PVGM1 loaded with 1.00 monolayer (1.19×10^{-3} mmole/mg) azomethane.

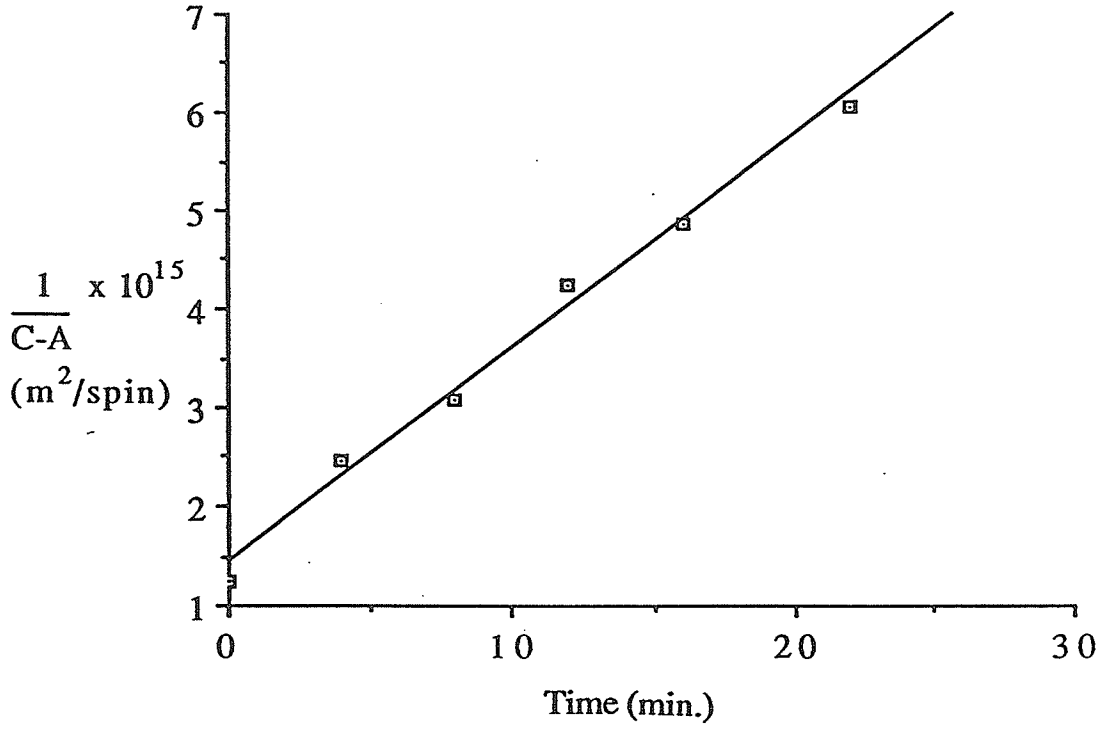

Figure 3-25: Modified second order plot for the decay of methyl radicals at -164°C (109 K) on PVGM3 loaded with 3.19 monolayers (3.80×10^{-3} mmole/mg) azomethane.

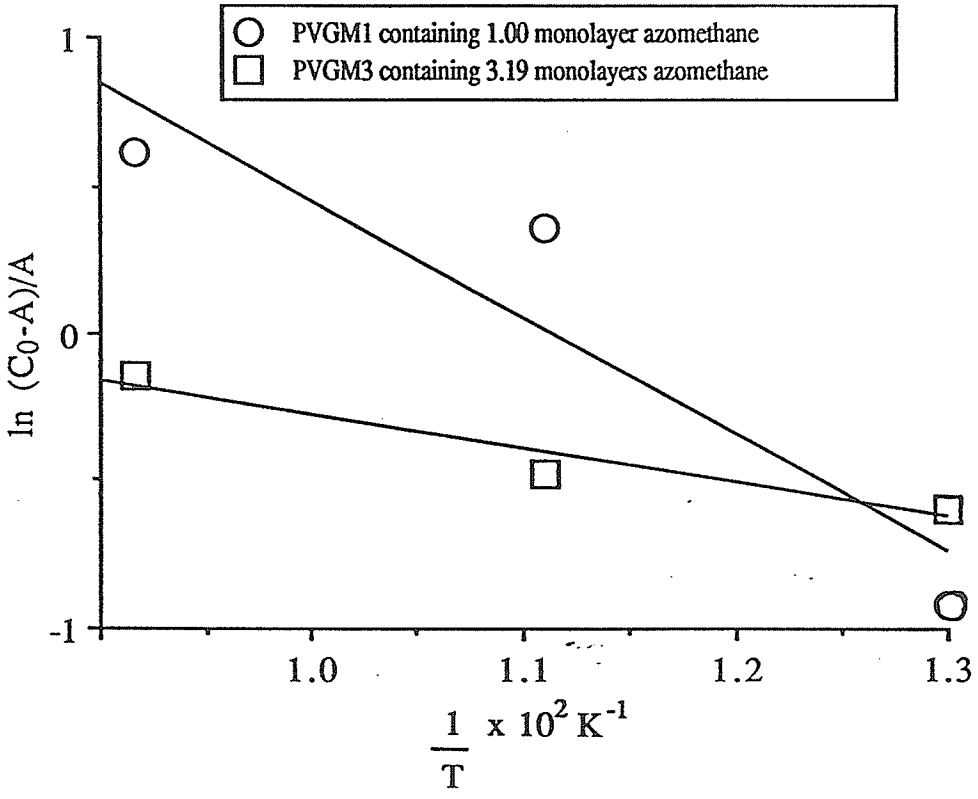

Figure 3-26: Plots of ln $(C_0-A)/A$ against 1/T for adsorbed methyl radicals on PVG samples containing different amounts of azomethane.

shown in Figures 3-27 and 3-28 for experiment numbers 3 and 8, respectively.

(b) Long time decay kinetics results

None of the decay studies of methyl radicals, the results of which are presented in Tables 3-1 to 3-3 as well as 3-14 to 3-16 for experiments 1 to 8 , was done for longer than 100 minutes. In order to study the effect of time of decay on the decay kinetics of the radicals, decay experiments were also performed for much longer periods of time. Furthermore, Waite[79] has derived the following equation for a second-order diffusion-controlled reaction

$$\frac{1}{C} = 4\pi rD\left[1 + \frac{2r}{(\pi Dt)^{1/2}}\right]t + \frac{1}{C_0} \qquad 3\text{-}13$$

where D is the sum of diffusion coefficients of the individual reacting species, C is the concentration at time t and r is the free-radical separation distance within which they react and outside of which the potential of an unreacted radical is independent of the position (Smoluchowski boundary condition). In other words, r is the radius of the reaction cage. At long times, equation 3-13 becomes

$$\frac{1}{C} = 4\pi rDt + \frac{1}{C_0} \qquad 3\text{-}14$$

and the second-order rate constant becomes the familiar steady state Smoluchowski expression, $4\pi rD$.[80] Equation 3-14 therefore predicts a slope of -1 when ln C is plotted against ln t. Hence, the decay studies

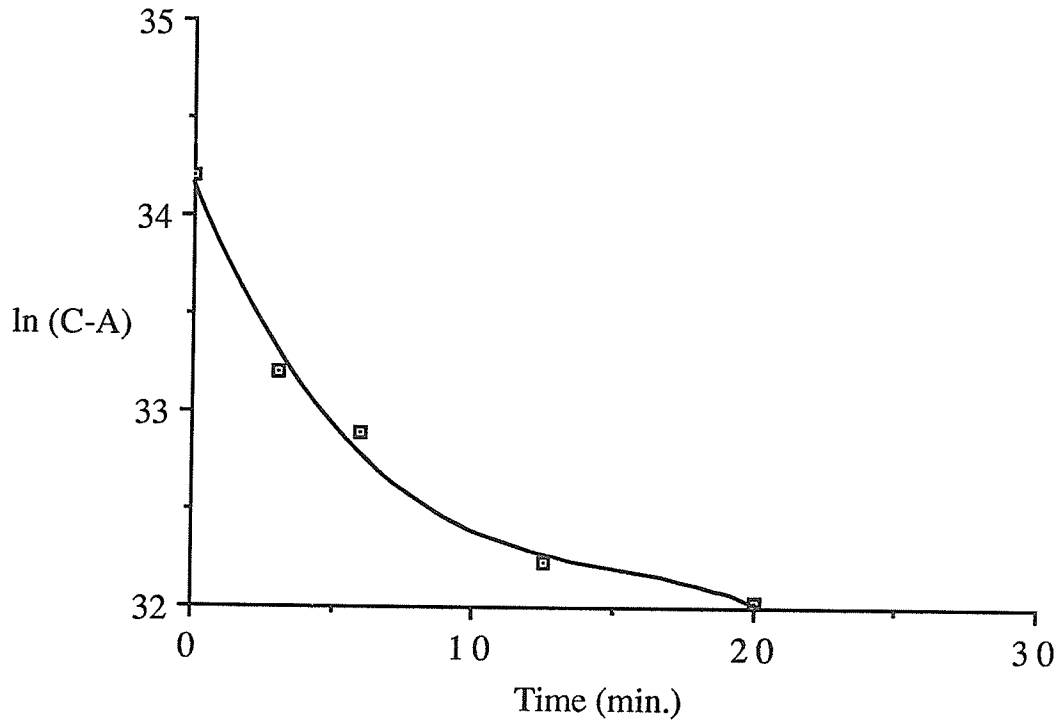

Figure 3-27: Modified first order plot for the decay of methyl radicals at -164°C (109 K) on PVGM1 loaded with 1.00 monolayer (1.19×10^{-3} mmole/mg) azomethane.

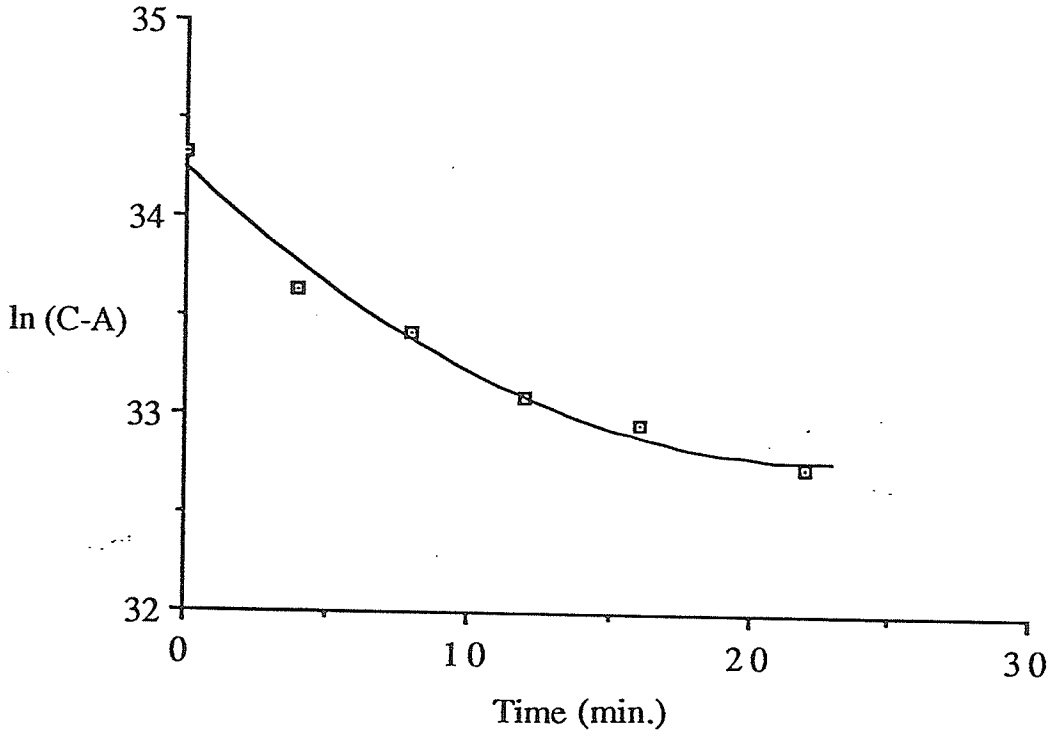

Figure 3-28: Modified first order plot for the decay of methyl radicals at -164°C (109 K) on PVGM3 loaded with 3.19 monolayers (3.19×10^{-3} mmole/mg) azomethane.

of methyl radicals were done at long times to test the applicability of equation 3-14 to the kinetics data. Similarly, at short times, equation 3-13 becomes

$$\frac{1}{C} = 8r^2(\pi D)^{1/2}t^{1/2} + \frac{1}{C_0} \qquad 3\text{-}15$$

or

$$\frac{1}{C} - \frac{1}{C_0} = 8r^2(\pi D)^{1/2}t^{1/2} \qquad 3\text{-}16$$

and the rate constant becomes $8r^2(\pi D)^{1/2}$.[80] A slope of 1/2 is therefore predicted from equation 3-16 for a plot of ln $(1/C - 1/C_0)$ against ln t. This has been experimentally observed by Hasinoff[80] for the recombination of CO with myoglobin in a supercooled very high viscosity glycerol-water solvent. The applicability of equation 3-16 to methyl radicals decay kinetics data obtained at both short and long times was therefore also tested.

As before all the decay curves obtained at much longer times than 100 minutes gave the best fit to Dole's revised second order equation (Equation 3-11). Typical decay curves obtained at such long times are presented in Figures 3-29 to 3-31 while the Dole plot data for such relatively long time decay of the radicals on various PVG surfaces are given in Tables 3-6 and 3-7. It should be noted that the decay curves in Figures 3-29 to 3-31 indicate that the concentrations of the radicals approach a constant value at long times which may then suggest the possibility of the existence of multiple sites on the surface. The Dole plots for experiments 9 to 14 as well as for

Table 3-6: Dole plot data for the decay of methyl radicals at 77 K on different PVG surfaces containing approximately 2 monolayers azomethane

PVG sample	Expt. No.	Length of decay	$(C_0 - A)$ x 10^{-15} (spins/ m^2)	A x 10^{-15} (spins/ m^2)	$(C_0-A)/A$	k_2* (m^2 $spin^{-1}$ min^{-1})
PVGM4	9	270 min.	0.709	1.92	0.369	2.04 x10^{-17}
	10**	147.8 hr.	1.55	1.51	1.03	7.28 x10^{-19} (or 4.37 x 10^{-17})
PVGM6	11	460 min.	0.982	2.57	0.382	1.24 x10^{-17}
	12¶	175.6 hr.	1.69	1.86	0.909	9.06 x10^{-19} (or 5.44 x 10^{-17})
PVGM6d	13	250 min.	0.990	2.71	0.365	2.17 x10^{-17}
	14¶	138.2 hr.	2.02	1.68	1.20	8.02 x10^{-19} (or 4.81 x 10^{-17})

*The values of k_2 written in parentheses are in the units of m^2 $spin^{-1}$ hr^{-1}.

**Experiment 10 was done after 68 hours 10 minutes decay at 77 K and subsequent re-irradiation for 120 minutes.

¶Experiments 12 and 14 are simply continuation experiments of experiments 11 and 13, respectively.

Table 3-7: Dole plot data for the decay of methyl radicals at different temperatures on PVG samples* containing approximately 0.1 monolayer azomethane

Expt. No.	Temp. (K)	Length of decay	$(C_0 - A) \times 10^{-15}$ (spins/m^2)	$(C_0-A)/A$	$k_2 \times 10^{17}$ (m^2 $spin^{-1}$ min^{-1})	E_a (kJ mol^{-1}) Fig. 3-35	
						Calculated	Least squares value
15a	77	252 min.	4.48	0.959	0.140**	7.30	7.31
15b	77	231.1 hr.	8.97	2.96	0.00748 (4.49)¶		
16	90	195 min.	3.96	0.615	0.726**		
17a¶¶	109	240 min.	10.3	8.58	4.06**	7.39	
17b¶¶	109	145 min.	7.11	9.00	5.22		

* PVGM5 was used for experiments 15b, PVGM5d for experiments 15a and 17b and PVGM5d_2 for experiments 16 and 17a [refer to section 3.3.1 (b)].

**k_2 values for experiments 15a, 16 and 17a were used for the determination of the activation energies.

¶The value of k_2 for experiment 15b written in parentheses is the actual value multiplied by 10^{18} in the units of m^2 $spin^{-1}$ hr^{-1}.

¶¶For experiment 17a, ESR measurements were recorded at 77 K while for experiment 17b, measurements were taken at 109 K.

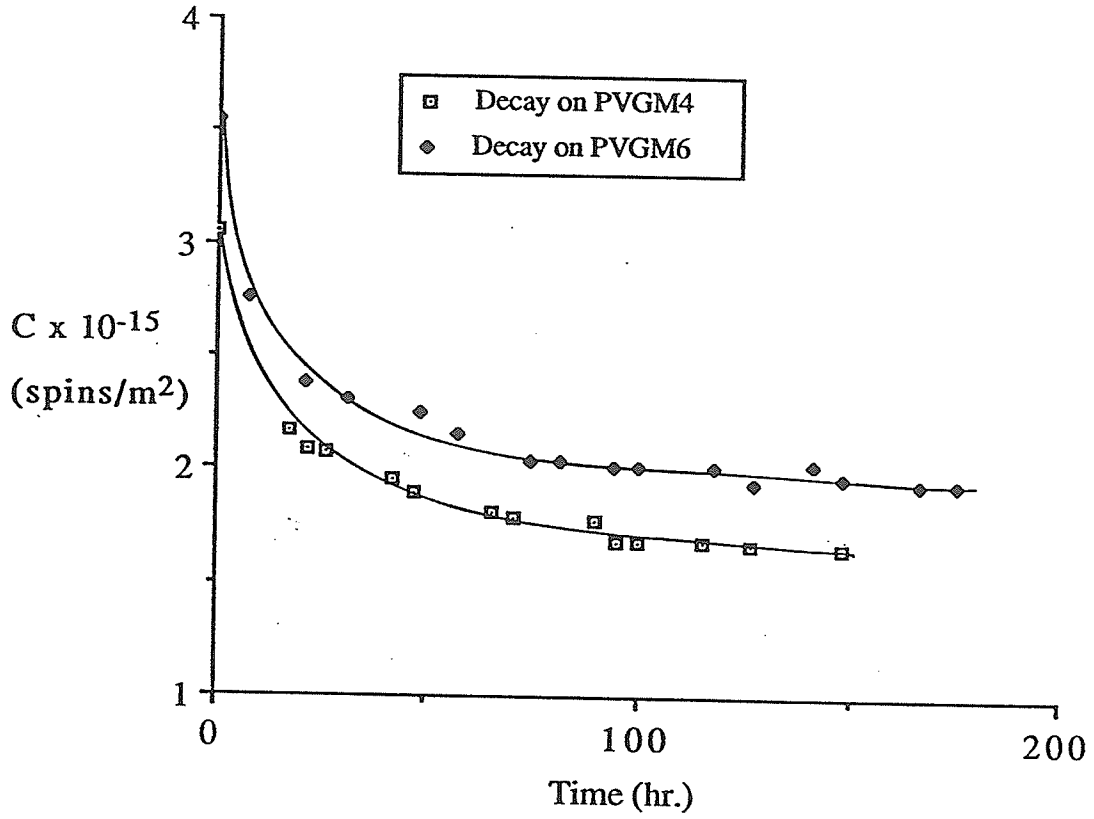

Figure 3-29: Long time decay of methyl radicals at 77 K on PVGM4 and PVGM6 surfaces containing 2.01 monolayers azomethane.

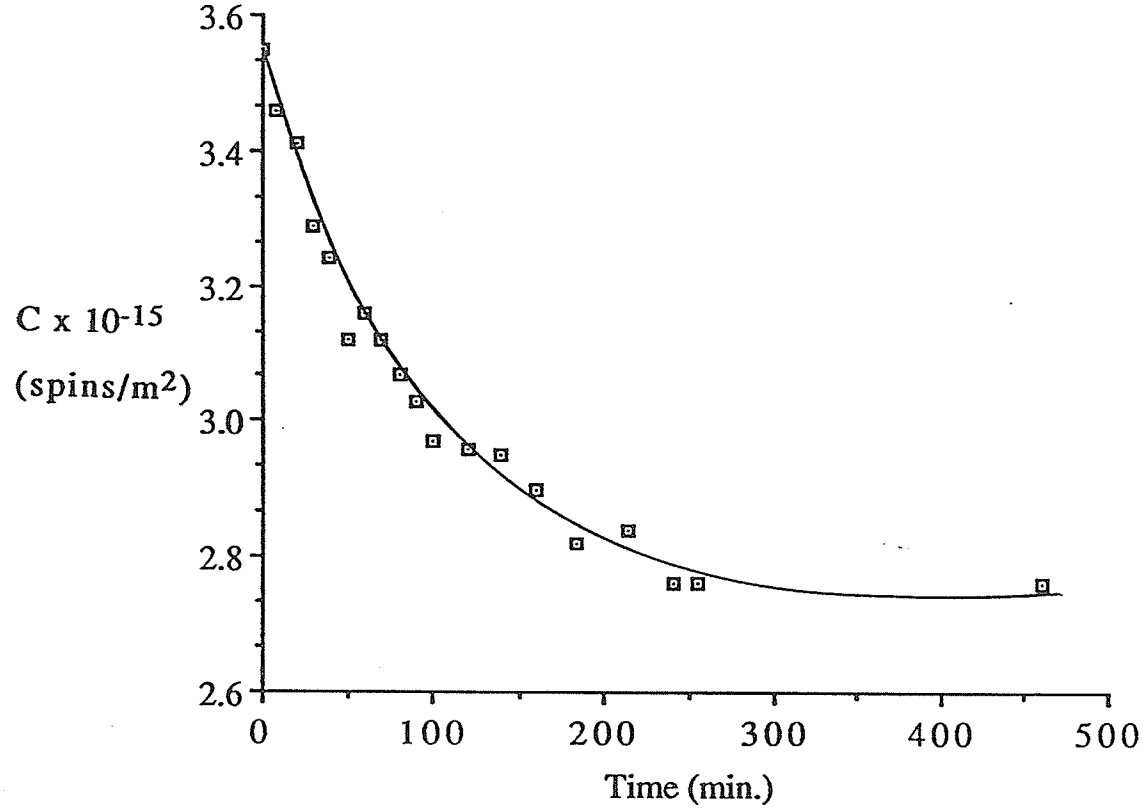

Figure 3-30: Decay of methyl radicals at 77 K on PVGM6 containing 2.01 monolayers (2.40 x 10^{-3} mmole/mg) azomethane.

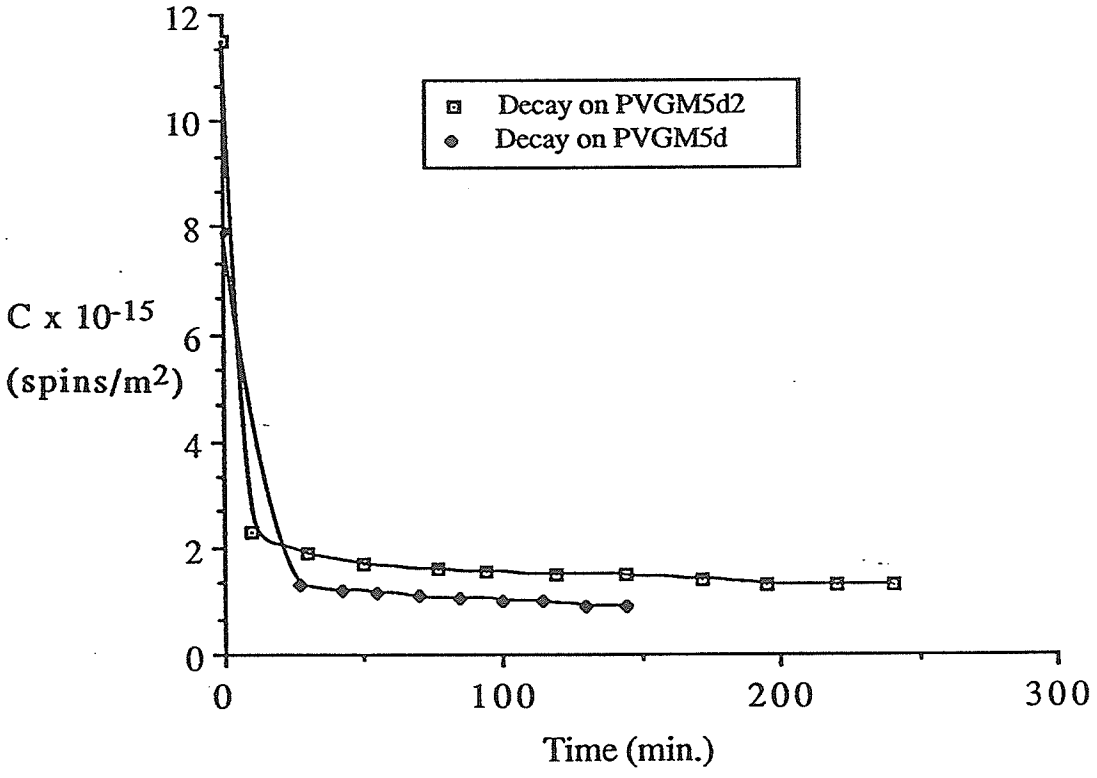

Figure 3-31: Decay of methyl radicals at 109 K on PVGM5d and PVGM5d$_2$ surfaces containing 0.103 monolayer azomethane. (Note that ESR measurements were taken at 109 K for decay on PVGM5d and at 77 K for decay on PVGM5d$_2$).

experiments 15a, 16, 17a and 17b are shown in Figures 3-32 to 3-34. The Arrhenius plot for the data in Figure 3-34 is shown in Figure 3-35. Values of k_2 for experiments 15a, 16 and 17a are used to obtain the plot.

Generally, when the values of A measured from the long time decay curves are substituted into equation 3-8, straight line graphs are obtained on plotting 1/(C-A) against t and the values of k_2, (C_0-A), A and $(C_0-A)/A$ obtained in this way are in good agreement with the corresponding values obtained from the Dole plots (Equation 3-11). This confirms further the applicability of equation 3-8 to the kinetic data on the condition that the decay was followed for a period of time long enough to make A measurable. This observation is illustrated in Figure 3-36 and Table 3-8 for experiments numbers 10 and 15b.

Although many plots of ln C against ln t are straight lines as shown in Figures 3-37 and 3-38 none of the plots gave a slope of -1; the slopes of the plots actually vary from -0·06 to 0·3. Hence, equation 3-14 cannot be applied to the kinetics data obtained in this work. Similarly, many plots of ln $(1/C - 1/C_0)$ against ln t are linear as illustrated in Figures 3-39 and 3-40. However, most of the plots did not yield a slope of 0·5 but rather slopes ranging from 0·2 to 0·8 were obtained for the plots. It therefore follows that equation 3-16 is also not very applicable to the kinetics data obtained in this study.

It should be noted that the PVG samples used were subjected to the following treatments:

Table 3-8: Rate constants and concentration values obtained from both modified second order and Dole plots for the long time decay of methyl radicals on PVGM4 and PVGM5 at -196°C (77 K)

	PVGM4 containing 2.01 monolayers (2.38×10^{-3} mmole/mg) azomethane		PVGM5 containing 0.104 monolayer (1.24×10^{-4} mmole/mg) azomethane	
	Modified 2nd order plot (Fig. 3-36) value	Dole plot (Eqn. 3-11) value	Modified 2nd order plot (Fig. 3-36) value	Dole plot (Eqn. 3-11) value
$k_2 \times 10^{18}$ (m^2 $spin^{-1}$ min^{-1})	1.08	0.728	0.125	0.0748
$(C_0\text{-}A) \times 10^{-15}$ ($spins/m^2$)	1.36	1.55	9.31	8.97
$A \times 10^{-15}$ ($spins/m^2$)	1.65	1.51	3.92	3.03
$(C_0\text{-}A)/A$	0.824	1.03	2.38	2.96

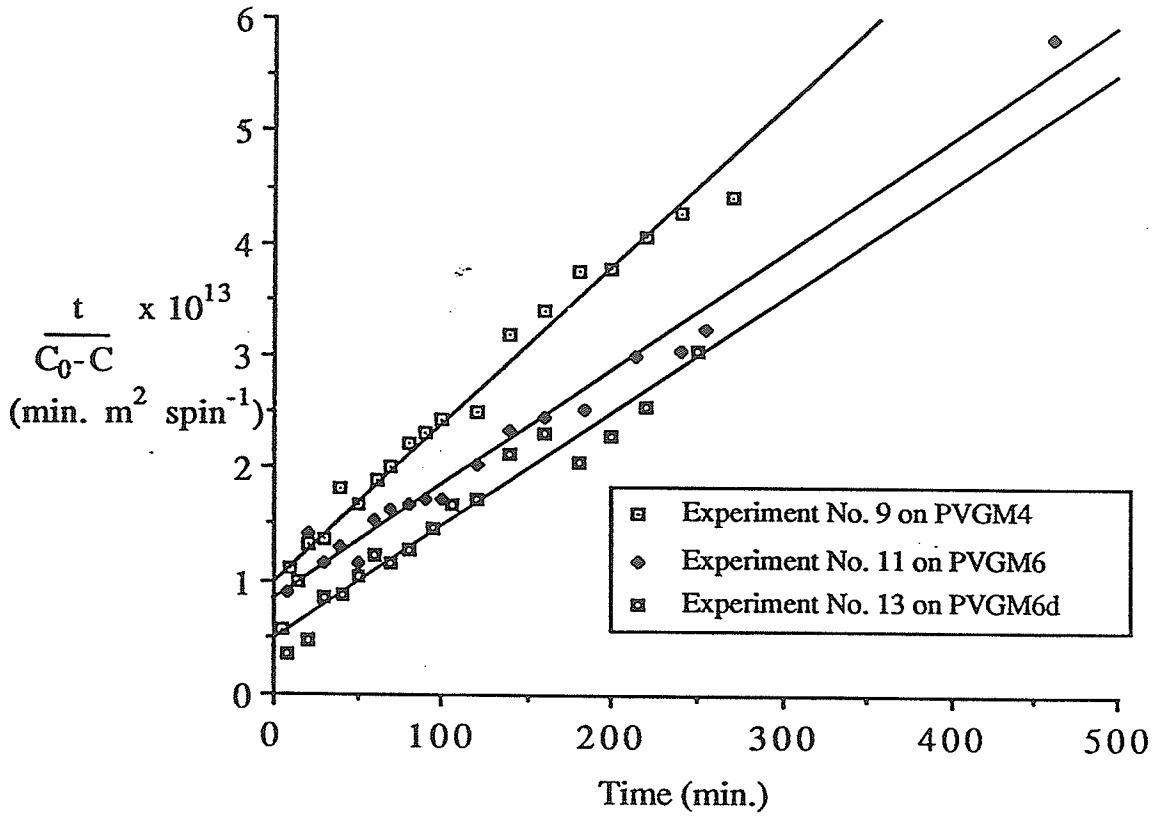

Figure 3-32: Second order Dole plots for the decay of methyl radicals at 77 K on PVGM4, PVGM6 and PVGM6d surfaces containing about 2 monolayers azomethane.

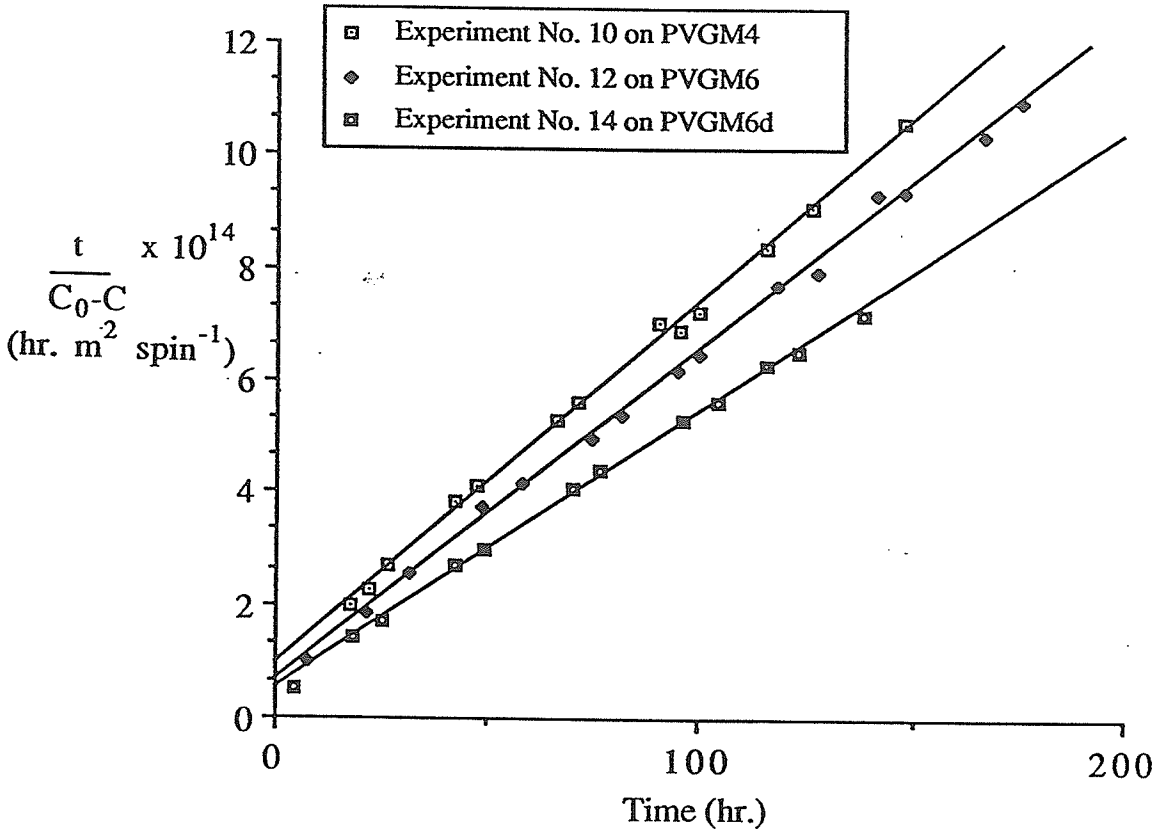

Figure 3-33 : Second order Dole plots for the long time decay of methyl radicals at 77 K on PVGM4, PVGM6 and PVGM6d surfaces containing about 2 monolayers azomethane.

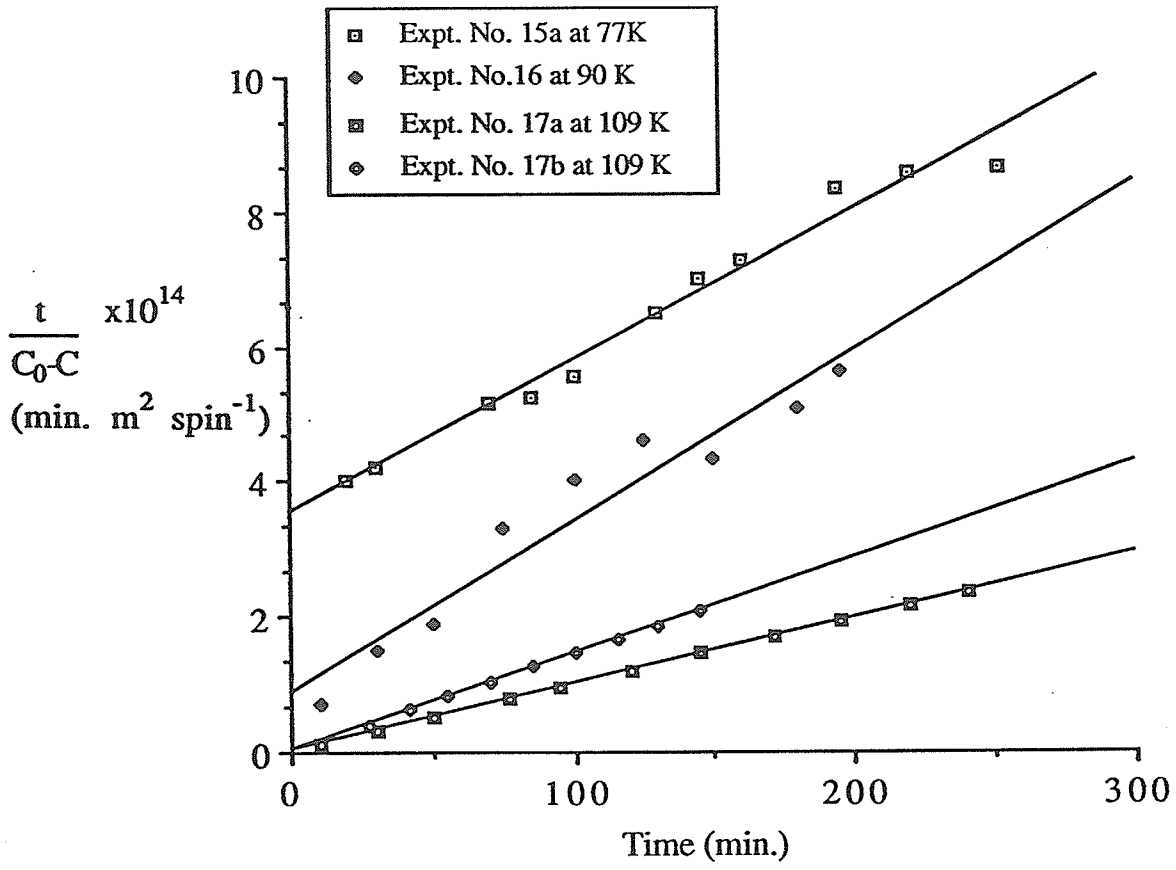

Figure 3-34: Second order Dole plots for the decay of methyl radicals at different temperatures on PVG surfaces loaded with about 0.1 monolayer azomethane. (Note that for experiment 17a, ESR measurements were taken at 77 K while for experiment 17b, measurements were recorded at 109 K).

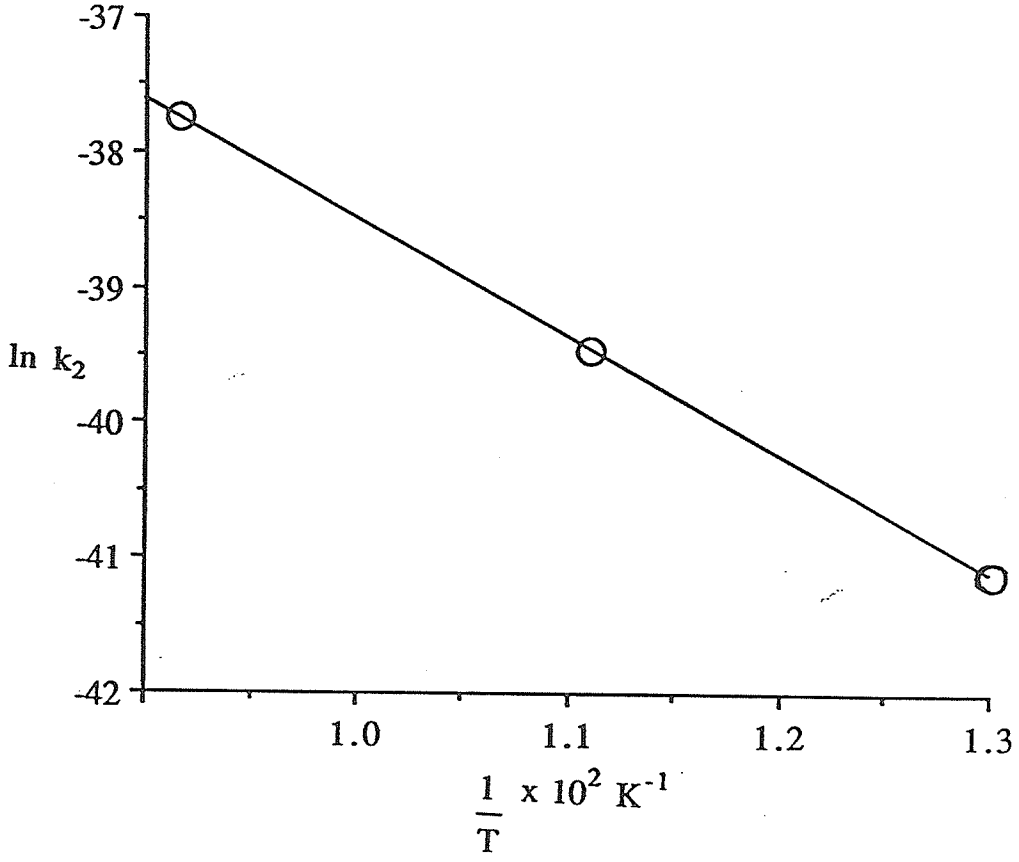

Figure 3-35: Arrhenius plot for the decay of methyl radicals on PVG surfaces loaded with about 0.1 monolayer azomethane.

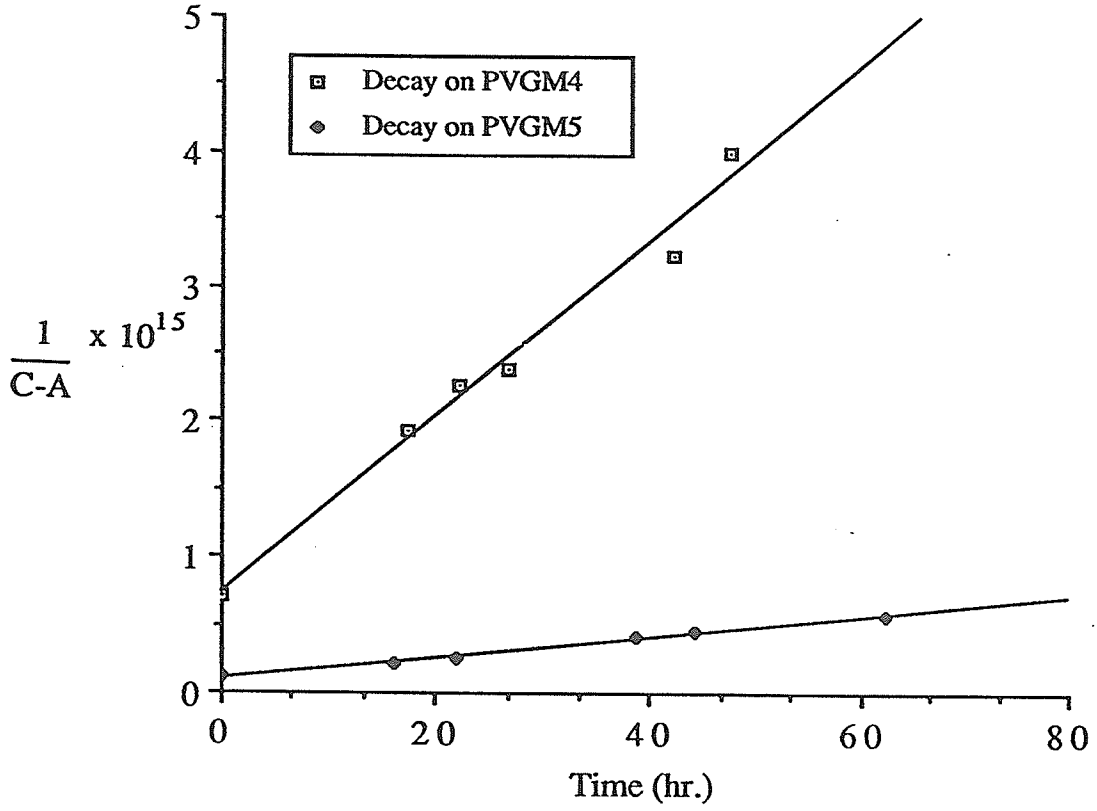

Figure 3-36: Modified second order plots for the long time decay of methyl radicals at -196°C (77 K) on PVGM4 and PVGM5 surfaces loaded with 2.01 and 0.104 monolayers azomethane, respectively.

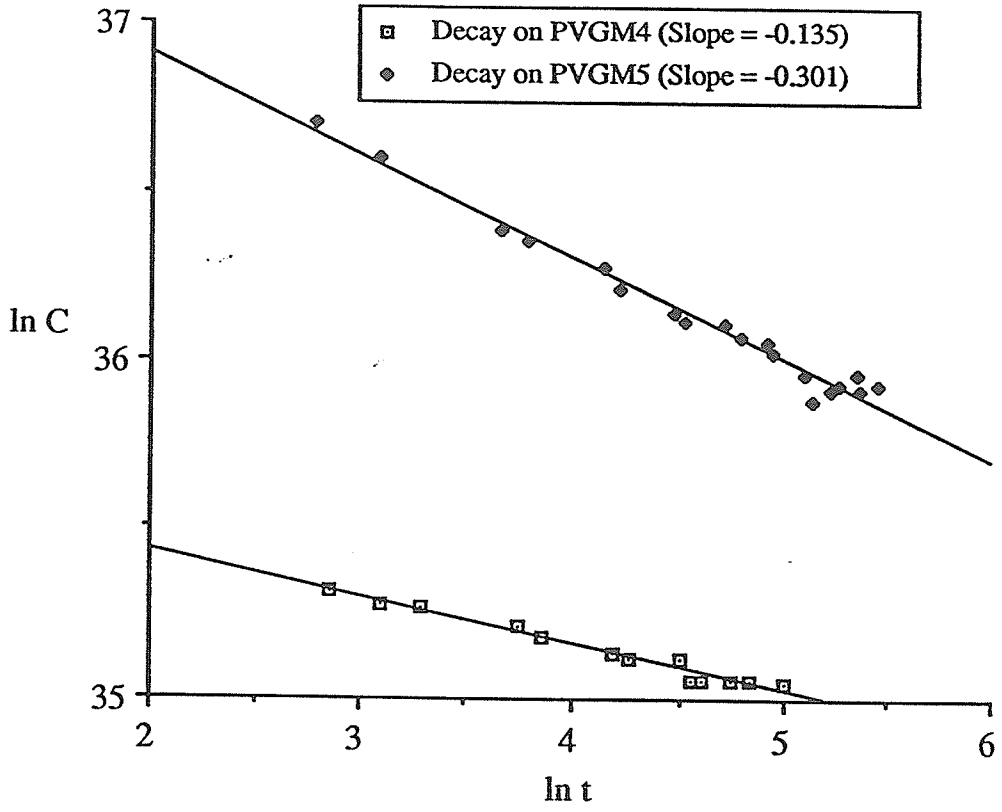

Figure 3-37: Plots of ln C against ln t for long time decay of methyl radicals at 77 K on PVGM4 and PVGM5 surfaces loaded with 2.01 and 0.104 monolayers azomethane, respectively.

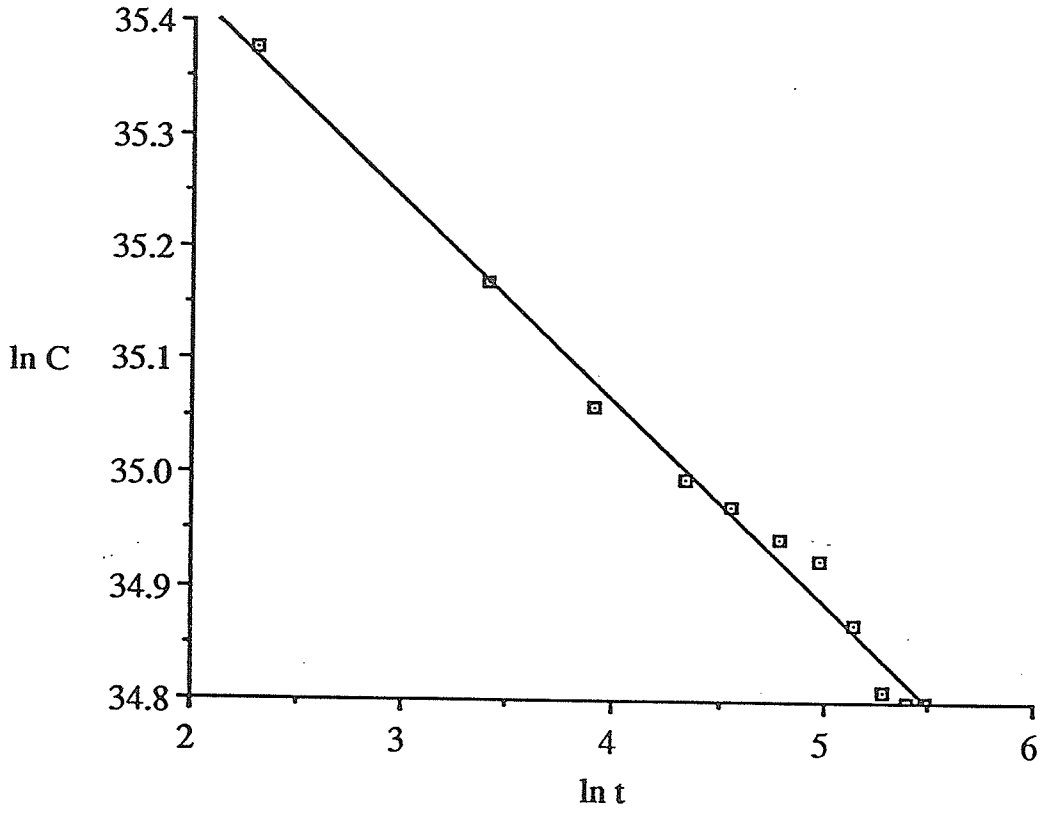

Figure 3-38: Plot of ln C against ln t for the decay of methyl radicals at -164°C (109 K) on PVGM5d_2 surface loaded with 0.103 monolayer (1.23×10^{-4} mmole/mg) azomethane. (Slope = -0.180).

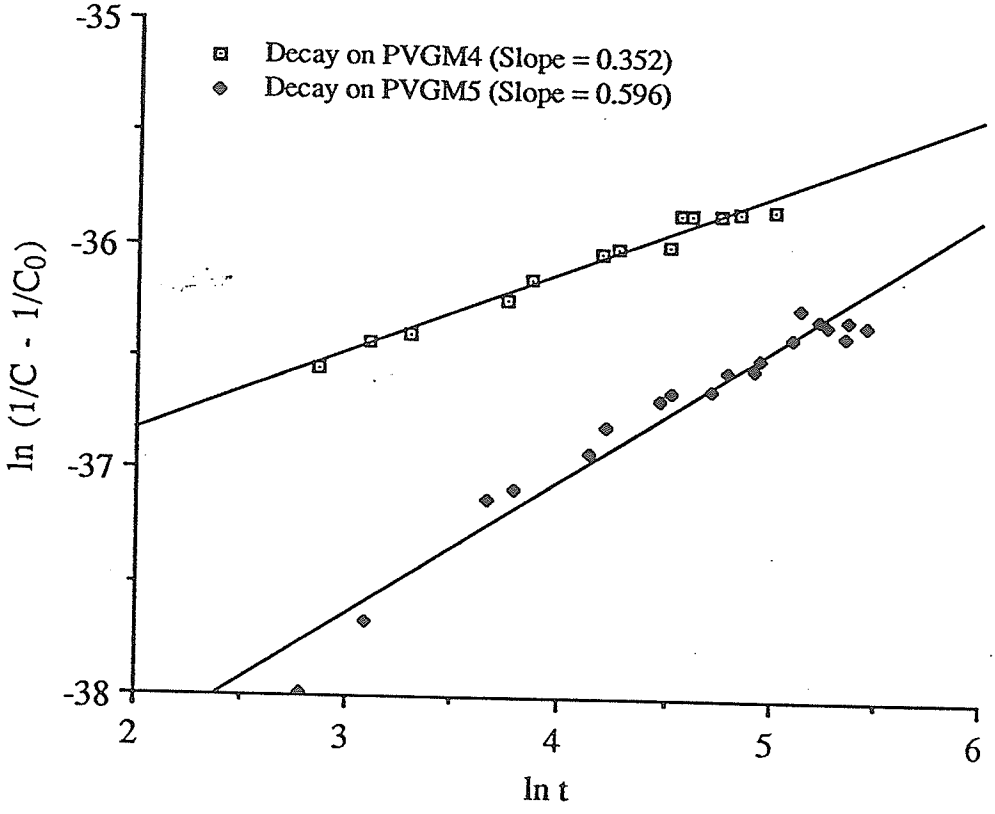

Figure 3-39: Plots of ln (1/C - $1/C_0$) against ln t for long time decay of methyl radicals at 77 K on PVGM4 and PVGM5 surfaces loaded with 2.01 and 0.104 monolayers azomethane, respectively.

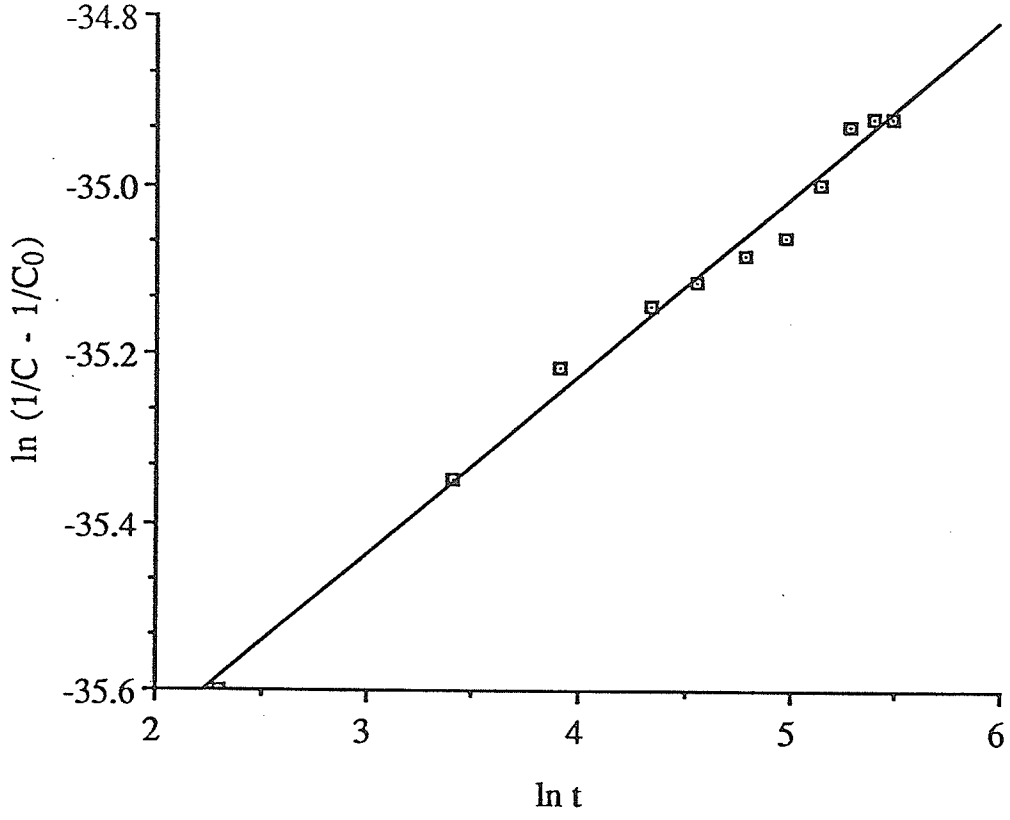

Figure 3-40: Plot of ln (1/C - $1/C_0$) against ln t for the decay of methyl radicals at -164°C (109 K) on PVGM5d_2 surface loaded with 0.103 monolayer (1.23 x 10^{-4} mmole/mg) azomethane. (Slope = 0.211).

(i) PVGM4 was evacuated at 750°C for 8 hours followed by thermoleaching in 171 torr O_2 at 500°C and subsequent evacuation at 500°C prior to loading with 2·01 monolayers (2.38×10^{-3} mmole/mg) azomethane.

(ii) PVGM6 was also pretreated at 750°C for $8^1/_2$ hours, thermoleached in 203 torr O_2 at 500°C, evacuated at 500°C and then loaded with 2·01 monolayers ($2{\cdot}40 \times 10^{-3}$ mmole/mg) azomethane.

(iii) PVGM6d was obtained by evacuating PVGM6 in (ii) (previously loaded with 2·01 monolayers azomethane) at 750°C for $8^1/_2$ hours, followed by thermoleaching in 211 torr O_2 at 500°C and subsequent evacuation at 500°C prior to re-loading with 2·02 monolayers ($2{\cdot}41 \times 10^{-3}$ mmole/mg) azomethane.

(iv) PVGM5 was pretreated at 750°C for $8^3/_4$ hours, thermoleached in 168 torr O_2 at 500°C, evacuated at 500°C and then loaded with 0·104 monolayer ($1{\cdot}24 \times 10^{-4}$ mmole/mg) azomethane. Experiment 15b was done using PVGM5.

(v) PVGM5d was obtained by evacuating PVGM5 in (iv), (previously loaded with 0·104 monolayer azomethane) at 750°C for 9 hours followed by thermoleaching in 197 torr O_2 at 500°C and subsequent evacuation at 500°C. The PVG sample was then re-loaded with 0·103 monolayer ($1{\cdot}23 \times 10^{-4}$ mmole/mg) azomethane. PVGM5d was used for experiments 15a and 17b.

(vi) PVGM5d_2 was obtained by evacuating PVGM5d in (v), (previously loaded with 0·103 monolayer azomethane) at 750°C for 8

hours followed by thermoleaching in 207 torr O_2 at 500°C and subsequent evacuation at 500°C prior to re-loading the sample with 0·103 monolayer azomethane. PVGM5d_2 was employed for experiments 16 and 17a.

As mentioned in section 2.1.4, some ESR measurements were done at liquid natural gas temperature (-164°C) for the purpose of comparing the results of the decay kinetics with those obtained at the same temperature by keeping the sample in liquid natural gas for a specified period of time and then transferring it quickly to the cavity dewar containing liquid nitrogen for ESR measurements at -196°C. The decay data for experiment 17a were obtained by taking ESR measurements at liquid nitrogen temperature (-196°C) while the data for experiment 17b were obtained by taking ESR measurements at liquid natural gas temperature (-164°C). Table 3-7 shows clearly that the values of $(C_0\text{-}A)/A$ and k_2 obtained for experiment 17a data recorded at -196°C are not significantly different from those obtained for experiment 17b data recorded at -164°C.

(c) Reproducibility of decay kinetics results

In order to verify how reproducible the decay kinetics results are, experiments were performed using (i) PVGM4 containing about 2 monolayers azomethane (ii) PVGM6 containing about the same amount of azomethane and (iii) PVGM6d which was obtained by pumping out PVGM6 previously loaded with about 2 monolayers azomethane prior to re-loading it with about the same amount of azomethane. The results presented in Table 3-6 clearly indicate that

they are reproducible. $(C_0\text{-}A)/A$ and k_2 values for experiments 9, 11 and 13 are in close agreement. Similarly, the values of $(C_0\text{-}A)/A$ and k_2 for experiments 10, 12 and 14 done at much longer times are also very close.

(d) Discussion

The applicability of Equations 3-8 and 3-11 to the decay kinetics data of methyl radicals as illustrated in Figures 3-14 to 3-16, 3-32 to 3-34 as well as in figures 3-24, 3-25 and 3-36 indicates clearly the presence of a fraction of the radicals decaying by a second order recombination mechanism while the remaining radicals which concentration is denoted by A, are completely unreactive. Tables 3-4 and 3-8 demonstrate that the modified second order equation (Equation 3-8) can simply be used to obtain values of k_2, $(C_0\text{-}A)$, A and $(C_0\text{-}A)/A$ close to the corresponding values obtained from the Dole Plots (Equation 3-11) provided the decay of the radicals was followed for a period of time long enough to make A measurable. It can therefore be concluded that the decay of methyl radicals is second order in mobile reactive radicals, consistent with a diffusion-controlled recombination process. These results imply that there are at least two types of surface adsorbed radicals for each temperature namely, weakly, physically adsorbed mobile and immobile, unreactive radicals. Results similar to these observations have been obtained by (1) Bader and Gesser[71] for the decay of hydrogen atoms on glass surfaces at -196°C, -185°C and -161°C, by (2) Fujimoto et. al.[2] for the decay of methyl radicals on porous Vycor glass and by (3) Joppien and Willard[3] for the decay of methyl radicals on silica gel.

Since the PVG samples were pretreated at a high temperature of 750°C, siloxane bridge structures must have been introduced by not only the removal of all the surface adsorbed contaminants but also by progressive dehydration of vicinal surface hydroxyl groups.[81] The immobile, unreactive radicals are identified with such siloxane bridge sites. Such radicals might also be associated with stabilization by caging effects in pores. The removal of vicinal hydroxyl groups on the PVG surfaces evacuated at 750°C also leaves a large number of geminal hydroxyl groups as well as B-OH groups on the surface.[9,81] The mobile reactive radicals might be identified with such sites.

The least squares values of activation energies obtained for the decay of methyl radicals between 77 K and 109 K as presented in Tables 3-1 to 3-3 as well as in Table 3-7 are higher than the value of 0±2·93 kJ mol^{-1} obtained by Gomer and Kistiakowsky[34] (or the value of 0±1·5 kJ mol^{-1} reported more recently by Baulch and Duxbury[35]) for the recombination reaction of the radicals in the gas phase. These values are , however, comparable with the value of 4·2 kJ mol^{-1} obtained by Bader and Gesser[71] for the recombination of hydrogen atoms on porous Vycor glass. This implies that methyl radicals can be stabilized on the surface of porous Vycor glass as previously observed by many workers.[2,4,25,82] The possibility of existence of a continuum of trapping potentials on the surface when the decay is carried out for relatively long time makes it possible for the stabilization to be achieved over a wide range of temperatures as previously noted.[2,3] The results summarized in Tables 3-1 to 3-3 also show that the ratio of the concentration of mobile, reactive methyl

radicals to the concentration of the immobile, unreactive radicals, $(C_0\text{-}A)/A$, increases with increase in temperature implying that some of the immobile, unreactive radicals are released from their sites and become converted to reactive radicals at higher temperatures by becoming trapped at the trapping sites for the latter radicals so that more radicals decay by recombination at the higher temperatures. However, the fact that some unreactive radicals are still present at the higher temperatures confirms further that the radicals can be stabilized over a wide range of temperatures.

Generally, the activation energies for the decay of methyl radicals were observed to vary erratically with temperatures as shown in Tables 3-1 to 3-3 as well as in Figures 3-17 and 3-19. However, the results presented in Tables 3-2 and 3-7 as well as in Figure 3-35 do not show any variation of activation energies with temperature. In spite of the erratic variation of E_a with temperature, the results presented in Tables 3-1 to 3-3 and in Table 3-7 also indicate that the average activation energies for the decay of the radicals between 77 K and 109 K decrease slightly with increase in surface coverage of azomethane on the PVG samples from 0.1 monolayer to 3 monolayers so that k_2 generally increases slightly as the surface coverage is raised from 0.1 to 3 monolayers. This is expected since the radicals are further away from the surface adsorption sites at the higher coverage so that they become more readily available for recombination reaction on the surface. The erratic variation of the activation energies with temperature may be attributed to experimental error since the results given in Tables 3-2

and 3-7 and in Figure 3-35 do not show any such variation. However, the variation of activation energies with both temperature and surface coverage needs to be studied in more details e.g. by obtaining results of more trials of the decay kinetics of the radicals at different temperatures and studying the variation of the activation energies over a wider range of temperatures and surface coverages. The fact that the erratic variation of activation energy with temperature was not obtained for the radicals on PVGM5 and PVGM2 covered with about 0.1 and 2 monolayers azomethane, respectively, subtantiates the need to do more trials of the decay kinetics.

Table 3-5 indicates the the adsorption energy of methyl radicals on PVG surface decreases with increase in surface coverage implying that the immobile radicals are less strongly bonded to the siloxane bridge sites at the higher coverage. This is consistent with the observation that the radicals decay faster when the surface coverage is raised from 0.1 to 3 monolayers in that the weaker bonding of the immobile radicals to the siloxane bridge sites on the higher-coverage surface makes it easier for them to be converted to the mobile, reactive radicals so that more radicals become available for decay on the PVG surface. Furthermore, as already mentioned, the radicals at the higher-coverage surface are further away from the surface adsorption sites and become more readily available for decay by recombination on the surface. It should be noted that the value of k_2 for methyl radicals on PVGM1 loaded with 1 monolayer azomethane is out of line probably due to experimental error. The values of adsorption energy obtained in this work cannot be

compared with the value of 6.7 kJ mol^{-1} obtained by Bader and Gesser[71] for the adsorption of immobile hydrogen atoms on PVG surface. This is because their value was erroneously obtained from the plot of the logarithm of concentration of the immobile atoms against 1/T rather than from the plot of logarithm of the ratio of the concentration of mobile atoms to the concentration of the immobile atoms against 1/T which was employed here for both methyl and ethyl radicals. Nevertheless, the values of the rate constants obtained in this work for methyl radicals can be compared with the value of 1.8×10^{-12} cm^2 $atom^{-1}$ s^{-1} (or 1.1×10^{-14} m^2 $atom^{-1}$ min^{-1}) reported by these workers for the decay of hydrogen atoms on PVG surface at 77 K. Table 3-5 clearly shows that the values of k_2 obtained in this study are much lower than the value obtained for hydrogen atoms. The slower decay of methyl radicals than hydrogen atoms on the PVG surface is actually expected since methyl radicals are much larger in size than hydrogen atoms.

Based on the foregoing experimental observations, the following mechanism similar to the one presented for hydrogen atoms is proposed for the decay of methyl radicals on porous Vycor glass:

$$(CH_3)_2N_2 + h\nu \longrightarrow 2CH_3 + N_2 \qquad 1\text{-}27$$

$$CH_3 \xrightarrow{77\ K} (CH_3)_A \qquad 3\text{-}17$$

$$CH_3 \xrightarrow{77\ K} (CH_3)_I \qquad 3\text{-}18$$

$$(CH_3)_A \rightleftharpoons CH_3 \qquad 3\text{-}19,\ 3\text{-}20$$

$$CH_3 + CH_3 \longrightarrow C_2H_6 \qquad 1\text{-}14$$

$$(CH_3)_I \longrightarrow (CH_3)_A \qquad 3\text{-}21$$

where CH_3, $(CH_3)_A$ and $(CH_3)_I$ are all surface adsorbed radicals; CH_3 is the mobile adsorbed radical capable of decaying by recombination while $(CH_3)_A$ exists as a constant (but temperature dependent) concentration of adsorbed, immobile radicals which are unreactive because of their stronger adsorption forces. $(CH_3)_A$ can be described further as active, immobile radicals since they are capable of being converted to the mobile, reactive radicals at higher temperatures. On the other hand, $(CH_3)_I$ are inactive, immobile radicals which are more strongly adsorbed than $(CH_3)_A$ radicals but can be converted to $(CH_3)_A$ radicals at higher temperatures. E_a is identified with reaction 1-14 and $-\Delta H_A$ with reaction 3-19. If reaction 3-20 occurs, it would have a very low activation energy and would therefore proceed unobserved.

Finally, it was observed that methyl radicals decay much faster when the decay was followed for less than 8 hours than when the decay was carried out for several days as shown clearly in Tables 3-6 and 3-7. Table 3-6 shows that the values of k_2 obtained for experiments 9, 11 and 13 done for 270, 460 and 250 minutes

respectively are much higher than the values obtained for experiments 10, 12 and 14 performed for 147.8, 175.6 and 138.2 hours respectively. Similarly, Table 3-7 indicates a much higher value of k_2 obtained for experiment 15a done for only 252 minutes than the value obtained for experiment 15b done for a period of 231.1 hours. These results are surprising and this anomaly may be due to systematic errors introduced into the ESR measurements in the case of the longer time experiments since both the sample and the cavity dewar flask containing liquid nitrogen are removed after each measurement thereby causing a change in their positioning in the cavity during subsequent measurements. Therefore, in future work, it is important to ensure that there is minimal change in the positioning of both the cavity dewar and sample during each measurement. Otherwise, any systematic error introduced has to be corrected for by the introduction of an internal standard such as a chip of ruby or a speck of carbon (diamond).

3.3.2 Ethyl radicals decay kinetics

(a) Results

A typical decay curve for the decay of ethyl radicals on PVG at -183°C after previous decay at -196°C is shown in Figure 3-41. Figure 3-42 presents a plot of the decay of the radicals at the three temperatures employed in this work. It is clear from Figure 3-42 that the decay of ethyl radicals is also a cascade type but only one adsorption site is postulated to be present on the surface since the

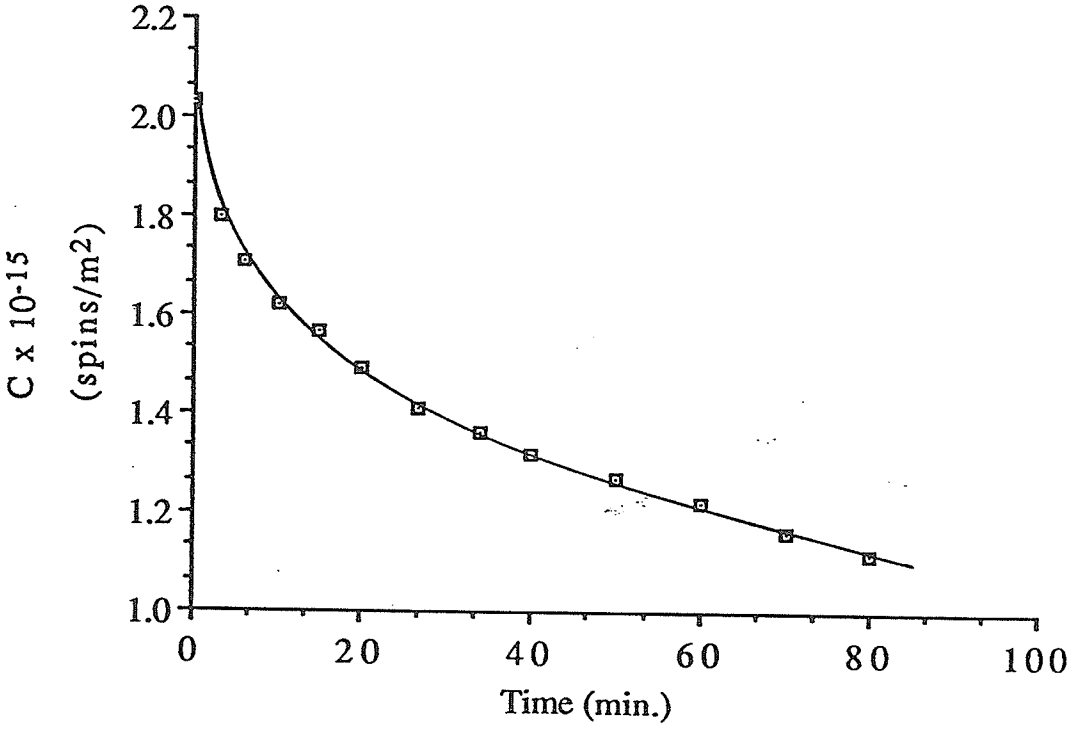

Figure 3-41: Decay of ethyl radicals on PVGE3 loaded with 3.09 monolayers (2.61×10^{-3} mmole/mg) azoethane at -183°C (90 K).

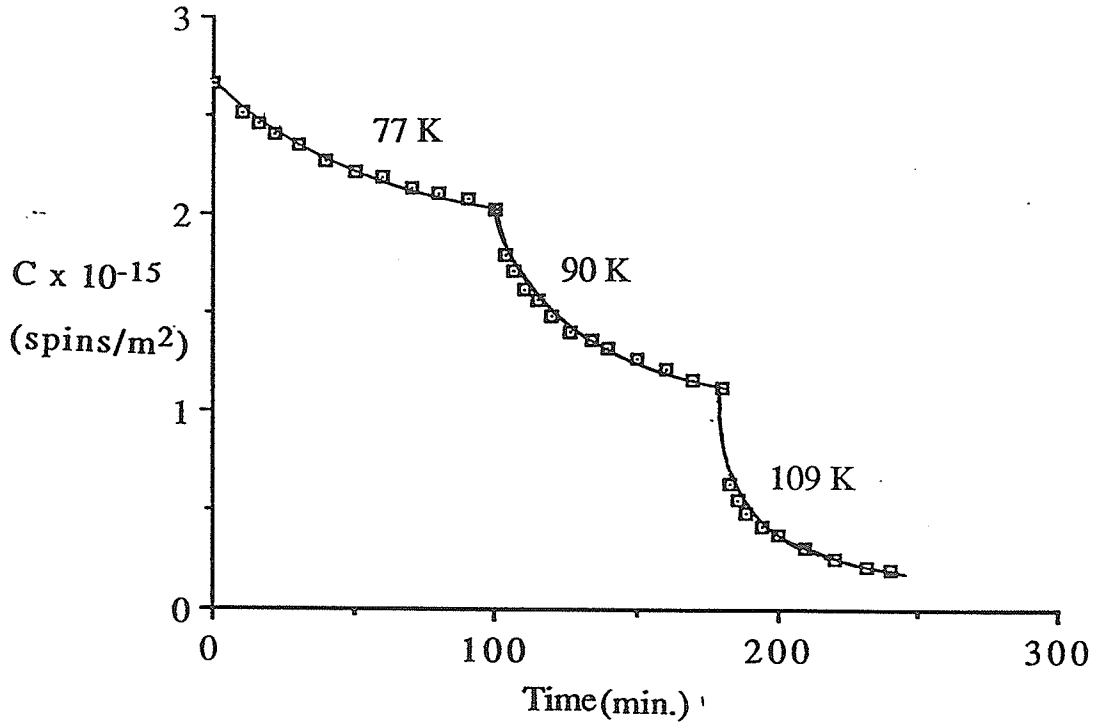

Figure 3-42: Decay of ethyl radicals on PVGE3 loaded with 3.09 monolayers (2.61 x 10^{-3} mmole/mg) azoethane at different temperatures.

decay studies were not carried out for a period of time long enough to make the concentrations of the radicals approach a constant value.

The decay of ethyl radicals was also found not to be a simple first or second order reaction as illustrated in Figures 3-43 and 3-44. However, all the kinetics data were again found to give the best fit to Dole's second order kinetics equation. The Dole plots for the decay of ethyl radicals adsorbed on three PVG samples at the three temperatures used in this work are presented in Figures 3-45 to 3-47. Figures 3-48 to 3-50 show the Arrhenius plots for the data in Figures 3-45 to 3-47, respectively. Activation energies, E_a, are again obtained from least squares analysis of the Arrhenius plots for the decay of the radicals. The values of E_a, k_2, $(C_0\text{-}A)$, A and $(C_0\text{-}A)/A$ at different temperatures for the PVG samples loaded with different amounts of azoethane are summarized in Tables 3-9 to 3-11. As it was done for methyl radicals, non-linear least squares analysis of the decay data given in Tables AI-8 to AI-10 was done using equation 3-12 and the values of $(C_0\text{-}A)$, A and k_2 were obtained. The values of E_a, k_2, $(C_0\text{-}A)$, A and $(C_0\text{-}A)/A$ obtained from the non-linear least squares analysis are written in parentheses in Tables 3-9 to 3-11. Figures 3-51 to 3-53 show typical non-linear least squares fits as well as the experimental points. It is clearly shown in Tables 3-9 to 3-11 that the Dole plot data agree well with the non-linear least squares fit data. Figures 3-51 to 3-53 also indicate that the non-linear least squares curves for the decay of ethyl radicals are in very good agreement with experimental points. The PVG samples, labelled PVGE1 and PVGE3, were evacuated at 750°C followed by

Table 3-9: Dole plot and non-linear least squares fit* data for the decay of ethyl radicals on PVGE1 loaded with 2·10 monolayers ($1{\cdot}78 \times 10^{-3}$ mmole/mg) azoethane

Expt. No.	Temp. (K)	$(C_0\text{-}A)$ $\times 10^{-14}$ (spins/m^2)	A $\times 10^{-14}$ (spins/m^2)	$(C_0\text{-}A)/A$	k_2 $\times 10^{17}$ (m^2 $spin^{-1}$ min^{-1})	E_a (kJ mol^{-1}) (Fig. 3-48) Calculated	E_a (kJ mol^{-1}) (Fig. 3-48) Least squares value
18	77	2.20 ± 0.17 (2.27 ± 0.20)	6.66 ± 0.17 (6.56 ± 0.22)	0.330 ± 0.034 (0.346 ± 0.042)	10.8 ± 2.7 (9.23 ± 2.89)	4.56 (6.40)	3.77 ± 0.42 (4.52 ± 1.05)
19	90	4.96 ± 0.17 (4.79 ± 0.20)	4.15 ± 0.17 (4.32 ± 0.15)	1.20 0.09 (1.11 ± 0.08)	30.3 ± 8.3 (39.2 ± 8.2)		
20	109	7.19 ± 0.10 (7.05 ± 0.17)	1.03 ± 0.10 (1.17 ± 0.12)	6.98 ± 0.77 (6.03 ± 0.76)	61.5 ± 9.2 (74.5 ± 10.4)	3.04 (2.76)	

*The values written in parentheses are the values obtained from non-linear least squares analysis.

Table 3-10: Dole plot and non-linear least squares fit* data for the decay of ethyl radicals on PVGE2 having some adsorbed water on the surface and loaded with 2·01 monolayers ($1{\cdot}71 \times 10^{-3}$ mmole/mg) azoethane

Expt. No.	Temp. (K)	$(C_0\text{-}A)$ $\times 10^{-14}$ (spins/ m^2)	A $\times 10^{-14}$ (spins/ m^2	$(C_0\text{-}A)/A$	k_2 $\times 10^{17}$ (m^2 $spin^{-1}$ min^{-1})	E_a (kJ mol^{-1}) (Fig. 3-49) Calculated	E_a (kJ mol^{-1}) (Fig. 3-49) Least squares value
21	77	4.94 ± 0.27 (5.25 ± 0.36)	11.1 ± 0.3 (10.7 ± 0.4)	0.445 ± 0.036 (0.491 ± 0.052)	3.30 ± 0.62 (2.58 ± 0.59)	4.90 (5.65)	5.23 ± 0.21 (6.36 ± 0.46)
22	90	5.77 ± 0.36 (5.66 ± 0.42)	7.03 ± 0.36 (6.98 ± 0.44)	0.821 ± 0.093 (0.811 ± 0.111)	10.0 ± 2.7 (9.20 ± 2.94)		
23	109	6.64 ± 0.13 (6.38 ± 0.24)	1.37 ± 0.13 (1.61 ± 0.16)	4.85 ± 0.56 (3.96 ± 0.54)	36.6 ± 6.2 (48.5 ± 8.2)	5.56 (7.15)	

*The values written in parentheses are the values obtained from non-linear least squares analysis.

Table 3-11: Dole plot and non-linear least squares fit* data for the decay of ethyl radicals on PVGE3 loaded with 3·09 monolayers ($2{\cdot}61 \times 10^{-3}$ mmole/mg) azoethane

Expt. No.	Temp. (K)	$(C_0\text{-}A)$ $\times 10^{-14}$ (spins/ m^2)	A $\times 10^{-14}$ (spins/ m^2)	$(C_0\text{-}A)/A$	k_2 $\times 10^{17}$ (m^2 $spin^{-1}$ min^{-1})	E_a (kJ mol^{-1}) (Fig. 3-50)	
						Calculated	Least squares value
24	77	9.93 ± 0.36 (10.3 ± 0.4)	16.7 ± 0.4 (16.2 ± 0.4)	0.595 ± 0.036 (0.636 ± 0.040)	1.60 ± 0.17 (1.37 ± 0.18)	5.69 (5.36)	5.52 ± 0.04 (6.53 ± 0.71)
25	90	10.5 ± 0.4 (10.3 ± 0.5)	9.80 ± 0.39 (9.43 ± 0.51)	1.07 ± 0.08) (1.09 ± 0.11)	5.76 ± 0.99 (4.59 ± 0.91)		
26	109	9.80 ± 0.19 (9.20 ± 0.46)	1.40 ± 0.19 (1.86 ± 0.29)	7.00 ± 1.09 (4.95 ± 1.02)	20.4 ± 3.4 (27.9 ± 5.2)	5.44 (7.74)	

*The values written in parentheses are the values obtained from non-linear least squares analysis.

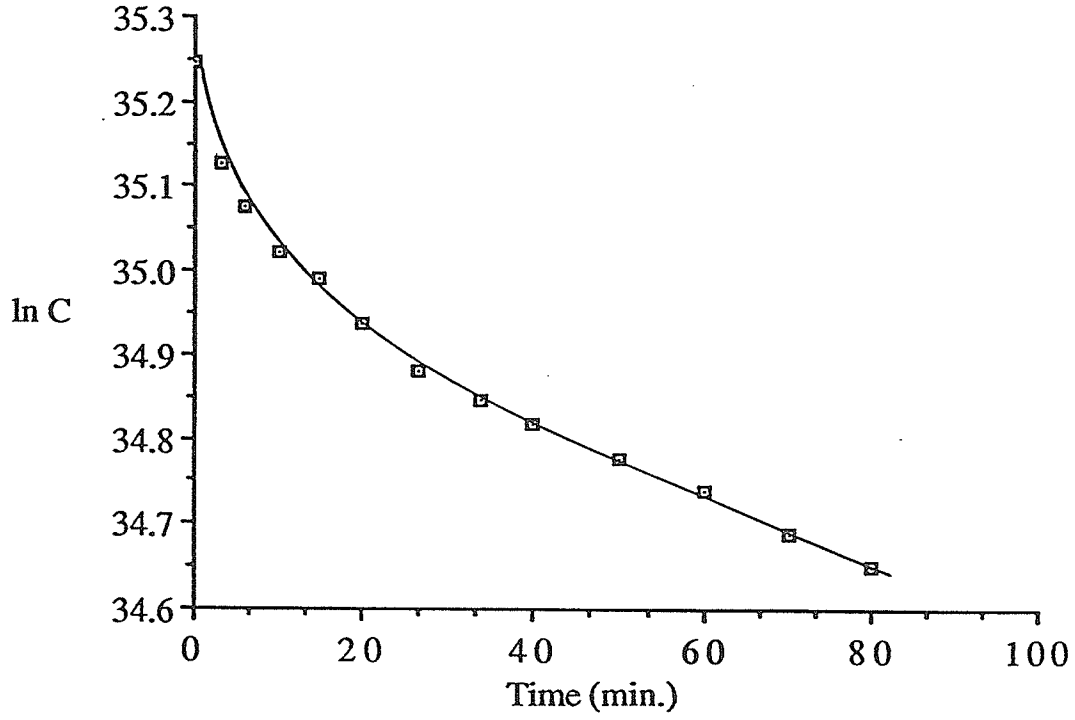

Figure 3-43: First order plot for the decay of ethyl radicals on PVGE3 loaded with 3.09 monolayers (2.61×10^{-3} mmole/mg) azoethane at -183°C (90 K).

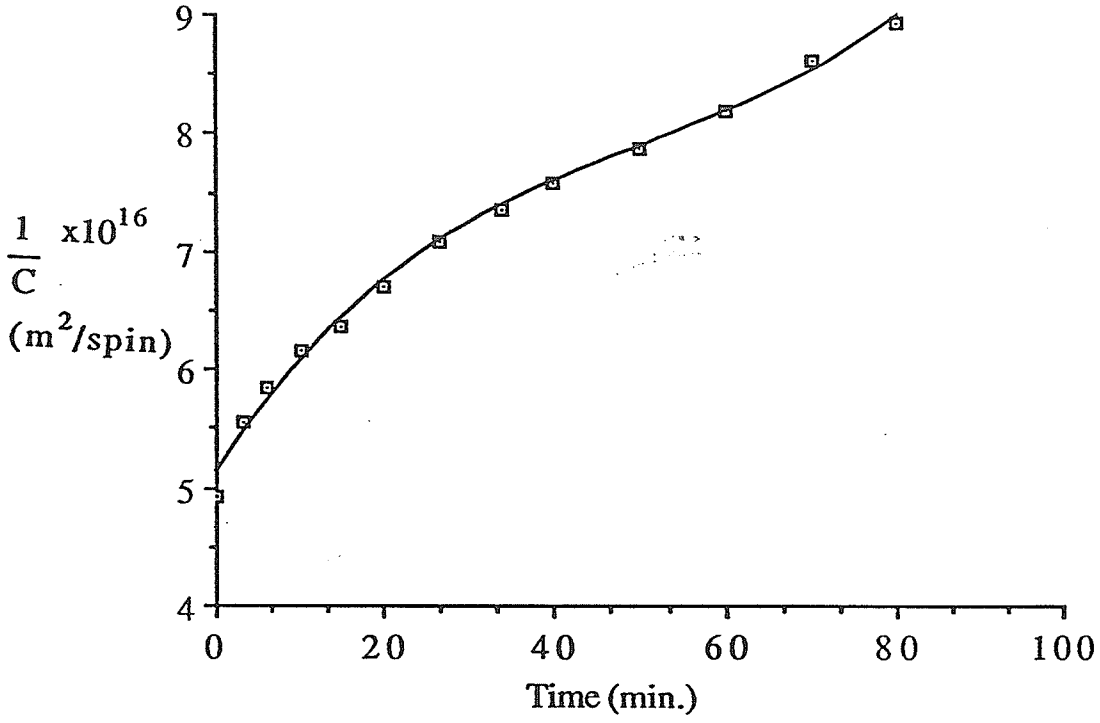

Figure 3-44: Second order plot for the decay of ethyl radicals on PVGE3 loaded with 3.09 monolayers (2.61 x 10^{-3} mmole/mg) azoethane at -183°C (90 K).

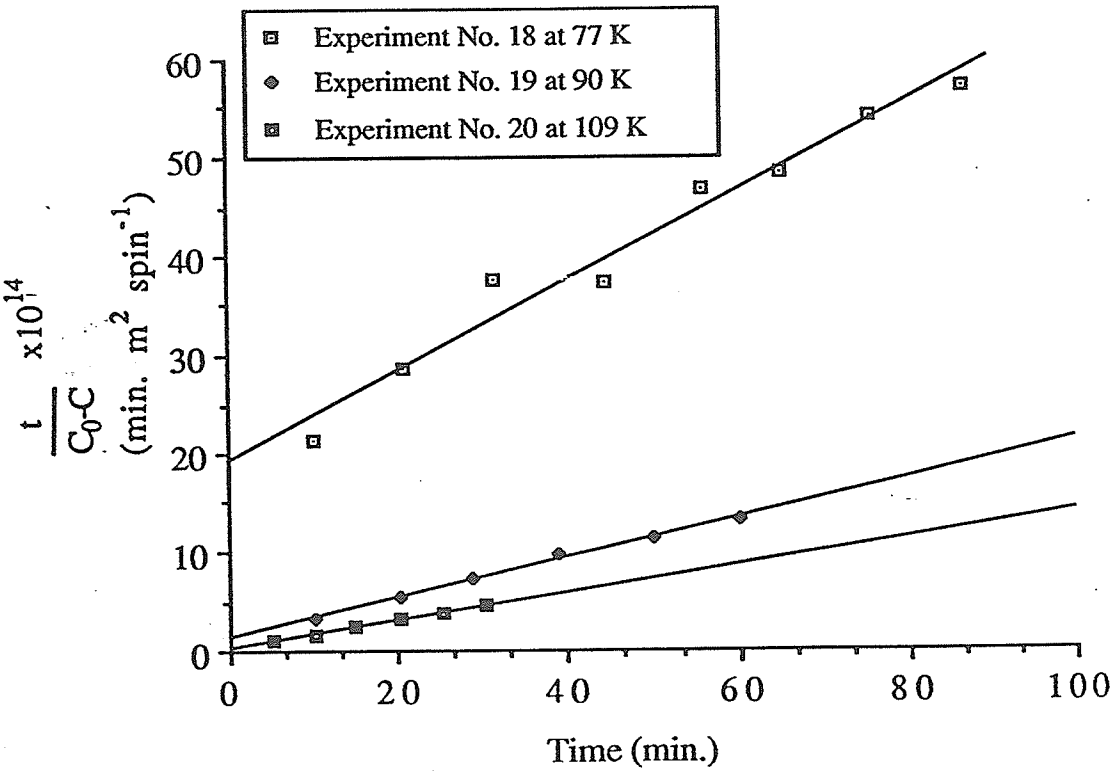

Figure 3-45: Second order Dole plots for the decay of ethyl radicals on PVGE1 loaded with 2.10 monolayers (1.78×10^{-3} mmole/mg) azoethane at different temperatures.

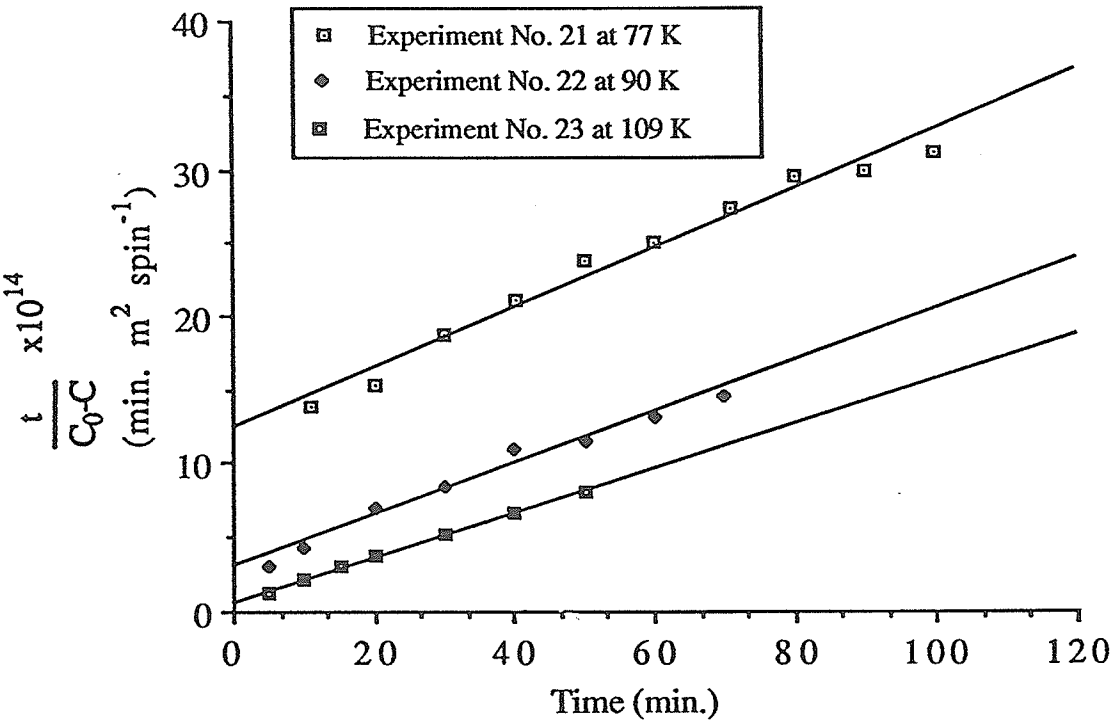

Figure 3-46: Second order Dole plots for the decay of ethyl radicals on PVGE2 loaded with 2.01 monolayers (1.71×10^{-3} mmole/mg) azoethane at different temperatures.

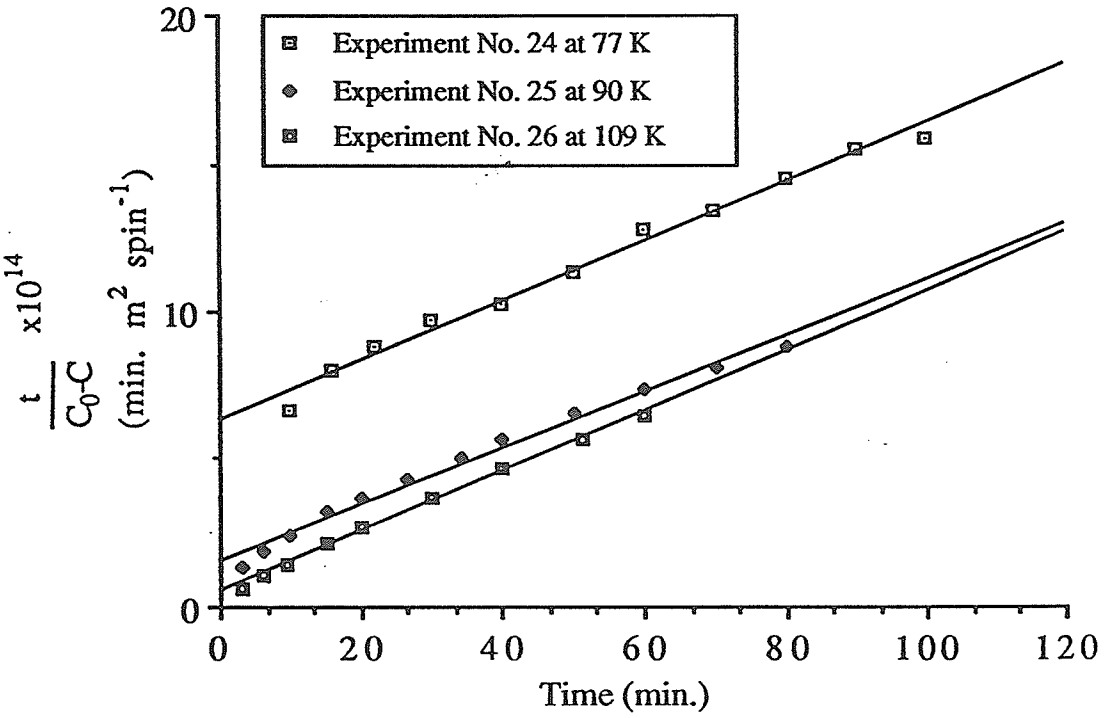

Figure 3-47: Second order Dole plots for the decay of ethyl radicals on PVGE3 loaded with 3.09 monolayers (2.61 x 10^{-3} mmole/mg) azoethane at different temperatures.

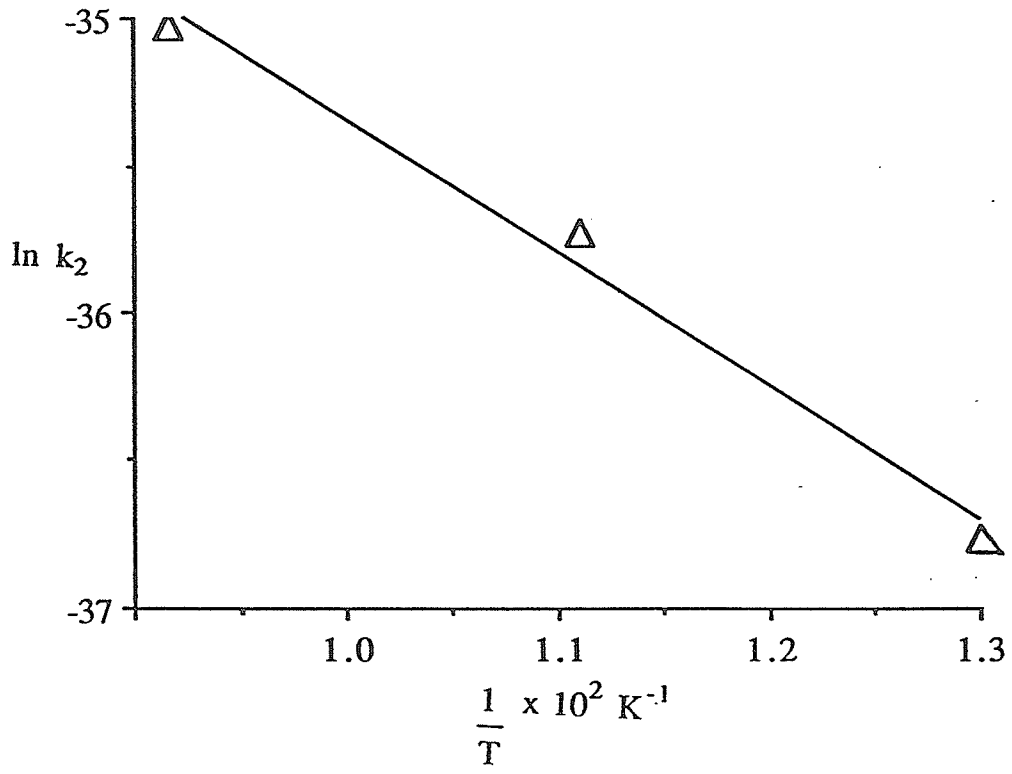

Figure 3-48: Arrhenius plot for the decay of ethyl radicals on PVGE1 loaded with 2.10 monolayers (1.78 x 10^{-3} mmole/mg) azoethane.

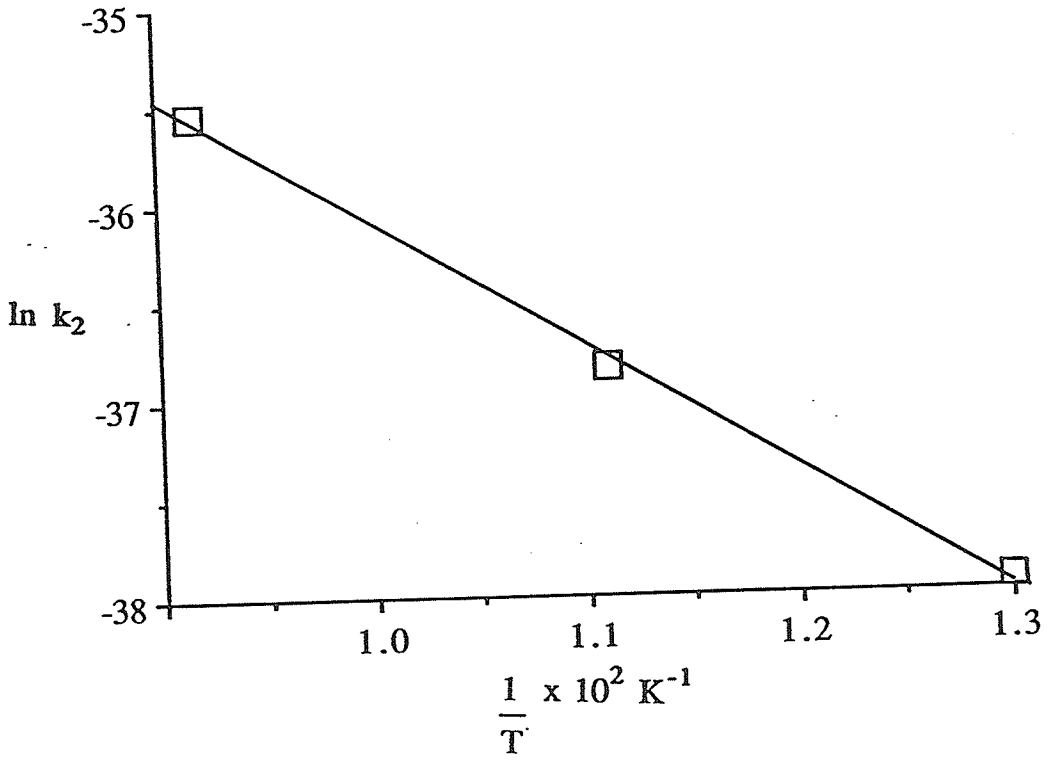

Figure 3-49: Arrhenius plot for the decay of ethyl radicals on PVGE2 loaded with 2.01 monolayers (1.71 x 10^{-3} mmole/mg) azoethane.

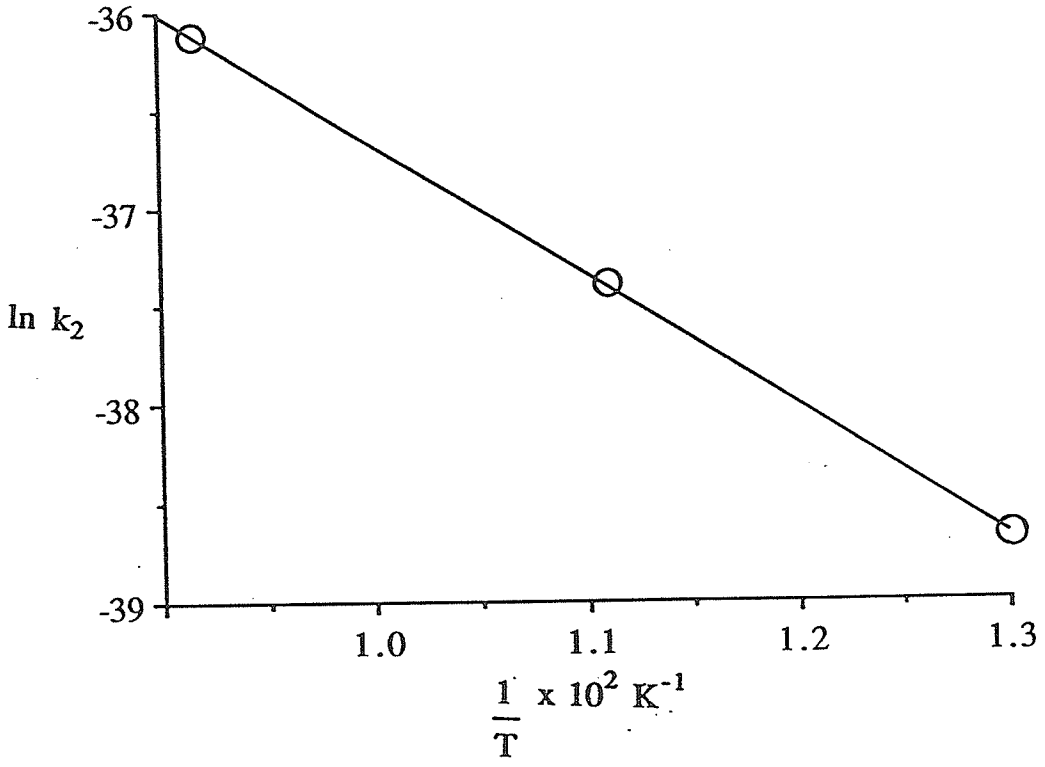

Figure 3-50: Arrhenius plot for the decay of ethyl radicals on PVGE3 loaded with 3.09 monolayers (2.61 x 10^{-3} mmole/mg) azoethane.

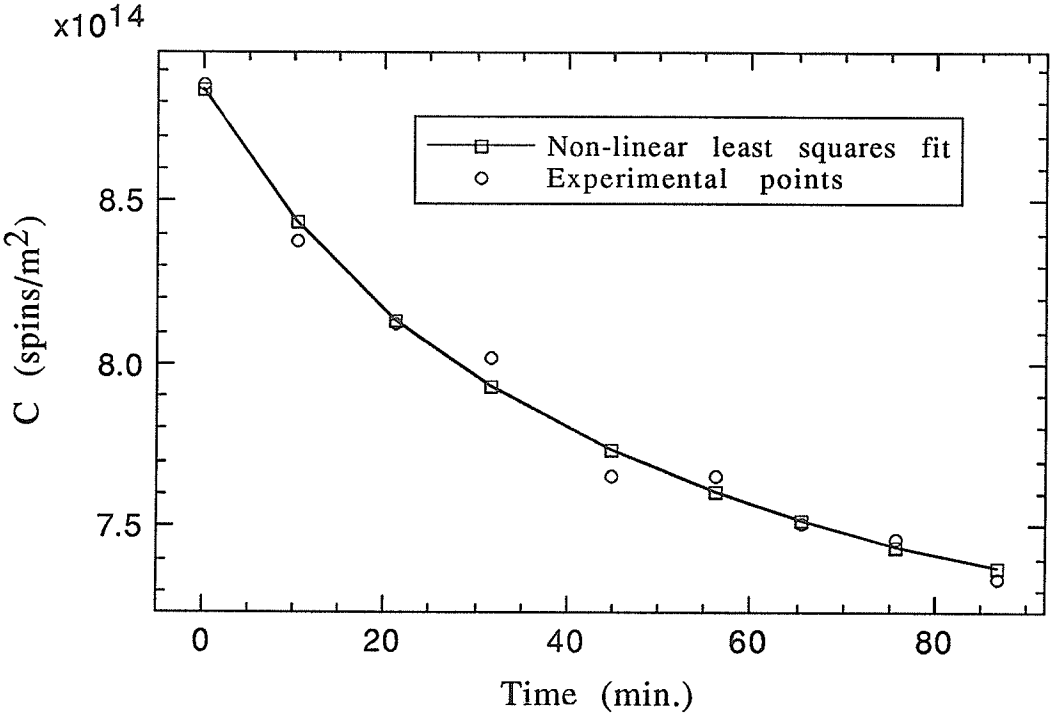

Figure 3-51: Non-linear least squares fit for the decay of ethyl radicals at 77 K on PVGE1 containing 2.10 monolayers (1.78 x 10^{-3} mmole/mg) azoethane.

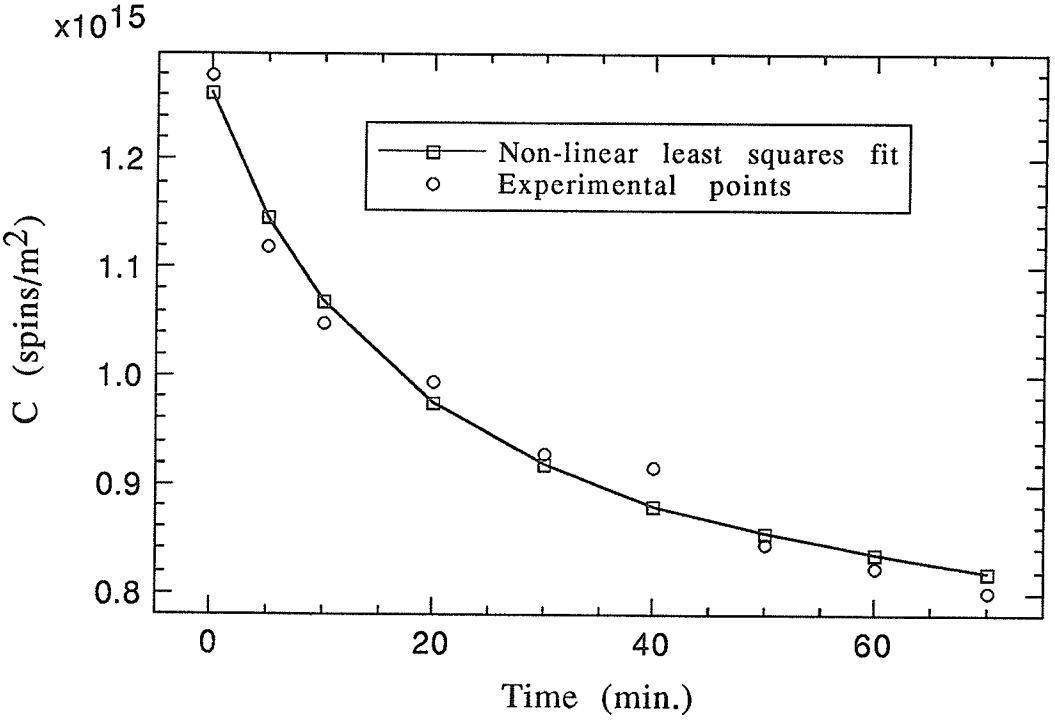

Figure 3-52: Non-linear least squares fit for the decay of ethyl radicals at 90 K on PVGE2 containing 2.01 monolayers (1.71×10^{-3} mmole/mg) azoethane.

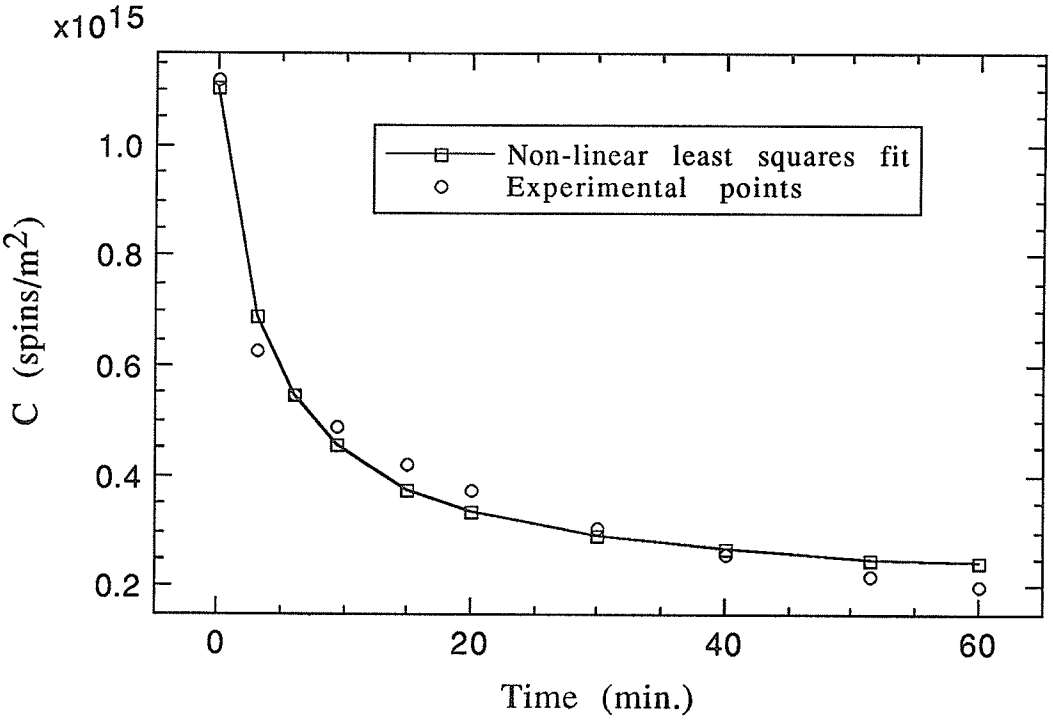

Figure 3-53: Non-linear least squares fit for the decay of ethyl radicals at 109 K on PVGE3 containing 3.09 monolayers (2.61 x 10^{-3} mmole/mg) azoethane.

thermoleaching in O_2 and subsequent evacuation at 500°C prior to loading with 2·10 and 3·09 monolayers azoethane, respectively. In order to leave some adsorbed water on the surface, the sample PVGE2 was degassed at 300°C after which it was thermoleached at 500°C prior to loading with 2·01 monolayers azoethane.

As illustrated in Figures 3-42, 3-54 and 3-55, the decay curves obtained for ethyl radicals did not reach steady states to make A measurable. However, it was still possible to estimate the values of A from the curves. This estimation was done for the curves 3-54 and 3-55 for experiment numbers 22 and 26, respectively. The estimated values of A, and therefore $(C_0\text{-}A)/A$, for the data in Figures 3-54 and 3-55 together with the corresponding values calculated from the Dole plots of $t/(C_0\text{-}C)$ against t (Equation 3-11) are presented in Table 3-12. Table 3-12 clearly shows that the calculated values are very close to the estimated values. Hence, the values of A can actually be estimated to be the concentration of the unreactive radicals at large times. When the calculated values of A for the same data in 3-54 and 3-55 are substituted into Equation 3-8, straight line graphs are obtained on plotting $1/(C\text{-}A)$ against t as shown in Figures 3-56 and 3-57, respectively. The values of k_2 and $(C_0\text{-}A)$ obtained from Figures 3-56 and 3-57 together with the corresponding Dole plot values for comparison are presented in Table 3-13.

It should be noted too that the value of A for ethyl radicals was also found to decrease with increase in temperature due to the decreased adsorption of the immobile, unreactive radicals at higher temperatures. This is shown clearly in Tables 3-9 to 3-11. The plots of $\ln (C_0\text{-}A)/A$ against $1/T$ for the data in Tables 3-9 to 3-11 are

Table 3-12: Comparison of estimated and calculated values of A and A/C_0 for the decay of ethyl radicals on PVGE2 and PVGE3

	PVGE2 containing 2·01 monolayers ($1·71 \times 10^{-3}$ mmole/mg) azoethane at -183°C (90 K)		PVGE3 containing 3·09 monolayers ($2·61 \times 10^{-3}$ mmole/mg) azoethane at -164°C (109 K)	
	Value estimated from Fig. 3-54	Value calculated from Dole plot (Eqn. 3-11)	Value estimated from Fig. 3-55	Value calculated from Dole plot (Eqn. 3-11)
A $\times 10^{-14}$ (spins/m^2)	7·65	7·03	1·60	1·40
$(C_0-A)/A$	0·697	0·821	5·24	7·00

Table 3-13: Rate constants and (C_0-A) values obtained from both modified second order and Dole plots for the decay of ethyl radicals on PVGE2 and PVGE3

	PVGE2 containing 2·01 monolayers ($1·71 \times 10^{-3}$ mmole/mg) azoethane at -183°C (90 K)		PVGE3 containing 3·09 monolayers ($2·61 \times 10^{-3}$ mmole/mg) azoethane at -164°C (109 K)	
	Modified 2nd order plot (Fig. 3-56) value	Dole plot (Eqn. 3-11) value	Modified 2nd order plot (Fig. 3-57) value	Dole plot (Eqn. 3-11) value
$k_2 \times 10^{16}$ (m^2 $spin^{-1}$ min^{-1})	0·841	1·00	1·71	2·04
(C_0-A) $\times 10^{-14}$ ($spins/m^2$)	5·33	5·77	8·39	9·80

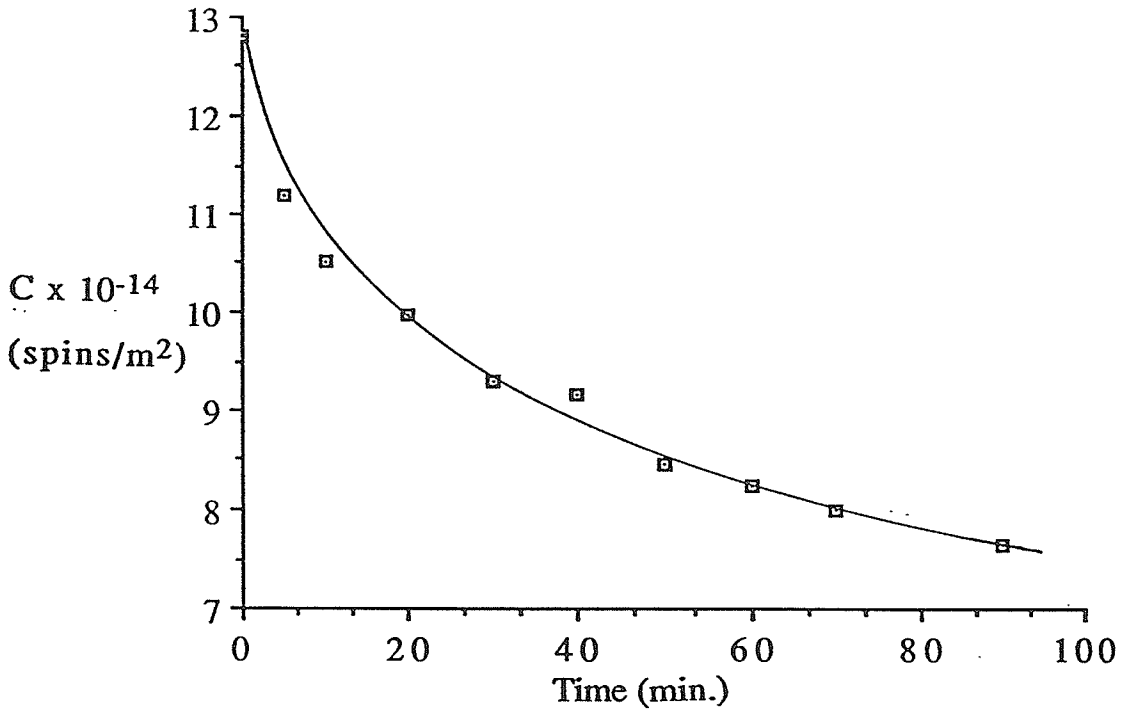

Figure 3-54: Experimental curve foı the decay of ethyl radicals at -183°C (90 k) on PVGE2 loaded with 2.01 monolayers (1.71 x 10^{-3} mmole/mg) azoethane.

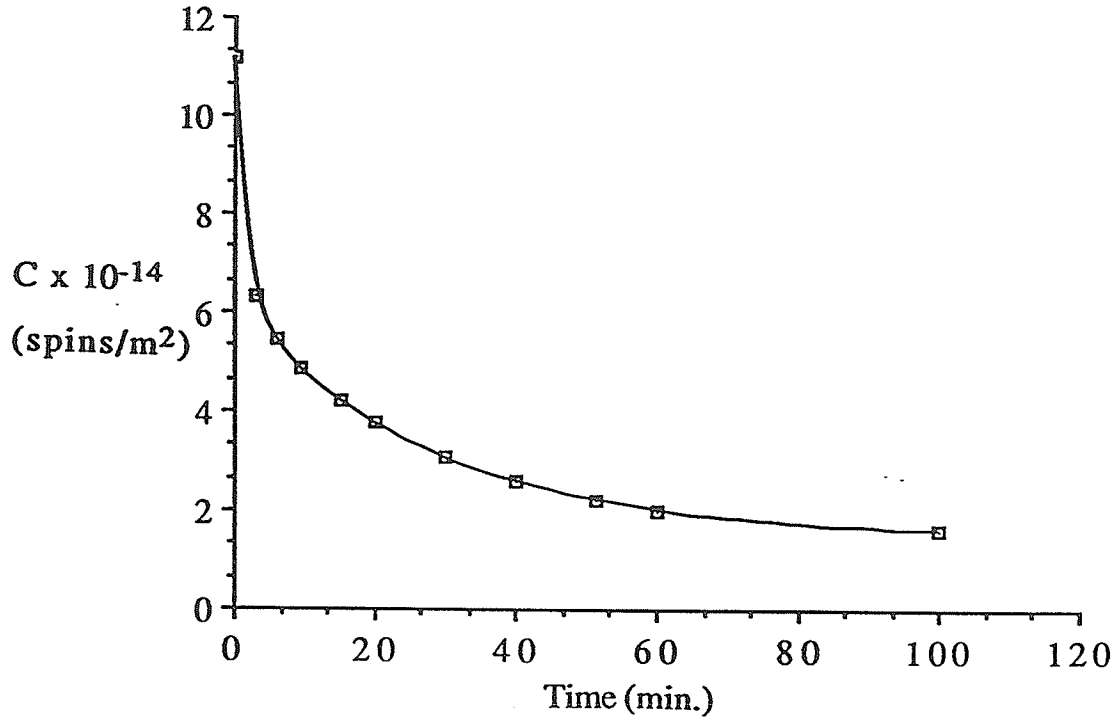

Figure 3-55: Experimental curve for the decay of ethyl radicals at -164°C (109 K) on PVGE3 loaded with 3.09 monolayers (2.61 x 10^{-3} mmole/mg) azoethane.

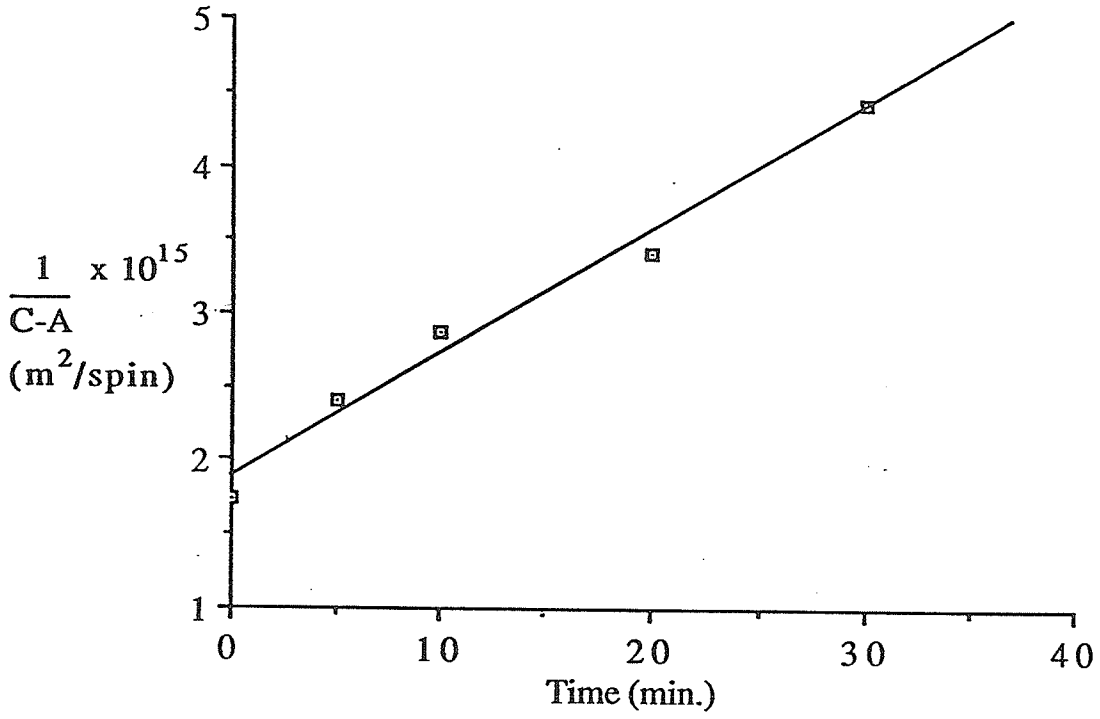

Figure 3-56: Modified second order plot for the decay of ethyl radicals at -183°C (90 K) on PVGE2 loaded with 2.01 monolayers (1.71 x10^{-3} mmole/mg) azoethane.

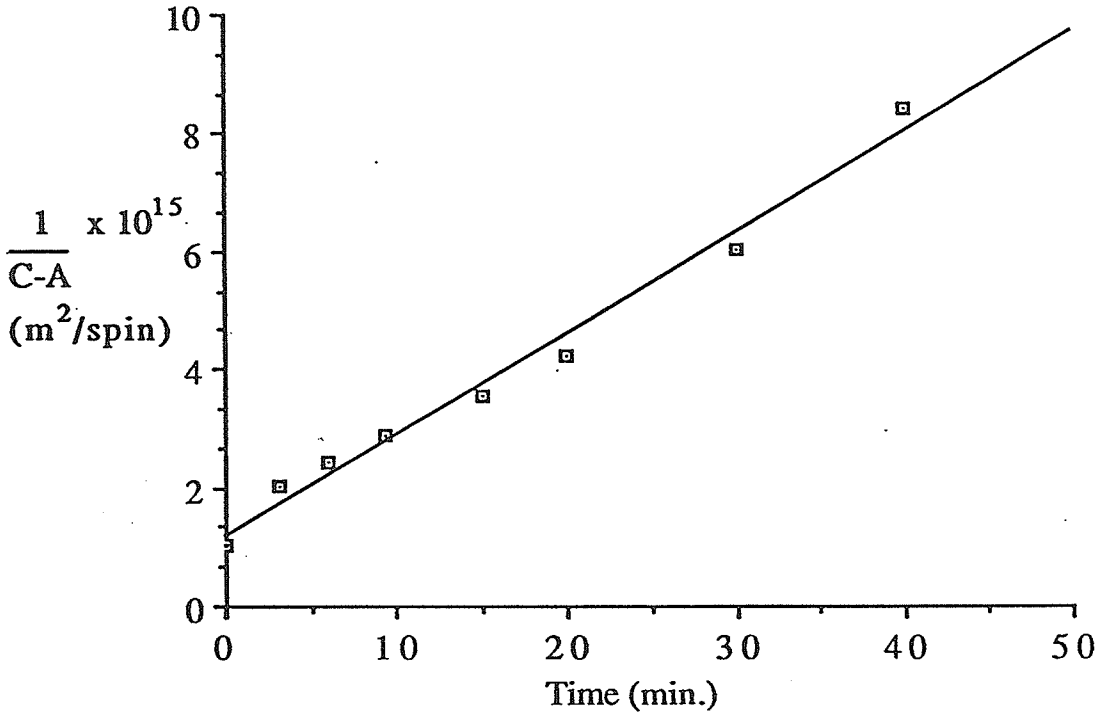

Figure 3-57: Modified second order plot for the decay of ethyl radicals at -164°C (109 K) on PVGE3 loaded with 3.09 monolayers (2.61×10^{-3} mmole/mg) azoethane.

shown in Figure 3-58. The heats of adsorption, ΔH_A, obtained from Figure 3-58 are given in Table 3-14.

As in the case of methyl radicals adsorbed on PVG samples, the decay of ethyl radicals on PVG samples was found not to follow a modified first order plot of ln (C-A) against time as illustrated in Figures 3-59 and 3-60 for experiment numbers 22 and 26, respectively. The calculated values of A were used to obtain the plots.

(b) Discussion

Results similar to those obtained for methyl radicals were obtained for ethyl radicals. The decay of the radicals did not give a good fit to a simple first or second order equation (Figures 3-43 and 3-44) but gave the best fit to Dole's second order equation (Figures 3-45 to 3-47). The applicability of the modified second order equation (Equation 3-8) to the kinetics data is also clearly demonstrated in Figures 3-56 and 3-57 as well as in Tables 3-12 and 3-13. Hence, it can be concluded that the decay of ethyl radicals is also second order in mobile, reactive radicals corresponding to a diffusion-controlled recombination process so that there are at least two adsorption sites for the decay of the radicals: one for weakly, physically adsorbed mobile radicals and the other for immobile, unreactive radicals. The PVG samples on which ethyl radicals were adsorbed were also pretreated at 750°C like those on which methyl radicals were adsorbed. Hence, the immobile, unreactive radicals might also be identified with siloxane bridge sites or caging sites in pores while the mobile reactive radicals might be asociated with the geminal hydroxyl groups as well B-OH groups on the PVG surface.

Table 3-14: Decay and adsorption energies for adsorbed ethyl radicals on PVG samples

PVG sample	Surface coverage (monolayer)	Decay activation energy, E_a (kJ mol^{-1})	Adsorption energy, $-\Delta H_A$ (kJ mol^{-1})	k_2 at 77 K (m^2 $spin^{-1}$ min^{-1})
PVGE1	2.10	3.77	6.63	1.08×10^{-16}
PVGE2*	2.01	5.23	5.19	3.30×10^{-17}
PVGE3	3.09	5.52	5.36	1.60×10^{-17}

*PVGE2 has some adsorbed water on the surface.

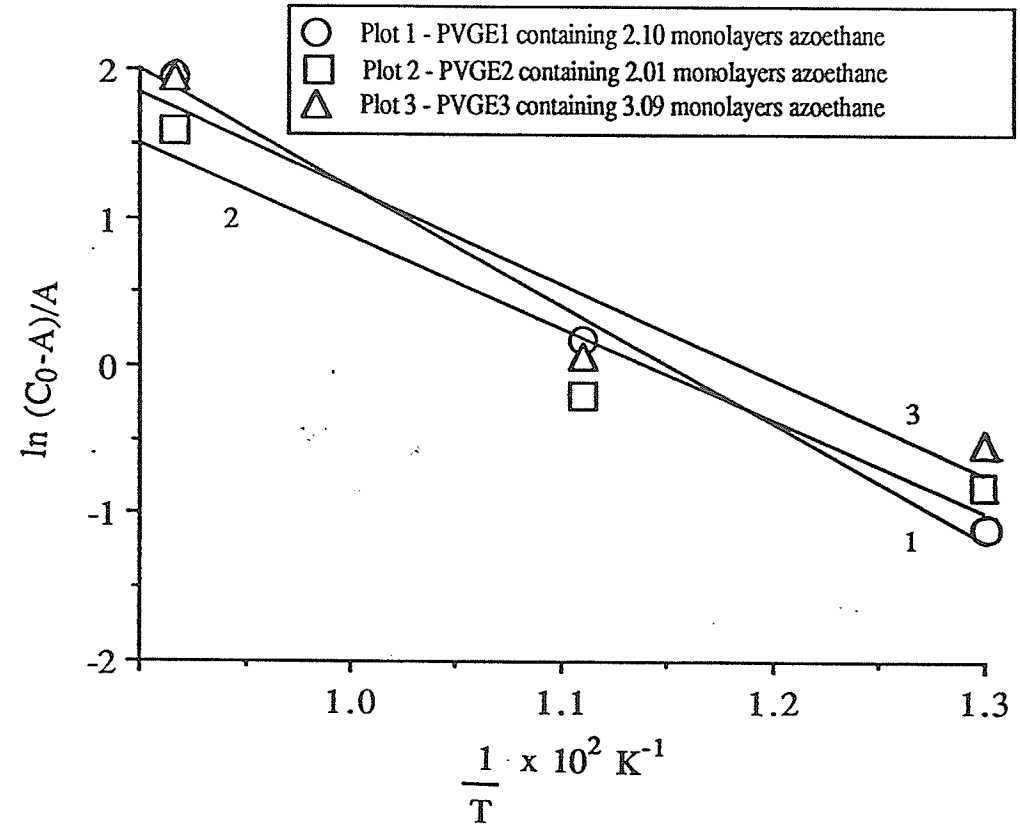

Figure 3-58: Plots of ln $(C_0-A)/A$ against 1/T for adsorbed ethyl radicals on PVG samples containing different amounts of azoethane. (Note that PVGE2 contains some surface adsorbed water).

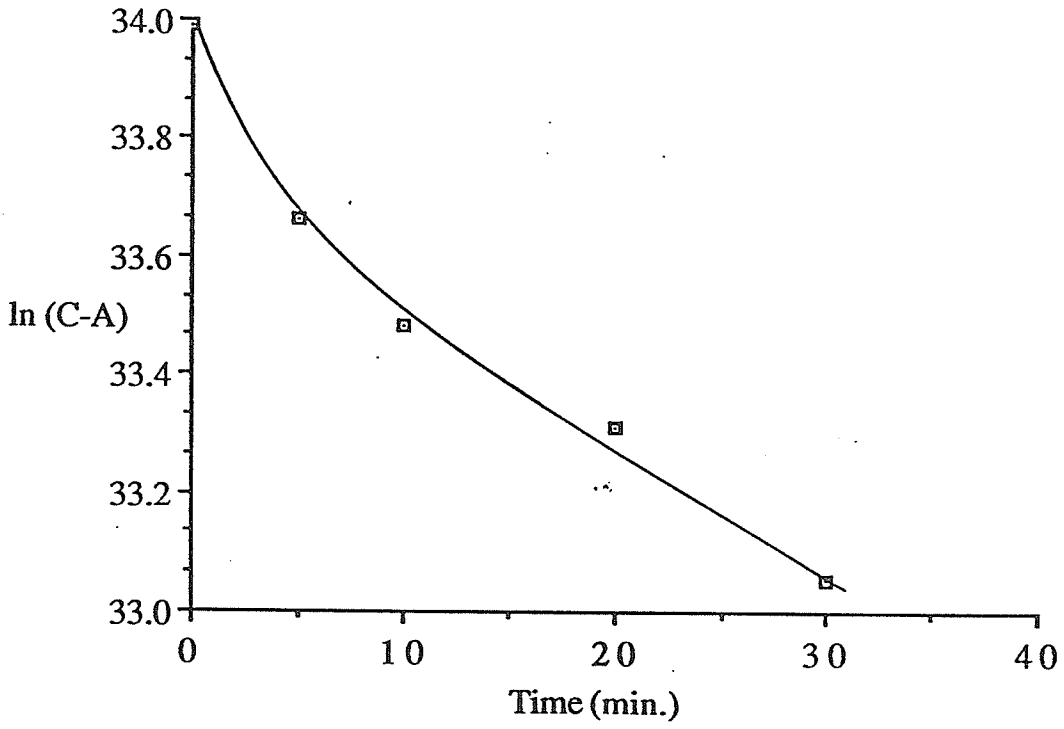

Figure 3-59: Modified first order plot for the decay of ethyl radicals at -183°C (90 K) on PVGE2 loaded with 2.01 monolayers (1.71×10^{-3} mmole/mg) azoethane.

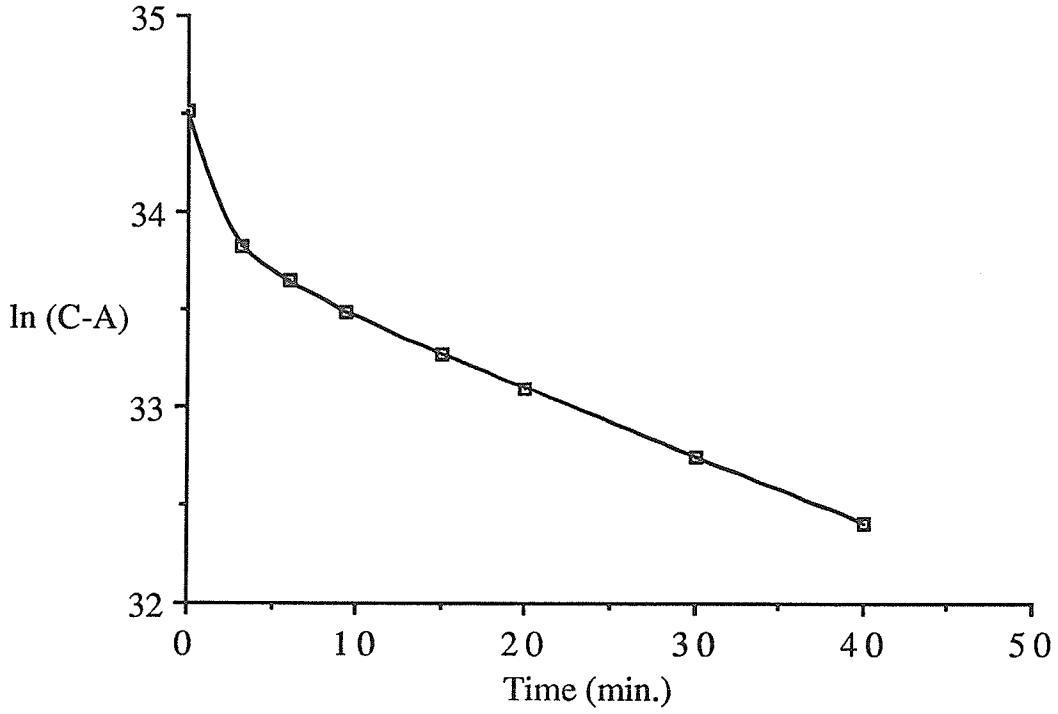

Figure 3-60: Modified first order plot for the decay of ethyl radicals at -164°C (109 K) on PVGE3 loaded with 3.09 monolayers (2.61 x 10^{-3} mmole/mg) azoethane.

The activation energies for the decay of ethyl radicals between 77 K and 109 K as given in Tables 3-9 to 3-11 are much higher than the value of zero obtained by Arthur[42] as well as by Dobis and Benson[43] for the recombination reaction of the radicals in the gas phase. Moreover, these values are comparable with the value of 4·2 kJ mol^{-1} obtained by Bader and Gesser[71] for the recombination of hydrogen atoms on Vycor glass. It therefore follows that ethyl radicals can also be stabilized on the surface of porous Vycor glass as previously shown.[23,68,70] Figure 3-61 also shows clearly that there is no significant difference between the activation energies obtained for ethyl radical decay and those obtained for methyl radical decay. However, the rate constants obtained for the decay of ethyl radicals as listed in Tables 3-9 to 3-11 are generally slightly higher than the values obtained for the decay of methyl radicals (Tables 3-1 to 3-3) implying that ethyl radicals are slightly less stable on the PVG surface than methyl radicals. This behaviour can be explained in terms of the orientation of the radicals and their motion in the adsorbed state. Pariiskii et. al.[22] have reported that for methyl radicals, there is a loss of two rotational degrees of freedom leaving only the three-fold symmetry axis of rotation. These workers[22] then thought of methyl radicals as being bound to the surface by a one-electron bond due to the attraction of the unpaired electron to the adsorbent. Kazanskii and Pariiskii[23] have also shown ethyl radicals to be bound to the surface at one end only. These workers observed that the adsorbed radicals are similar to free radicals in gaseous and liquid phases and that their free electron took no appreciable part in forming a chemical bond with the surface. Their interpretation of the

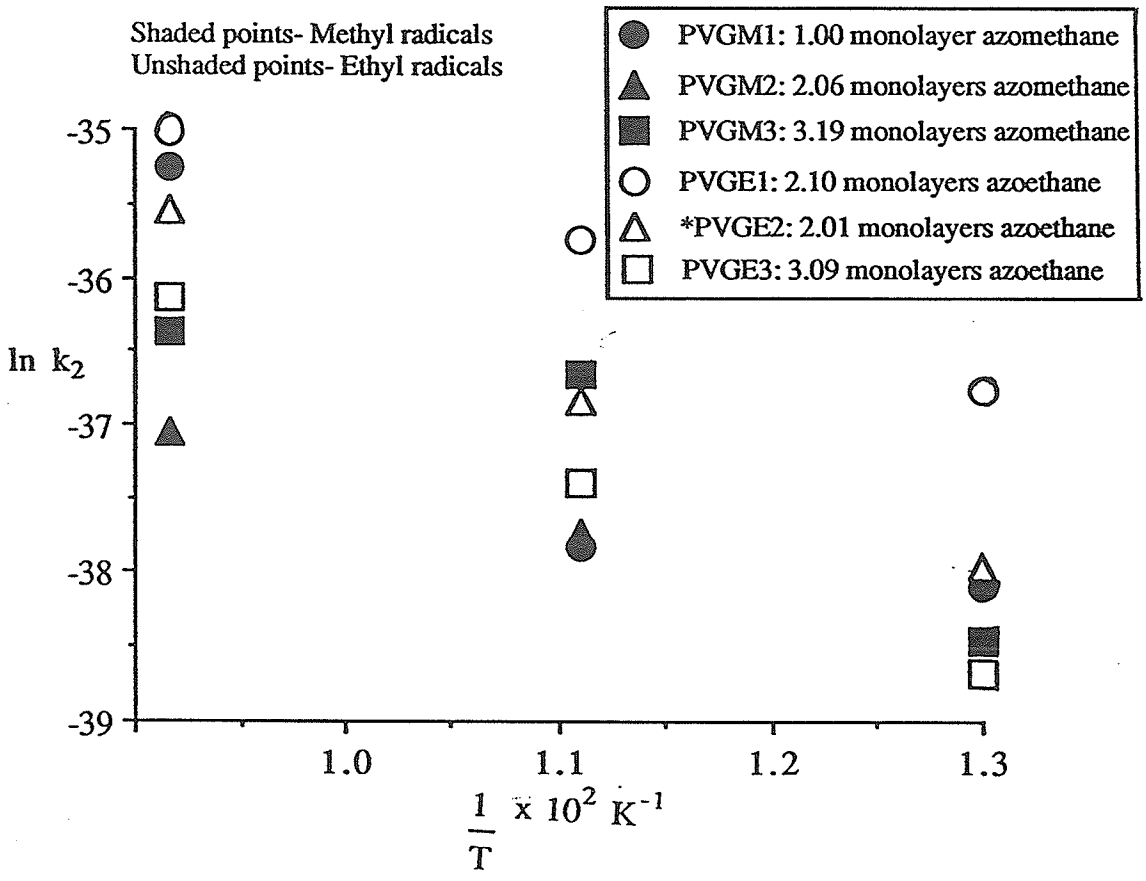

Figure 3-61: Arrhenius plot for the decay of both methyl and ethyl radicals on the various PVG samples containing different amounts of adsorbed azomethane and azoethane. (*PVGE2 contains some surface adsorbed water).

spectrum of adsorbed ethyl radical showed that the radical "lies on the adsorbent surface on its side" and that there is rotation of its CH_3 and CH_2 groups relative to each other. The ethyl radical was also postulated to "roll" along the surface. More recently, Shiga and Lund[83] have also reported the results of their analysis of the asymmetric ESR spectra of methyl and ethyl radicals adsorbed on silica gel which indicated that at 77 K the methyl radicals rotate about the axis perpendicular to the plane of the radical, whereas the ethyl radicals rotate about the C-C bond axis. Although the results of Shiga and Lund[83] indicate that the adsorbed methyl and ethyl radicals are both axially symmetric, the results obtained earlier by Pariiskii et. al.[22] and by Kazanskii and Pariiskii[23] also show that there is the possibility of mobile, reactive ethyl radicals being less strongly bound to the surface than methyl radicals thereby making them to decay faster on the surface by recombination, as observed in this work.

Like the results obtained for methyl radicals, Tables 3-9 to 3-11 indicate that the ratio of the concentration of mobile, reactive ethyl radicals to the concentration of immobile, unreactive radicals, $(C_0\text{-}A)/A$, increases with increase in temperature implying that larger number of ethyl radicals also decay at the higher temperatures. The presence of some unreactive radicals at the higher temperatures also confirms further the possibility of stabilizing the radicals over a wide range of temperatures. It is also observed in Tables 3-9 to 3-11 that the values of the ratio $(C_0\text{-}A)/A$ for ethyl radicals are generally much higher than the values of the ratio for methyl radicals. This behaviour implies that a greater number of

immobile ethyl radicals than immobile methyl radicals are converted to the corresponding mobile, reactive radicals when the temperature is raised which is consistent with the observed faster decay of ethyl radicals on the surface.

It is shown clearly in Table 3-14 that the adsorption energy, ΔH_A, of ethyl radicals on PVG surface decreases slightly when the surface coverage is raised from 2 to 3 monolayers implying a slightly weaker bonding of the immobile radicals to the siloxane bridge sites at the higher coverage. This is, however, inconsistent with the observation that the radicals decay at a slightly lower rate on the higher-coverage surface since the weaker bonding of the immobile radicals on this surface should make it possible for more of the radicals to become available for decay on the surface by conversion to mobile, reactive radicals. Since the radicals are further away from surface adsorption sites, it is expected too that they should be more readily available for decay on the surface but the opposite seems to be true probably because the radicals are simply just rolling along the surface thereby slowing down their decay by recombination. Furthermore, as explained later, the radicals are probably not able to react faster on the higher-coverage surface, in spite of the smaller adsorption energy, because of the presence of more azoethane molecules on the surface that constitutes a barrier to the interaction of the radicals with each other. Table 3-14 also shows that the adsorption energy of ethyl radicals on PVGE2 surface loaded with 2 monolayers azoethane and containing some adsorbed water on the surface is lower than the value obtained for the radicals on PVGE1 loaded with approximately the same amount of azoethane. This is

also not in agreement with the observed slower decay rate constant, k_2, obtained for the radicals on PVGE2. As mentioned later, at the lower heat pretreatment of PVGE2 sample, the presence of adsorbed water on the surface must have introduced vicinal hydroxyl groups and removed some geminal hydroxyl groups and all the B-OH groups present on the surface. Thus, both the smaller adsorption energy and lower decay rate on PVGE2 may be attributed to their possible interaction with the silanol groups present on the surface. There is, however, no significant difference between the adsorption energy obtained for ethyl radicals on PVGE2 and that obtained for the radicals on PVGE3 loaded with about 3 monolayers azoethane. It is also observed from Tables 3-5 and 3-14 that the adsorption energies obtained for ethyl radicals are much higher than those obtained for methyl radicals which is not in agreement with the slightly faster decay rate constants obtained for ethyl radicals. Thus, the slightly faster decay of ethyl radicals on the surface might probably have resulted from not only recombination on the surface but also from additional interaction with both geminal hydroxyl and B-OH groups present on the surface which is consistent with the observed higher adsorption energy. Table 3-14 also clearly shows that the values of k_2 for ethyl radicals are much lower than the value of 1.1×10^{-14} m^2 $atom^{-1}$ min^{-1} obtained by Bader and Gesser[71] for hydrogen atoms. This is expected since ethyl radical has a much larger size than hydrogen atom.

From the preceding discussion, it is clear that the same mechanism given in section 3.3.1 for the decay of methyl radicals on PVG surface can be proposed for the decay of ethyl radicals. So, ethyl

radicals also recombine on the surface via the following kinetic scheme:

$$(C_2H_5)_2N_2 + h\nu \longrightarrow 2C_2H_5 + N_2 \qquad 3\text{-}22$$

$$C_2H_5 \xrightarrow{77\ K} (C_2H_5)_A \qquad 3\text{-}23$$

$$C_2H_5 \xrightarrow{77\ K} (C_2H_5)_I \qquad 3\text{-}24$$

$$(C_2H_5)_A \rightleftharpoons C_2H_5 \qquad 3\text{-}25,\ 3\text{-}26$$

$$C_2H_5 + C_2H_5 \longrightarrow C_4H_{10} \qquad 1\text{-}15$$

$$(C_2H_5)_I \longrightarrow (C_2H_5)_A \qquad 3\text{-}27$$

where C_2H_5, $(C_2H_5)_A$ and $(C_2H_5)_I$ are all surface adsorbed radicals; C_2H_5 is the mobile adsorbed radical while $(C_2H_5)_A$ exists as a constant (but temperature dependent) concentration of adsorbed, immobile, unreactive radicals. $(C_2H_5)_A$ are again active immobile radicals capable of being converted to mobile reactive radicals at higher temperatures while $(C_2H_5)_I$ are inactive immobile radicals which are more strongly adsorbed than $(C_2H_5)_A$ but which can be converted to $(C_2H_5)_A$ at higher temperatures. Similarly, E_a for ethyl radicals is identified with reaction 1-15 and $-\Delta H_A$ with reaction 3-25.

It is also clear that the activation energies for the decay of ethyl radicals increase slightly with increase in surface loading of the azoethane from two monolayers on PVGE1 (Table 3-9) to three monolayers on PVGE3 (Table 3-11). This observation indicates that the ethyl radicals are probably not interacting with the azoethane molecules and since it is already assumed that the rate controlling step is the recombination of the radicals on the surface, the presence

of more azoethane molecules on the surface at a higher surface coverage would constitute a barrier to the interaction of the ethyl radicals with each other thereby slowing down the decay by recombination on the surface of the Vycor glass. Unlike in the case of methyl radicals, the activation energies did not vary significantly with increase in temperature. It should also be noted that there is no significant difference between the activation energies obtained for the decay of ethyl radicals on PVGE2 (Table 3-10) having some adsorbed water on the surface and loaded with about two monolayers of azoethane and those obtained for the decay of the radicals on PVGE3 (Table 3-11) loaded with about three monolayers. However, the variation of activation energies with both temperature and surface coverage needs to be studied over a wider range of temperatures and surface coverages in order to obtain a clearer picture of the variation.

Lastly, the results of the decay kinetics of ethyl radicals on PVGE2 sample having some adsorbed water on the surface and loaded with 2·01 monolayers azoethane (Table 3-10) indicate clearly that the value of 5·23 kJ mol^{-1} for E_a is higher than, and the rate constants, k_2, at the three temperatures lower than the corresponding values for the decay of the radicals on PVGE1 which was pretreated at 750°C prior to loading with approximately the same amount of azoethane (Table 3-9). At the lower heat pretreatment of PVGE2 sample, the presence of adsorbed water on the surface must have introduced vicinal hydroxyl groups and there also fewer geminal hydroxyl groups and no B-OH groups present on

the surface as already shown previously.[9,81] The lower rates of decay of ethyl radicals on PVGE2 may therefore be attributed to their possible interaction with the silanol groups present on the surface. However, this behaviour of ethyl radicals on PVG sample having some adsorbed water on the surface needs to be studied in more details for clearer understanding of the effect of surface adsorbed water on the decay of the radicals.

CHAPTER 4
CONCLUSIONS

4.1 Conclusions

The following conclusions are evident from the foregoing results and discussions presented in Chapter 3.

(1) Methyl (or ethyl) radicals can be produced and stabilized on the surface of porous Vycor glass by UV photolysis of adsorbed azomethane (or azoethane) at 77 K and the stabilization can be achieved over a wide range of temperatures due to the possibility of existence of a continuum of trapping potentials on the surface as evident from the cascade type of decay observed in this work. It is worthy of mention that this is the first time of using azoethane as a source of ethyl radicals for stabilization on the surface at low temperatures. Little or no work seems to have been done too on the ESR study of the decay kinetics of ethyl radicals adsorbed on surfaces. The cascade type of decay has also not been previously reported for ethyl radicals.

(2) Within the period of irradiation in this work, the build-up of methyl and ethyl radicals does not approach saturation probably due to the fact that only a very small fraction of the azomethane and azoethane molecules decomposed to produce the radicals during photolysis.

(3) It is slightly more difficult to generate ethyl radicals by UV photolysis of azoethane than methyl radicals by irradiation of azomethane probably due to a lower quantum yield for the photodecomposition of azoethane adsorbed on the PVG surface than the value for the photodecomposition of azomethane.

(4) Ethyl radicals are formed much faster and in larger quantity when they are left to decay overnight at 77 K after several hours of irradiation. This is attributed to the possible addition reaction of the radicals with azoethane molecules during the decay at 77 K to produce tetraethylhydrazine so that when the PVG sample containing the surface stabilized radicals are subsequently re-irradiated, ethyl radicals are probably formed from tetraethylhyrazine molecules rather than from azoethane molecules. On the other hand, the rate of formation of methyl radicals remains almost the same when they are left to decay for several hours at 77 K after previous irradiation for a certain period of time implying that the radicals are probably still formed from the azomethane molecules during re-irradiation.

(5) Methyl radicals are generated much faster and in larger quantity on a PVG surface containing less than 1 monolayer (about 0.1 monolayer) azomethane than on a surface containing more than 1 monolayer azomethane. This is interpreted to be probably due to the possibility of the radicals decaying much more slowly during irradiation on the low-coverage surface in support of experimental observation. Furthermore, the observed gradual increase in the percentage decomposition of azomethane molecules during irradiation might contribute to the higher rate of formation of the radicals on the low-coverage surface.

(6) The decay data obtained in this work for methyl and ethyl radicals gave the best fit to Dole's revised second order kinetics equation which was derived for the decay of free radicals in polymers from a second order equation modified on the assumption that a fraction of the radicals recombine by a second order

mechanism while the remaining radicals are completely unreactive. It is therefore postulated in this work that the decay of both radicals is second order in mobile reactive radicals, consistent with a diffusion-controlled recombination process. Thus, two types of surface adsorbed radicals are identified for each temperature viz the weakly, physically adsorbed mobile radicals and immobile, unreactive radicals. The immobile, unreactive radicals are identified with siloxane bridge sites or stabilization by caging effects in pores while the mobile reactive radicals are associated with the large number of geminal hydroxyl and B-OH groups on the PVG surface pretreated at 750°C.

(7) The decay of ethyl radicals on the PVG surface is found to be slightly faster than the decay of methyl radicals. This is explained to be due to the possibility of ethyl radicals being less strongly bound to the surface than methyl radicals since earlier findings[23] have indicated that adsorbed ethyl radicals are similar to free radicals in gaseous and liquid phases and that their free electron takes no appreciable part in forming a chemical bond with the surface. These earlier findings also show that the adsorbed ethyl radicals lie on their side on the adsorbent surface and that they "roll" along the surface. On the other hand, earlier studies[22] have also shown that for methyl radicals, there is a loss of two rotational degrees of freedom leaving only the 3-fold symmetry axis and the radicals are then postulated to be bound to the surface by a one-electron bond due to the attraction of the unpaired electron to the adsorbent. The slightly faster decay of ethyl radicals is also attributed to additional interaction with both geminal hydroxyl and B-OH groups present on

the surface in agreement with the observed higher adsorption energies obtained for the radicals. However, there seems to be no significant difference between the activation energies for the decay of ethyl radicals and those for the decay of methyl radicals.

(8) Values of $(C_0-A)/A$, the ratio of mobile, reactive radicals concentration to immobile, unreactive radicals concentration are found to increase with increase in temperature for both methyl and ethyl radicals implying that some of the unreactive radicals are released from their sites and become converted to reactive radicals so that greater number of the radicals decay at the higher temperatures.

(9) In some experiments, the activation energies for the decay of methyl radicals are observed to vary erratically with temperatures. Nevertheless, the average activation energies for the decay of the radicals between 77 K and 109 K which vary from 3.2 to 7.3 kJ mol^{-1}, are found to decrease slightly with increase in surface coverage of azomethane on the PVG samples from 0.1 monolayer to 3 monolayers. These observations are attributed to the possible association reaction between the radicals and the adsorbed azomethane molecules. Least squares values of activation energies for the decay of ethyl radicals between 77 K and 109 K are found to range from 3·8 to 5·5 kJ mol^{-1}. In contrast to the results obtained for the decay of methyl radicals, the activation energies for the decay of ethyl radicals are observed not to vary significantly with increase in temperature. The activation energies for ethyl radical decay are also found to increase slightly with increase in surface coverage of azoethane from 2 monolayers to 3 monolayers making the decay to

be slower at the higher coverage. This is explained to be due to the fact that the presence of more azoethane molecules on the PVG surface at the higher coverage probably constitutes a barrier to the interaction of ethyl radicals with each other thereby slowing down the decay by recombination.

(10) The adsorption energies are found to decrease with increase in surface coverage for both radicals which is consistent with the increase in decay rate constant with increase in surface coverage observed for methyl radicals but inconsistent with decrease in rate constant with increase in surface coverage observed for ethyl radicals. In addition to the possibility of more azoethane molecules at the higher coverage constituting a barrier to the interaction of ethyl radicals, the situation in the case of ethyl radicals is explained to be probably due to the fact that the radicals are simply rolling along the surface thereby slowing down their recombination reaction while the observation in the case of methyl radicals is expected since the radicals at the higher-coverage surface are further away from the surface adsorption sites and are therefore readily available for recombination on the surface.

(11) Lastly, it is observed that the presence of adsorbed water on a PVG surface pretreated at 500°C increases the activation energy for the decay of ethyl radicals thereby slowing down the rate of decay of the radicals. The presence of adsorbed water on the surface is also found to lower the adsorption energy for ethyl radicals. These observations are attributed to the possible interaction of the radicals with the silanol groups present on such a surface.

4.2 Suggestions for further work

It is suggested that the following studies could be done in order to obtain a better understanding of the growth and decay characteristics of both radicals as well as their reactions on surfaces.

Azomethane and azoethane adsorbed on porous Vycor glass could be UV photolyzed at 77 K for a much longer time to see if there would be any approach to saturation in the build-up of methyl and ethyl radicals on the surface. One could also UV irradiate tetraethylhydrazine, the product of the possible addition reaction of ethyl radicals with azoethane, at 77 K to see if ethyl radicals would be produced, and if produced, to see whether they would be formed faster than by the irradiation of azoethane. It would be good too to see if tetraethylhydrazine could be detected on GC/MS after photolysis of azoethane.

The variation of activation energies for the decay of both radicals needs to be studied in greater details by investigating the decay over a wider range of temperatures and surface coverages.

The effect of adsorbed water on the decay kinetics of both methyl and ethyl radicals on surfaces pretreated at different low temperatures should be studied more closely. The decay of the radicals on such surfaces should also be investigated over a wide range of temperatures and surface coverages. One could also study the effect of a pre-adsorbed gas such as neopentane on the decay kinetics of both radicals.

It would be interesting too to compare the decay characteristics of both radicals on different surfaces. The investigation of the decay

kinetics of the radicals on the surface could therefore be extended to surfaces like the transparent aerogels of silica and alumina.

It would also be good if the compound CH_3-N=N-C_2H_5, could be produced, adsorbed on different surfaces and UV irradiated at 77 K to see what radicals would be generated on the surfaces and what the decay characteristics of the stabilized radicals would be.

More attempts could be made to generate abnormal methyl radicals from azomethane adsorbed on the surface. Efforts should also be made to produce abnormal ethyl radicals by UV irradiation of azoethane adsorbed on the surface. If these abnormal radicals could be produced, one could then proceed to studying their decay kinetics on the surface.

Unsuccessful attempts were made in this work to generate methylperoxy and ethylperoxy radicals by addition of oxygen to adsorbed methyl and ethyl radicals, respectively. More efforts could be made to produce these peroxy radicals for the purpose of studying their decay characteristics on the surface.

APPENDIX I

Measurement of absolute concentrations of the radicals

The numerical double integration method of Wyard[67] was used to obtain the areas of the first derivative ESR signals of methyl, ethyl and the standard DPPH radicals. In this method, the abscissa of the first derivative spectrum is divided into n equal divisions separated by a distance d and the value h_r of the ordinate at the centre of each division is measured (see Figure AI-1). The height of the absorption peak at the end of the p^{th} division is then approximately,

$$I_p = d \sum_{r=1}^{p} h_r \qquad \text{AI-1}$$

Thus, the absorption peak is approximated by a polygon with n units and whose area, which is approximately the required double integral of the first derivative curve, is given by:

$$A = {}^1/_2\, d^2\{h_1 + (2h_1 + h_2) + (2h_1 + 2h_2 + h_3) + \ldots + (2h_1 + 2h_2 + \ldots + 2h_{n-1} + h_n)\}$$

$$= {}^1/_2\, d^2 \sum_{r=1}^{n} (2n - 2r + 1)h_r \qquad \text{AI-2}$$

To correct for any base-line drift, the magnitude $({}^1/_2\, nd^2)\sum_{r=1}^{n} h_r$ is substracted from the total area given in Equation AI-2 so that the corrected value for the double integral becomes:

$$A = {}^1/_2\, d^2 \sum_{r=1}^{n} (n - 2r + 1)h_r \qquad \text{AI-3}$$

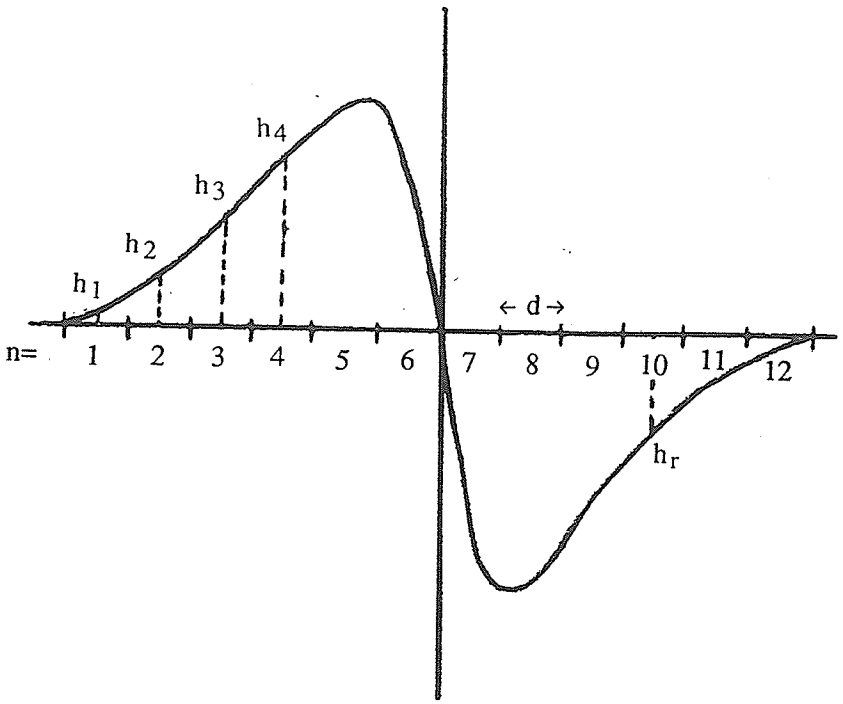

Figure AI-1: Division of the first derivative curve into equal parts for numerical double integration using the method of Wyard.[67]

Equation AI-3 was used to obtain all double integrations in this work. DPPH solution in benzene containing $7{\cdot}71 \times 10^{16}$ spins was used as standard. This was prepared by dissolving 0·1010 g DPPH in 10 mL benzene and withdrawing a 5 μL portion of the solution with a microsyringe.

Absolute concentration of methyl radicals

The area, A_{DPPH}, of the ESR of DPPH standard containing $7{\cdot}71 \times 10^{16}$ spins was calculated to be 1679552 ± 62891 mm^2 using Equation AI-3. The error in the area is the average deviation of three measurements on three different signals recorded under identical conditions. The three DPPH signals were obtained under the same conditions used for the study of methyl radicals (Table 2-1).

A sample of methyl radicals on PVGM3 loaded with 3·19 monolayers ($3{\cdot}80 \times 10^{-3}$ mmole/mg) azomethane was used as a representative sample of the radicals for the purpose of obtaining absolute radical concentrations during kinetic measurements. The ESR signal of the radicals was obtained under the standard conditions (Table 2-1). The double integration of line 3 (i.e. the second line from the low field side) using Equation AI-3 gave an area, A_{Me}, of 341442 mm^2 for the line. The peak to peak height of this line was measured to be 116·5 mm.

Using the intensity ratio of 1:3·7:3·5:1·1 obtained in this work, the total area, $A_{T(Me)}$, of the absorption spectrum of methyl radicals on PVGM3 is then given by:

$$A_{T(Me)} = A_{Me} \times \frac{9.3}{3.7} \text{ mm}^2$$

$$= 341442 \times \frac{9.3}{3.7} = 858219 \text{ mm}^2.$$

The number of methyl radical spins, N_{Me}, is then obtained from

$$N_{Me} = \frac{A_{T(Me)}}{A_{DPPH}} \times 7.71\times10^{16} \text{ spins}$$

$$= \frac{858219}{1679552} \times 7.71\times10^{16} \text{ spins}$$

$$= 3.94 \times 10^{16} \text{ spins.}$$

Since the surface area, S_{PVGM3}, of PVGM3 sample containing the radicals = 15·6 m^2, the concentration, C_{Me}, of the radicals in spins/m^2 is obtained from:

$$C_{Me} = \frac{N_{Me}}{S_{PVGM3}} = \frac{3.94\times10^{16}}{15.6} \text{ spins/m}^2$$

$$= 2.52\times10^{15} \text{ spins/m}^2.$$

Alternative calculation

Using the theoretical intensity ratio of 1:3:3:1, the total area, $A_{T(Me)}$, becomes:

$$A_{T(Me)} = A_{Me} \times \frac{8}{3} \text{ mm}^2$$

$$= 341442 \times \frac{8}{3} \text{ mm}^2$$

$$= 910512 \text{ mm}^2.$$

$$\therefore N_{Me} = \frac{A_{T(Me)}}{A_{DPPH}} \times 7.71 \times 10^{16} \text{ spins}$$

$$= \frac{910512}{1679552} \times 7.71 \times 10^{16} \text{ spins}$$

$$= 4.18 \times 10^{16} \text{ spins.}$$

$$\therefore C_{Me} = \frac{N_{Me}}{S_{PVGM3}} = \frac{4.18 \times 10^{16}}{15.6} \text{ spins/m}^2$$

$$= 2.68 \times 10^{15} \text{ spins/m}^2.$$

The concentration obtained using the intensity ratio obtained in this work was then only 6·35% different from the value obtained using the theoretical ratio. So, the theoretical ratio was conveniently used to obtain all absolute methyl radical concentrations.

During kinetic measurements, the peak to peak heights, I_{Me}, of the first derivative ESR signals were converted to absolute radical concentrations, C_{Me}, as follows:

$$C_{Me} = \frac{I_{Me} \times 4.18 \times 10^{16}}{116.5 \times S_{PVG}} \text{ spins/m}^2$$

where S_{PVG} is the surface area of the particular PVG sample on which the radicals were adsorbed.

The raw data for the spin concentrations of methyl radicals obtained during kinetic measurements for experiments 1 to 17 in Tables 3-1 to 3-3 and 3-6 to 3-7 are tabulated in Tables AI-1 to AI-7.

Table AI-1: Decay of methyl radicals on PVGM1 containing 1·00 monolayer ($1·19 \times 10^{-3}$ mmole/mg) azomethane at different temperatures

Decay at -196°C (77 K)		Decay at -183°C (90 K)*		Decay at -164°C (109 K)*	
Time (min.)	C x 10^{-15} (spins/m^2)	Time (min.)	C x 10^{-15} (spins/m^2)	Time (min.)	C x 10^{-14} (spins/m^2)
0	2·83	0	2·22	0	11·3
5·00	2·75	5·00	1·92	3·01	6·81
11·0	2·63	10·0	1·80	6·00	6·12
20·0	2·59	15·0	1·66	12·5	5·20
30·0	2·50	20·0	1·57	20·0	5·01
40·0	2·42	30·0	1·46	30·0	4·88
50·0	2·42	40·0	1·36	40·0	4·55
60·0	2·40	50·0	1·33	50·0	4·35
70·0	2·37	60·0	1·26	60·0	4·37
80·0	2·32	70·0	1·18	70·0	4·14
90·0	2·28	80·0	1·18		
100	2·22	90·0	1·13		

*ESR measurements were recorded at liquid nitrogen temperature, -196°C (77 K).

Table AI-2: Decay of methyl radicals on PVGM2 containing 2·06 monolayers ($2{\cdot}45 \times 10^{-3}$ mmole/mg) azomethane at different temperatures

Decay at -183°C (90 K)*		Decay at -164°C (109 K)*	
Time (min.)	C x 10^{-15} (spins/m^2)	Time (min.)	C x 10^{-15} (spin/m^2)
0	4·86	0	3·68
3·00	4·57	3·00	2·99
7·00	4·38	7·00	2·74
13·0	4·33	13·0	2·66
20·0	4·10	20·0	2·46
30·0	3·85	30·0	2·24
40·0	3·80	40·0	2·21
50·0	3·71	50·0	2·14
60·0	3·68	60·0	2·09
70·0	3·68	66·5	2·08

*ESR measurements were recorded at liquid nitrogen temperature, -196°C (77 K).

Table AI-3: Decay of methyl radicals on PVGM3 containing 3·19 monolayers ($3{\cdot}80 \times 10^{-3}$ mmole/mg) azomethane at different temperatures

Decay at -196°C (77 K)		Decay at -183°C (90 K)*		Decay at -164°C (109 K)*	
Time (min.)	C x 10^{-15} (spins/m^2)	Time (min.)	C x 10^{-15} (spins/m^2)	Time (min.)	C x 10^{-15} (spins/m^2)
0	4·02	0	2·97	0	1·92
5·00	3·82	4·00	2·54	4·00	1·52
10·0	3·69	8·00	2·35	8·00	1·44
15·0	3.58	12·0	2·26	12·0	1·35
19·0	3·55	16·0	2·22	16·0	1·32
29·0	3·45	22·0	2·14	22·0	1·28
39·0	3·26	30·0	2·04	30·0	1·22
49·0	3·18	50·0	2·01	40·0	1·15
60·0	3·15	60·0	1·97	50·0	1·13
70·0	3·11	70·0	1·93	60·0	1·13
80·0	3·02	80.0	1·92	70·0	1.10
90·0	2.95				
100	2·97				

*ESR measurements were recorded at liquid nitrogen temperature, -196°C (77 K).

Table AI-4: Decay of methyl radicals at 77 K on PVGM4, PVGM6 and PVGM6d containing about 2 monolayers azomethane

Decay on PVGM4 containing 2.01 monolayers azomethane		Decay on PVGM6 containing 2.01 monolayers azomethane		Decay on PVGM6d containing 2.02 monolayers azomethane	
Time (min.)	C x 10^{-15} (spins/m^2)	Time (min.)	C x 10^{-15} (spins/m^2)	Time (min.)	C x 10^{-15} (spins/m^2)
0	2.63	0	3.55	0	3.70
5	2.54	8	3.46	8	3.47
10	2.54	20	3.41	20	3.27
15	2.48	30	3.29	30	3.35
20	2.48	40	3.24	41	3.23
30	2.41	50	3.12	50	3.22
40	2.41	60	3.16	60	3.21
50	2.33	70	3.12	70	3.09
62	2.30	80	3.07	80	3.07
70	2.28	90	3.03	95	3.05
80	2.27	100	2.97	106	3.07
90	2.24	120	2.96	120	3.00
100	2.22	140	2.95	140	3.04
120	2.15	160	2.90	160	3.01
140	2.19	184	2.82	180	2.82
160	2.16	213	2.84	200	2.83
180	2.15	240	2.76	220	2.84
200	2.10	255	2.76	250	2.88
220	2.09	460	2.76		
240	2.07				
270	2.02				

Table AI-5: Long time decay of methyl radicals at 77 K on PVGM4, PVGM6 and PVGM6d containing about 2 monolayers azomethane

Decay on PVGM4 containing 2.01 monolayers azomethane		Decay on PVGM6 containing 2.01 monolayers azomethane		Decay on PVGM6d containing 2.02 monolayers azomethane	
Time (hr.)	C x 10^{-15} (spins/m^2)	Time (hr.)	C x 10^{-15} (spins/m^2)	Time (hr.)	C x 10^{-15} (spins/m^2)
0	3.06	0	3.55	0	3.70
17.5	2.17	7.67	2.76	4.2	2.88
22.1	2.09	21.7	2.38	18.0	2.43
26.8	2.07	31.7	2.31	25.0	2.24
42.2	1.96	48.7	2.25	42.5	2.11
47.5	1.90	57.9	2.16	49.0	2.06
66.0	1.81	74.6	2.04	69.8	1.98
71.2	1.79	81.6	2.04	76.6	1.96
90.0	1.78	94.4	2.02	95.6	1.90
95.2	1.68	99.9	2.01	103.8	1.86
99.7	1.68	117.7	2.02	115.3	1.86
115.5	1.68	127.3	1.95	122.9	1.81
126.4	1.67	141.4	2.03	138.2	1.77
147.8	1.66	147.8	1.97		
		166.4	1.94		
		175.6	1.95		

Table AI-6: Decay of methyl radicals on PVG samples containing about 0.1 monolayer azomethane at different temperatures

Decay at -196°C (77 K) on PVGM5d containing 0.103 monolayer azomethane		Decay at -183°C (90 K)* on PVGM5d_2 containing 0.103 monolayer azomethane		Decay at -164°C (109 K)* on PVGM5d_2 containing 0.103 monolayer azomethane	
Time (min.)	C x 10^{-15} (spins/m^2)	Time (min.)	C x 10^{-15} (spins/m^2)	Time (min.)	C x 10^{-15} (spins/m^2)
0	9.15	0	10.4	0	11.5
20	8.65	10.0	9.00	10.0	2.31
30	8.44	30.0	8.37	30.0	1.88
70	7.79	50.1	7.76	50.0	1.68
85	7.53	75.1	8.12	76.7	1.58
100	7.35	100.0	7.91	95.0	1.54
130	7.15	125.0	7.69	120.0	1.50
145	7.08	150.0	6.95	145.0	1.47
160	6.95	180.0	6.85	171.3	1.39
194	6.83	195.0	6.93	195.0	1.31
220	6.59			220.0	1.30
252	6.24			240.0	1.30

* ESR measurements were recorded at liquid nitrogen temperature, -196°C (77 K).

Table AI-7 : Decay of methyl radicals at 77 K on PVGM5 containing 0.104 monolayer azomethane and at 109 K* on PVGM5d containing 0.103 monolayer azomethane

Decay at -196°C (77 K) on PVGM5 containing 0.104 monolayer azomethane		Decay at -164°C (109 K)* on PVGM5d containing 0.103 monolayer azomethane	
Time (hr.)	C x 10^{-15} (spins/m^2)	Time (min.)	C x 10^{-15} (spins/m^2)
0	12.0	0	7.90
16.2	8.70	27.0	1.30
21.9	7.87	42.0	1.19
38.7	6.32	55.0	1.16
44.1	6.17	70.0	1.08
62.4	5.68	85.2	1.04
68.1	5.33	100.0	1.02
87.1	4.98	115.0	0.980
92.1	4.86	130.0	0.912
110.9	4.82	145.0	0.898
120.3	4.61		
135.2	4.55		
140.1	4.42		
162.8	4.16		
168.1	3.83		
184.9	3.95		
190.8	4.02		
209.0	4.14		
211.9	3.95		
231.1	4.02		

* ESR measurements were recorded at liquid natural gas temperature, -164°C (109 K).

Absolute concentrations of ethyl radicals

The ESR signal of DPPH containing $7{\cdot}71 \times 10^{16}$ spins was obtained under ethyl radical conditions (Table 2-1). Equation AI-3 was then used to calculate the area, A_{DPPH}, of the DPPH signal. The average A_{DPPH} obtained by taking three measurements on three different signals was found to be 10750464 ± 178176 mm^2, somewhat different from that obtained for methyl radicals because of the different ESR conditions used.

A sample of ethyl radicals on PVGE4 containing 3·17 monolayers ($2{\cdot}68 \times 10^{-3}$ mmole/mg) azoethane was used as a representative sample of the radicals. The ESR signal of the radicals on this PVG sample was obtained under the standard conditions (Table 2-1). As before, the double integration of the high field most intense line (i.e. the 8^{th} line from the low field side) was obtained using Equation AI-3); this gave an area, A_{Et}, of 275574 ± 5231 mm^2 for the line. Again, the error in A_{Et} is the average deviation of three measurements on three signals recorded under the same conditions. The peak to peak height of this line was measured to be 79·5 mm. Using the intensity ratio of 1·0:9·8:5·1:1·3:38:5·9:5·2:38:1·2:4·0:10:0·94 obtained in this work, the total area, $A_{T(Et)}$, of the absorption spectrum of the radicals on PVGE4 is calculated from:

$$A_{T(Et)} = A_{Et} \times \frac{120.44}{38} \ mm^2$$

$$= 275574 \times \frac{120.44}{38} \ mm^2$$

$$= 873424 \pm 16580 \ mm^2.$$

Therefore, the number of ethyl radical spins, N_{Et}, is then given by:

$$N_{Et} = \frac{A_{T(Et)}}{A_{DPPH}} \times 7.71\times10^{16} \text{ spins}$$

$$= \frac{873424}{10750464} \times 7.71\times10^{16} \text{ spins}$$

$$= (6.26 \pm 0.12) \times 10^{15} \text{ spins.}$$

The surface area, S_{PVGE4}, of PVGE4 sample containing the radicals = 10·8 m^2. Hence, the concentration, C_{Et}, of the radicals in spins/m^2 is given by:

$$C_{Et} = \frac{N_{Et}}{S_{PVGE4}} = \frac{6.26\times10^{15}}{10.8} \text{ spins/m}^2$$

$$= (5.80 \pm 0.11) \times 10^{14} \text{ spins/m}^2 \text{ [i.e. } \approx 1.9\% \text{ error].}$$

Alternative calculation

Using the intensity ratio of 1:2:3:1:6:3:3:6:1:3:2:1 reported in the literature,[68,69] the total area, $A_{T(Et)}$, becomes:

$$A_{T(Et)} = A_{Et} \times \frac{32}{6} \text{ mm}^2$$

$$= 275574 \times \frac{32}{6} \text{ mm}^2$$

$$= 1469728 \pm 27899 \text{ mm}^2.$$

Hence, $N_{Et} = \frac{A_{T(Et)}}{A_{DPPH}} \times 7.71\times10^{16}$ spins

$$= \frac{1469728}{10750464} \times 7.71\times10^{16} \text{ spins}$$

$$= (1.05 \pm 0.02) \times 10^{16} \text{ spins.}$$

$$\therefore C_{Et} = \frac{N_{Et}}{S_{PVGE4}} = \frac{1.05\times10^{16}}{10.8} \text{ spins/m}^2$$

$$= (9.72 \pm 0.19) \times 10^{14} \text{ spins/m}^2 \text{ [i.e. } \approx 2.0\% \text{ error].}$$

Thus, the concentration obtained using the intensity ratio obtained in this work was about 67·6% different from the value obtained using the ratio reported in the literature. Nevertheless, the ratio reported in the literature was used to calculate all absolute concentrations of ethyl radicals.

The peak to peak heights, I_{Et}, of the first derivative ESR signals of ethyl radicals obtained during kinetic measurements were then converted to absolute radical concentrations, C_{Et}, using the relation:

$$C_{Et} = \frac{I_{Et} \times 1.05 \times 10^{16}}{79.5 \times S_{PVG}} \text{ spins/m}^2.$$

where S_{PVG} is, as before, the surface area of the particular PVG sample on which the radicals were adsorbed.

The spin concentrations of ethyl radicals obtained during kinetic measurements for experiments 18 to 26 are tabulated in the data presented in AI-8 to AI-10.

Table AI-8: Decay of ethyl radicals on PVGE1 containing 2·10 monolayers ($1{\cdot}78 \times 10^{-3}$ mmole/mg) azoethane at different temperatures

Decay at -196°C (77 K)		Decay at -183°C (90 K)*		Decay at -164°C (109 K)*	
Time (min.)	C x 10^{-14} (spins/m^2)	Time (min.)	C x 10^{-14} (spins/m^2)	Time (min.)	C x 10^{-14} (spins/m^2)
0	8·86	0	9·11	0	8·22
10·2	8·38	10·2	5·87	5·01	3·00
21·0	8·13	20·1	5·38	10·0	2·48
31·6	8·02	28·8	5·14	15·0	1·99
44·7	7·66	38·8	5·07	20·1	1·83
56·1	7·66	49·9	4·72	25·3	1·63
65·3	7·51	60·0	4·55	30·5	1·47
75·6	7·46				
86·8	7·34				

*ESR measurements were recorded at liquid nitrogen temperature, -196°C (77 K).

Table AI-9: Decay of ethyl radicals on PVGE2 containing 2·01 monolayers ($1{\cdot}71 \times 10^{-3}$ mmole/mg) azoethane at different temperatures

Decay at -196°C (77 K)		Decay at -183°C (90 K)*		Decay at -164°C (109 K)*	
Time (min.)	C x 10^{-15} (spins/m^2)	Time (min.)	C x 10^{-14} (spins/m^2)	Time (min.)	C x 10^{-14} (spins/m^2)
0	1·60	0	12·8	0	8·01
11·1	1·52	5.01	11·2	5·01	3·91
20·0	1·47	10·0	10·5	10·0	3·23
30·1	1·44	20·0	9·96	15·0	2·98
40·1	1·41	30·0	9·29	20·0	2·64
50·1	1·39	40·0	9·17	30·0	2·30
60·0	1·36	50·0	8·47	40·0	1·96
71·2	1·34	60·0	8·23	50·0	1·81
80·0	1·33	70·0	8·01		
90·0	1·30				
100	1·28				

*ESR measurements were recorded at liquid nitrogen temperature, -196°C (77 K).

Table AI-10: Decay of ethyl radicals on PVGE3 containing 3·09 monolayers ($2{\cdot}61 \times 10^{-3}$ mmole/mg) azoethane at different temperatures

Decay at -196°C (77 K)		Decay at -183°C (90 K)*		Decay at -164°C (109 K)*	
Time (min.)	C x 10^{-15} (spins/m^2)	Time (min.)	C x 10^{-15} (spins/m^2)	Time (min.)	C x 10^{-14} (spins/m^2)
0	2·66	0	2·03	0	11·2
10·0	2·51	3·01	1·80	3·18	6·30
16·0	2·46	6·01	1·71	6·01	5·48
22·0	2·41	10·0	1·62	9·34	4·89
30·1	2·35	15·0	1·57	15·0	4·21
40·0	2·27	20·0	1·49	20·0	3·76
50·0	2·22	26·7	1·41	30·0	3·06
60·0	2·19	34·0	1·36	40·0	2·59
70·0	2·14	40·0	1·32	51·3	2·22
80·0	2·11	50·0	1·27	60·0	2·01
90·0	2·08	60·0	1·22		
100	2·03	70·4	1·16		
		80·0	1·12		

*ESR measurements were recorded at liquid nitrogen temperature, -196°C (77 K).

APPENDIX II

Estimation of percentage decomposition of azomethane and azoethane during irradiation

The percentage of azomethane (or azoethane) molecules adsorbed on PVG samples that decomposed during the period of irradiation was estimated as follows:

$$\% \text{ azomethane (or azoethane) decomposed} = \frac{C_R \times S_{PVG}}{2\,n\,N} \times 100\ \%$$

where C_R = the maximum concentration of the methyl (or ethyl) radicals produced during irradiation; S_{PVG} = surface area of the particular PVG sample used; n = number of moles of azomethane (or azoethane) adsorbed on the PVG sample; N = Avogadro's constant.

Sample calculation

Sample PVGM1 having a surface area of 13·5 m^2 and loaded with 1·00 monolayer ($1{\cdot}19 \times 10^{-3}$ mmole/mg) azomethane contains $8{\cdot}06 \times 10^{-5}$ mole azomethane. This sample was irradiated for $5^1/_2$ hours to produce a maximum methyl radical concentration of $1{\cdot}10 \times 10^{16}$ spins/m^2. Hence, the percentage of azomethane decomposed is calculated thus:

$$\text{Percentage of azomethane decomposed} = \frac{1.10\times10^{16} \times 13.5}{2 \times 8.06\times10^{-5} \times 6.023\times10^{23}} \times 100\ \%$$

$$= 0.153\%.$$

The percentage of azomethane molecules that decomposed during the $3^1/_2$ to $5^1/_2$ hours of irradiation to produce methyl radicals was estimated to be about 1.41 to 1.71% for surfaces loaded

with about 0.1 monolayer azomethane, 0.0615 to 0.153% for surfaces covered with approximately 1 monolayer azomethane and 0.0182 to 0.0255% for surfaces containing about 2 monolayers azomethane. On the other hand, the percentage of azoethane molecules that decomposed during the 5 to 7 hours of irradiation to produce ethyl radicals was estimated to be about 0·00648 to 0·0279%.

APPENDIX III

Results of the first-order, non-linear least squares analysis for the decay of methyl and ethyl radicals on PVG samples

It was mentioned in sections 3.3.1(a) and 3.3.2(b) that the decay data of methyl and ethyl radicals do not follow a modified first-order plot of ln (C-A) against time. For methyl radicals, the values of A were measured from the decay curves while for ethyl radicals, these values were calculated from the Dole plots. The Dole plot values of A should not have been used for the modified first-order plots since the Dole equation is a second-order equation. The modified first-order equation can be written as

$$\ln (C-A) = \ln (C_0-A) - k_1 t \qquad \text{AIII-1}$$

so that,

$$C-A = (C_0-A)e^{-k_1 t} \qquad \text{AIII-2}$$

or,

$$C = A + (C_0-A)e^{-k_1 t} \qquad \text{AIII-3}$$

Therefore, non-linear least squares analysis of the decay data for both radicals presented in Tables AIII-1 to AIII-7 was done using equation AIII-3 and values of (C_0-A), A and first-order rate constant, k_1, were obtained accordingly. Surprisingly, all the non-linear least squares curves for the decay of methyl and ethyl radicals are found to agree well with experimental points as illustrated in Figures AIII-1 to AIII-7 indicating the possibility of a fraction of the radicals decaying by a first-order mechanism while the remaining radicals, which concentration is denoted by A, are completely

Table AIII-1: First- and second-order, non-linear least squares fit data for the decay of methyl radicals on PVG samples* containing approximately 0.1 monolayer azomethane

Expt. No.	Temp. (K)	Reaction order	(C_0-A) x 10^{-15} (spins/ m^2)	A x 10^{-15} (spins/ m^2)	k_1 (min^{-1})	E_a (kJ mol^{-1})
15a	77	1	3.15 ± 0.18	5.95 ± 0.20	0.00755 ± 0.00106	
		2	4.52 ± 0.32	4.62 ± 0.35		
16	90	1	2.88 ± 0.41	7.11 ± 0.29	0.0219 ± 0.0087	7.61 ± 1.68
		2	3.54 ± 0.43	6.71 ± 0.37		(9.04 ± 0.08)**
17a	109	1	10.0 ± 0.19	1.49 ± 0.06	0.250 ± 0.024	
		2	10.1 ± 0.11	1.36 ± 0.04		

*PVGM5d was used for experiment 15a and PVGM5d_2 for experiments 16 and 17a [refer to section 3.3.1(b)].

**The values of E_a written in parentheses is the value for second-order fit.

Table AIII-2: First- and second-order, non-linear least squares fit data for the decay of methyl radicals on PVGM1 containing 1.00 monolayer (1.19×10^{-3} mmole/mg) azomethane

Expt. No.	Temp. (K)	Reaction order	$(C_0\text{-}A) \times 10^{-15}$ (spins/m^2)	$A \times 10^{-15}$ (spins/m^2)	k_1 (min.)	E_a (kJ mol^{-1})
1	77	1	0.601 ± 0.048	2.20 ± 0.05	0.00221 ± 0.0048	
		2	0.825 ± 0.077	1.99 ± 0.09		
2	90	1	1.01 ± 0.04	1.15 ± 0.03	0.0428 ± 0.0044	5.69 ± 1.60
		2	1.30 ± 0.03	0.901 ± 0.032		(7.32 ± 3.26)*
3	109	1	0.657 ± 0.043	0.463 ± 0.016	0.303 ± 0.047	
		2	0.708 ± 0.020	0.420 ± 0.097		

*The value of E_a written in parentheses is the value for second-order fit.

Table AIII-3: First- and second-order, non-linear least squares fit data for the decay of methyl radicals on PVGM2 containing 2.06 monolayers (2.45 x 10^{-3} mmole/mg) azomethane

Expt. No.	Temp. (K)	Reaction order	(C_0-A) x 10^{-15} (spins/ m^2)	A x 10^{-15} (spins/ m^2)	k_1* (min.)	E_a (kJ mol^{-1})
11	77	1	-	-	0.0115 ± 0.0009	
4	90	1	1.17 ± 0.06	3.63 ± 0.06	0.0491 ± 0.0075	4.62 ± 0.99
		2	1.52 ± 0.10	3.30 ± 0.11		(4.36 ± 0.03)**
5	109	1	1.39 ± 0.12	2.14 ± 0.06	0.0967 ± 0.0208	
		2	1.67 ± 0.09	1.96 ± 0.07		

*The value of k_1 at 77 K given in this table is the value obtained for experiment 11 done on PVGM6 containing 2.01 monolayers azomethane.

**The value of E_a written in parentheses is the value for second-order fit.

Table AIII-4: First- and second-order, non-linear least squares fit data for the decay of methyl radicals on PVGM3 containing 3.19 monolayers (3.80×10^{-3} mmole/mg) azomethane

Expt. No.	Temp. (K)	Reaction order	$(C_0\text{-}A) \times 10^{-15}$ (spins/m^2)	$A \times 10^{-15}$ (spins/m^2)	k_1 (min.)	E_a (kJ mol^{-1})
6	77	1	1.08 ± 0.04	2.90 ± 0.04	0.0264 ± 0.0030	
		2	1.47 ± 0.06	2.53 ± 0.07		
7	90	1	0.948 ± 0.052	1.97 ± 0.03	0.0992 ± 0.0116	3.01 ± 1.58
		2	1.11 ± 0.02	1.85 ± 0.02		(5.23 ± 2.13)*
8	109	1	0.719 ± 0.053	1.15 ± 0.03	0.106 ± 0.017	
		2	0.855 ± 0.034	1.05 ± 0.02		

*The value of E_a written in parentheses is the value for second-order fit.

Table AIII-5: First- and second-order, non-linear least squares fit data for the decay of ethyl radicals on PVGE1 containing 2.10 monolayers (1.78×10^{-3} mmole/mg) azoethane

Expt. No.	Temp. (K)	Reaction order	$(C_0\text{-}A) \times 10^{-14}$ (spins/ m^2)	$A \times 10^{-14}$ (spins/ m^2)	k_1 (min.)	E_a (kJ mol^{-1})
18	77	1	1.62 ± 0.11	7.19 ± 0.12	0.0249 ± 0.0045	
		2	2.27 ± 0.20	6.56 ± 0.22		
19	90	1	4.24 ± 0.27	4.84 ± 0.13	0.123 ± 0.022	5.39 ± 0.91
		2	4.79 ± 0.20	4.32 ± 0.15		(4.52 ± 1.05)*
20	109	1	6.44 ± 0.32	1.76 ± 0.15	0.299 ± 0.044	
		2	7.05 ± 0.17	1.17 ± 0.12		

*The value of E_a written in parentheses is the value for second-order fit.

Table AIII-6: First- and second-order, non-linear least squares fit data for the decay of ethyl radicals on PVGE2 having some adsorbed water on the surface and containing 2.01 monolayers (1.71×10^{-3} mmole/mg) azoethane

Expt. No.	Temp. (K)	Reaction order	$(C_0\text{-}A) \times 10^{-14}$ (spins/m^2)	$A \times 10^{-14}$ (spins/m^2)	k_1 (min.)	E_a (kJ mol^{-1})
21	77	1	3.63 ± 0.23	12.3 ± 0.3	0.0171 ± 0.0025	
		2	5.25 ± 0.36	10.7 ± 0.4		
22	90	1	4.41 ± 0.36	8.03 ± 0.34	0.0451 ± 0.0110	5.33 ± 0.63
		2	5.66 ± 0.42	6.98 ± 0.44		(6.36 ± 0.46)*
23	109	1	5.68 ± 0.43	2.24 ± 0.20	0.200 ± 0.038	
		2	6.38 ± 0.24	1.61 ± 0.16		

*The value of E_a written in parentheses is the value for second-order fit.

Table AIII-7: First- and second-order, non-linear least squares fit data for the decay of ethyl radicals on PVGE3 containing 3.09 monolayers (2.61 x 10^{-3} mmole/mg) azoethane

Expt. No.	Temp. (K)	Reaction order	(C_0-A) x 10^{-14} (spins/ m^2)	A x 10^{-14} (spins/ m^2)	k_1 (min.)	E_a (kJ mol^{-1})
24	77	1	7.08 ± 0.25	19.4 ± 0.3	0.0182 ± 0.0016	
		2	10.3 ± 0.4	16.2 ± 0.4		
25	90	1	8.01 ± 0.42	11.4 ± 0.4	0.0420 ± 0.0064	4.83 ± 0.67
		2	10.3 ± 0.5	9.43 ± 0.51		(6.53 ± 0.71)*
26	109	1	7.91 ± 0.76	2.77 ± 0.35	0.168 ± 0.035	
		2	9.20 ± 0.46	1.86 ± 0.29		

*The value of E_a wiritten in parentheses is the value for second-order fit.

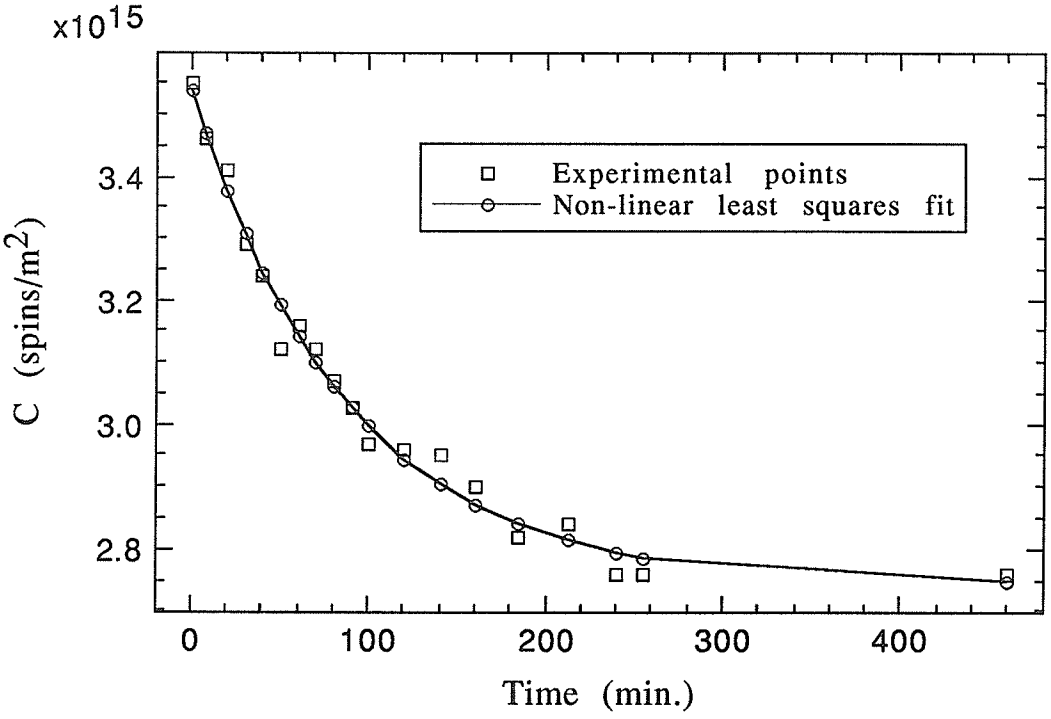

Figure AIII-1: First-order, non-linear least squares fit for the decay of methyl radicals at 77 K on PVGM6 containing 2.01 monolayers azomethane.

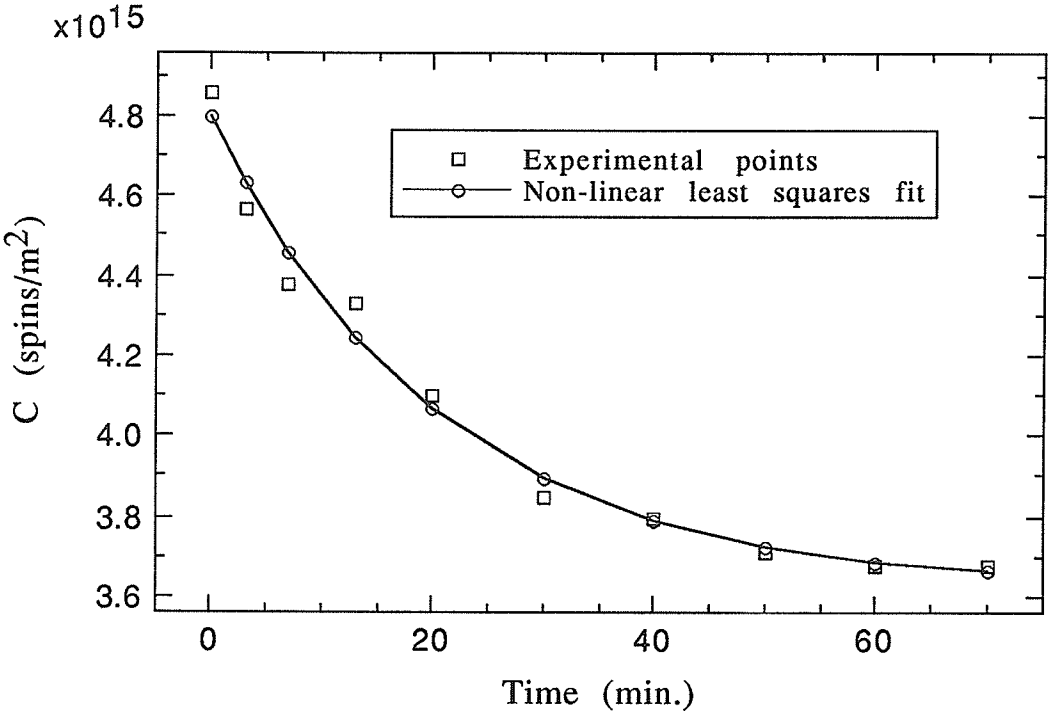

Figure AIII-2: First-order, non-linear least squares fit for the decay of methyl radicals at 90 K on PVGM2 containing 2.06 monolayers (2.45×10^{-3} mmole/mg) azomethane.

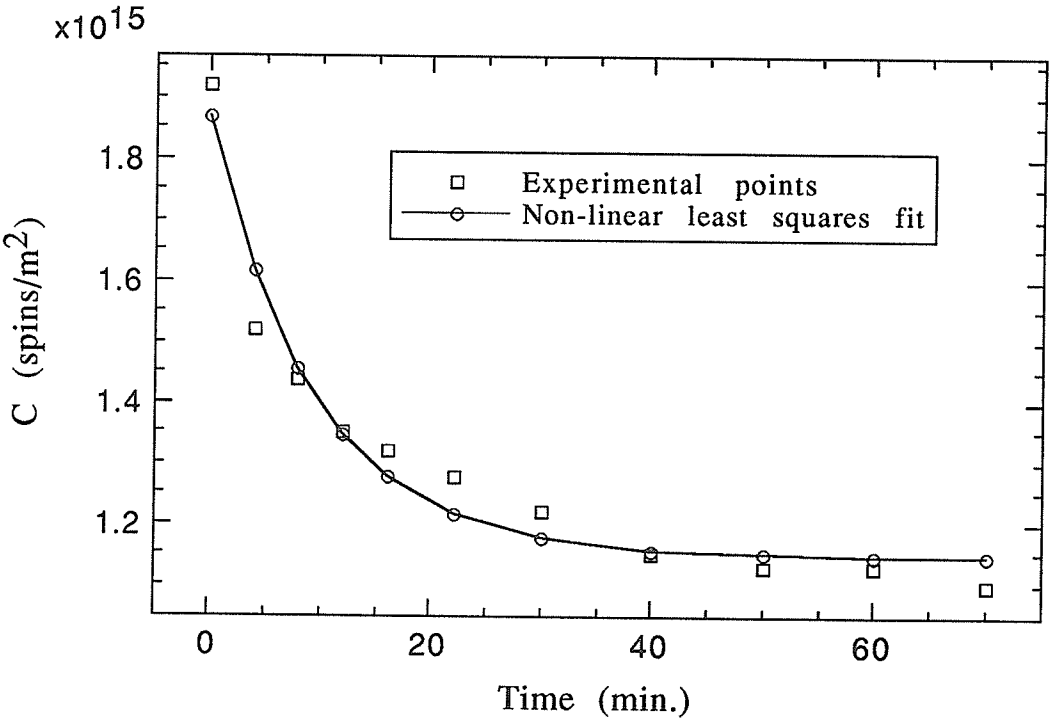

Figure AIII-3: First-order, non-linear least squares fit for the decay of methyl radicals at 109 K on PVGM3 containing 3.19 monolayers (3.80×10^{-3} mmole/mg) azomethane.

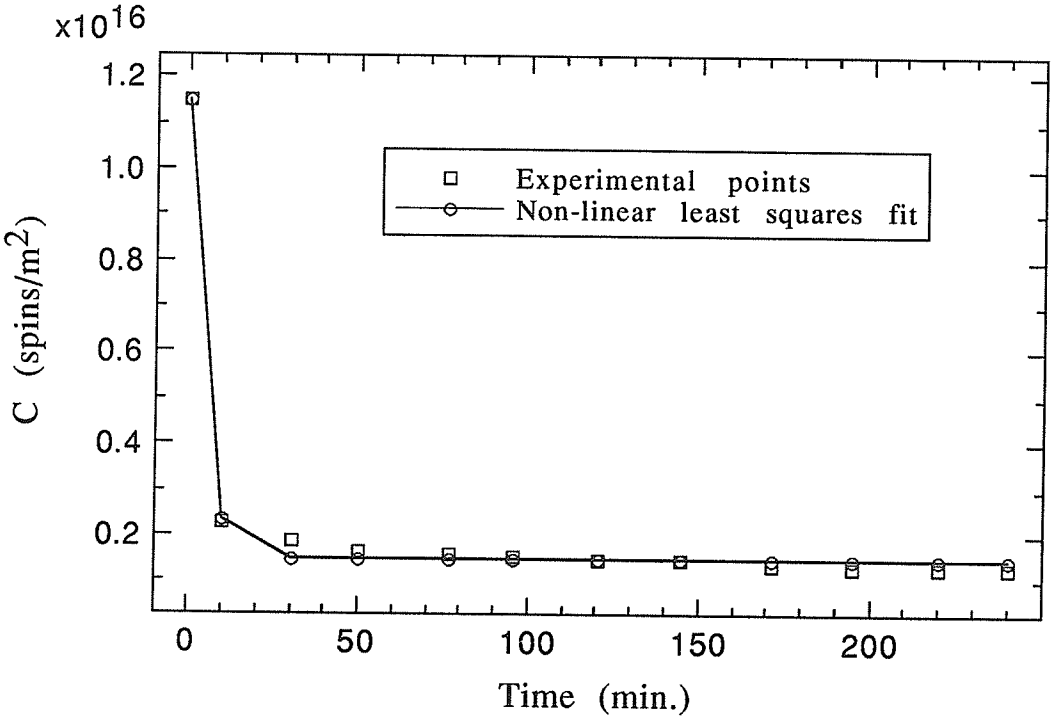

Figure AIII-4: First-order, non-linear least squares fit for the decay of methyl radicals at 109 K on PVGM5d_2 containing 0.103 monolayer azomethane.

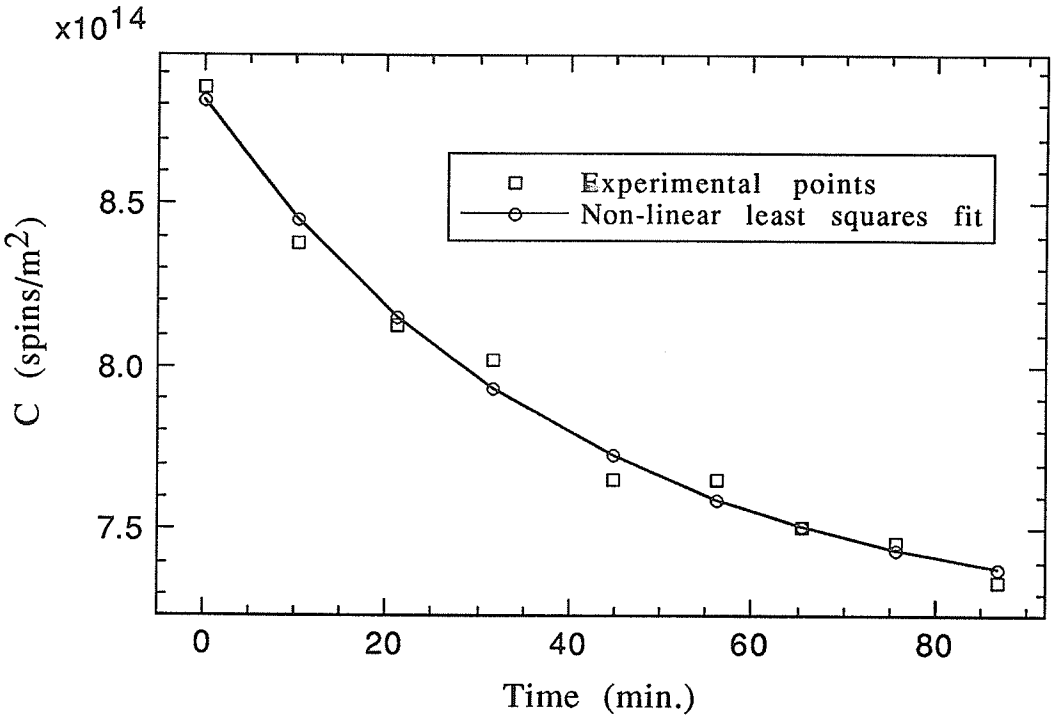

Figure AIII-5: First-order, non-linear least squares fit for the decay of ethyl radicals at 77 K on PVGE1 containing 2.10 monolayers (1.78 x 10^{-3} mmole/mg) azoethane.

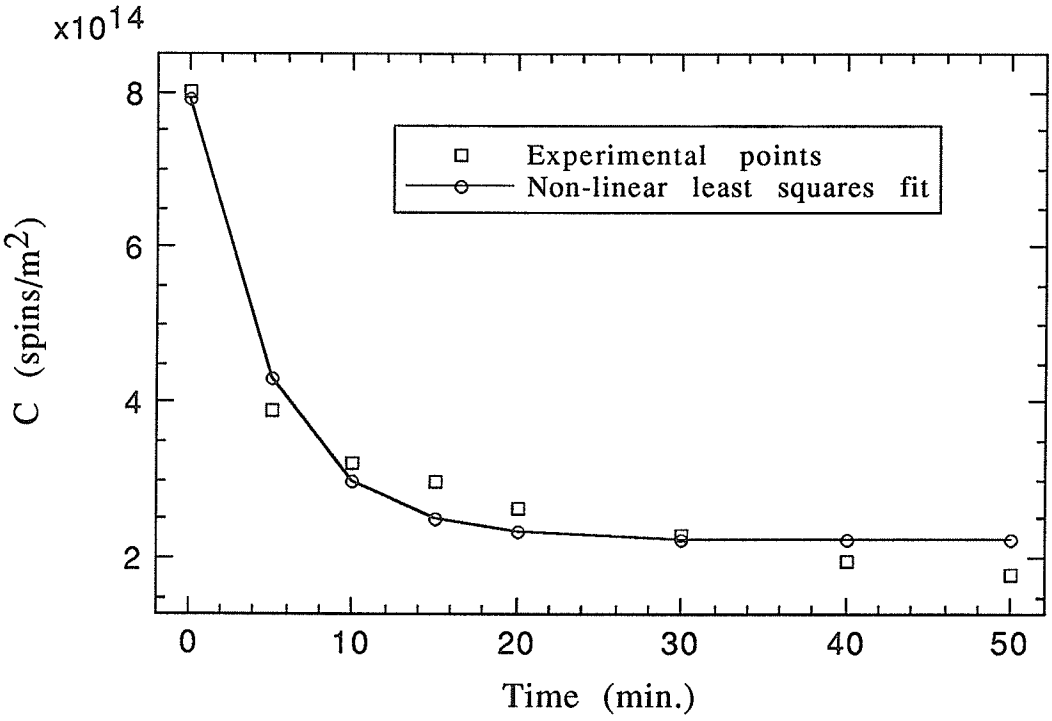

Figure AIII-6: First-order, non-linear least squares fit for the decay of ethyl radicals at 109 K on PVGE2 containing 2.01 monolayers (1.71 x 10^{-3} mmole/mg) azoethane.

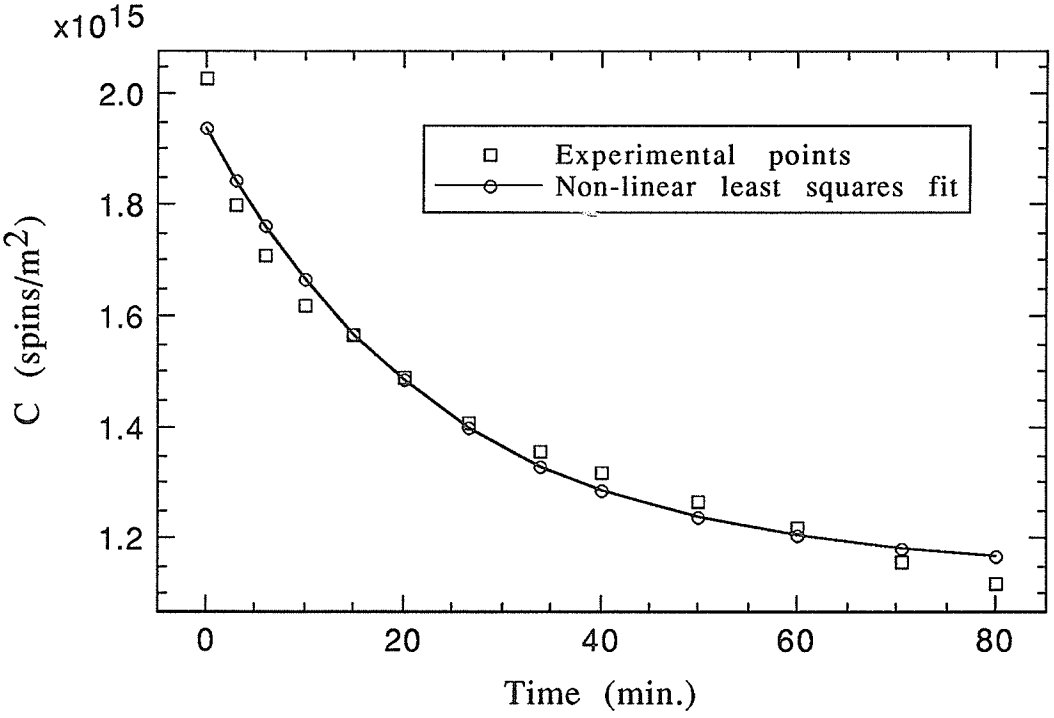

Figure AIII-7: First-order, non-linear least squares fit for the decay of ethyl radicals at 90 K on PVGE3 containing 3.09 monolayers (2.61 x 10^{-3} mmole/mg) azoethane.

unreactive. When the values of A obtained from the first-order, non-linear least squares analysis are substituted into equation AIII-1, straight line graphs are obtained on plotting ln (C-A) against t as illustrated in Figures AIII-8 and AIII-9. The values of k_1 and (C_0-A) obtained from the plots of ln (C-A) against t are in good agreement with the corresponding values obtained from the non-linear least squares analysis. This is illustrated in Tables AIII-8 and AIII-9. These results confirm further a first-order decay of a fraction of the radicals while the remaining radicals are unreactive. This is in conflict with the results of the Dole plots and second-order, non-linear least squares analysis presented in section 3.3 which indicate that a fraction of the radicals decay by a second-order recombination reaction while the remaining radicals are unreactive. Hence, this conflict needs to be resolved first by doing further analysis of the decay data and obtaining more experimental results prior to arriving at a more concrete conclusion about the mechanism of the decay of the radicals on the PVG surface.

It should be noted that the values of (C_0-A), A and E_a obtained from the second-order, non-linear least squares fits are included in Tables AIII-1 to AIII-7 for comparison with the corresponding values obtained from first-order, non-linear least squares fits. In the meantime, it should be mentioned that these tables clearly show that the values of A obtained from the first-order fits are generally slightly higher than, and the values of (C_0-A) slightly lower than the corresponding values obtained from the second-order fits. It is also observed from Tables AIII-1 to AIII-7 that the first-order values of activation energies, E_a, are generally lower than the corresponding

second-order values. The E_a values are obtained from Arrhenius plots of ln k_1 against reciprocal temperature as illustrated in Figure AIII-10 for samples loaded with 0.1 and 3.19 monolayers azomethane as well as in Figure AIII-11 for samples loaded with 2.10 and 3.09 monolayers azoethane. The E_a values are observed to decrease with increase in surface coverage for both radicals.

Table AIII-8: First-order rate constants and (C_0-A) values obtained from both modified first-order and non-linear least squares plots for the decay of methyl radicals on PVGM1, PVGM2 and PVGM3

	PVGM1 containing 1.00 monolayer azomethane at -196°C (77 K)		PVGM2 containing 2.06 monolayers azomethane at -183°C (90 K)		PVGM3 containing 3.19 monolayers azomethane at -164°C (109 K)	
	Modified 1st order plot (Eqn. AIII-1) value	Non-linear fit (Eqn. AIII-3) value	Modified 1st order plot (Eqn. AIII-1) value	Non-linear fit (Eqn. AIII-3) value	Modified 1st order plot (Eqn. AIII-1) value	Non-linear fit (Eqn. AIII-3) value
k_1 (min.)	0.0221	0.0221	0.0527	0.0491	0.0909	0.106
(C_0-A) (spins/ m^2)	5.96 x 10^{14}	6.01 x 10^{14}	1.20 x 10^{15}	1.17 x 10^{15}	6.39 x 10^{14}	7.19 x 10^{15}

Table AIII-9: First-order rate constants and (C_0-A) values obtained from both modified first-order and non-linear least squares plots for the decay of ethyl radicals on PVGE1, PVGE2 and PVGE3

	PVGE1 containing 2.10 monolayers azoethane at -164°C (109 K)		PVGE2 containing 2.01 monolayers azoethane at -183°C (90 K)		PVGE3 containing 3.09 monolayers azoethane at -196°C (77 K)	
	Modified 1st order (Eqn. AIII-1) value	Non-linear fit (Eqn. AIII-3) value	Modified 1st order (Eqn. AIII-1) value	Non-linear fit (Eqn. AIII-3) value	Modified 1st order (Eqn. AIII-1) value	Non-linear fit (Eqn. AIII-3) value
k_1 (min.)	0.214	0.299	0.0407	0.0451	0.0186	0.0182
(C_0-A) (spins/ m^2)	5.31 x 10^{14}	6.44 x 10^{14}	4.17 x 10^{14}	4.41 x 10^{14}	7.06 x 10^{14}	7.08 x 10^{14}

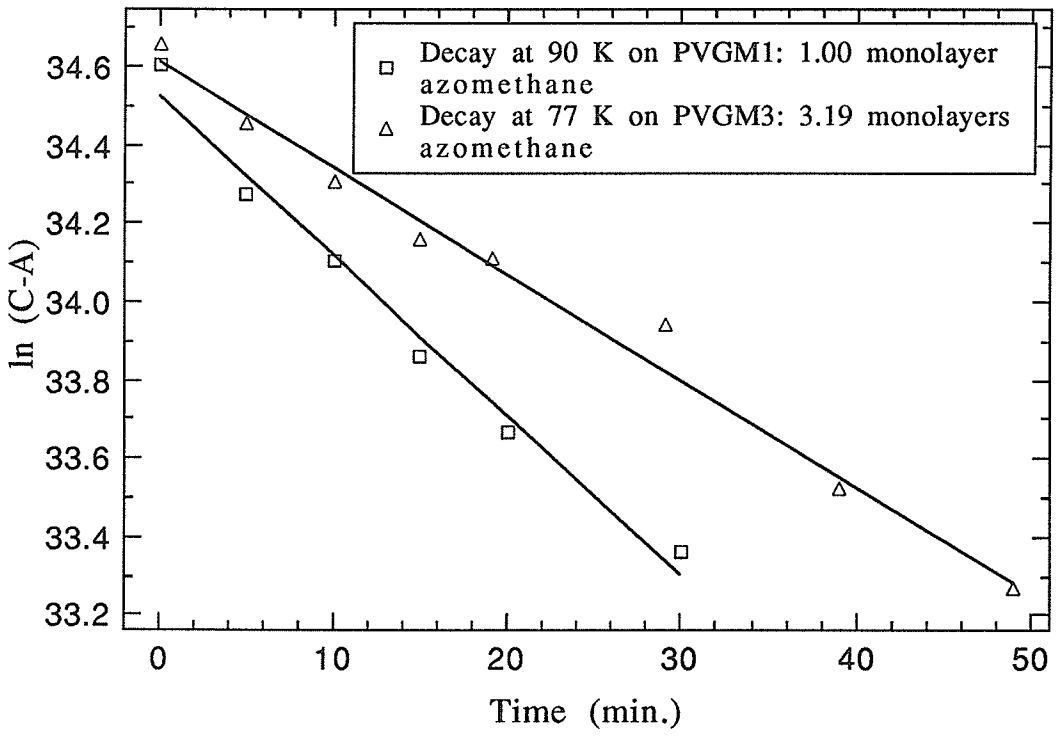

Figure AIII-8: Modified first-order plots for the decay of methyl radicals at two different temperatures on PVG samples containing 1.00 and 3.19 monolayers azomethane.

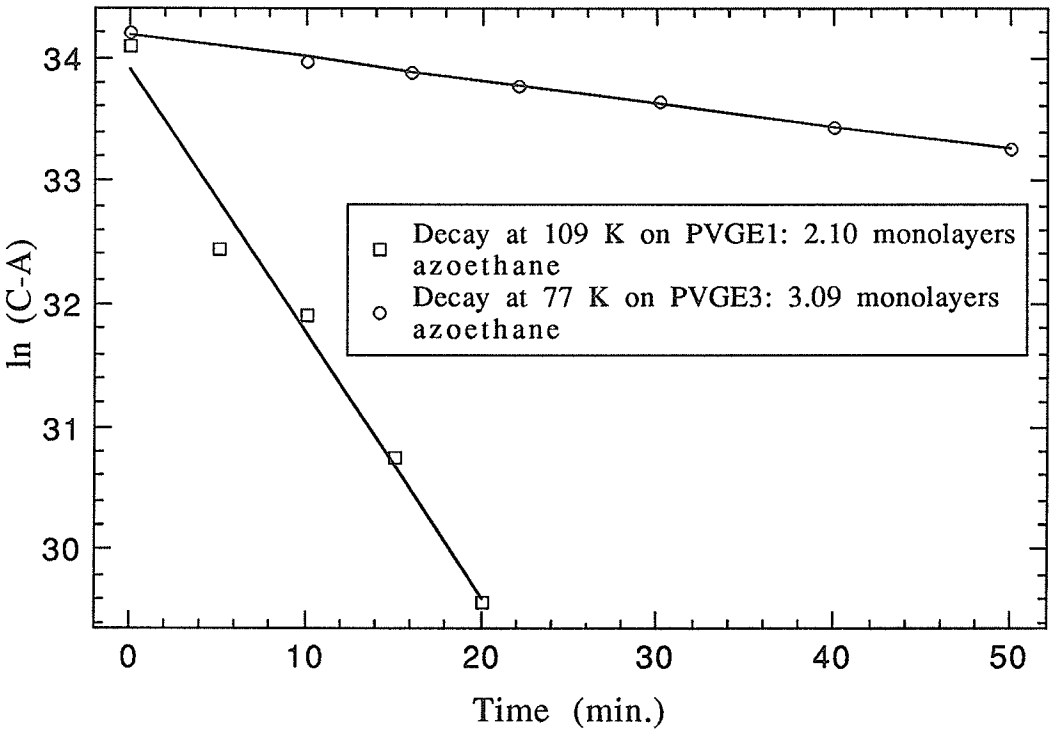

Figure AIII-9: Modified first-order plots for the decay of ethyl radicals at two different temperatures on PVG samples containing 2.10 and 3.09 monolayers azoethane.

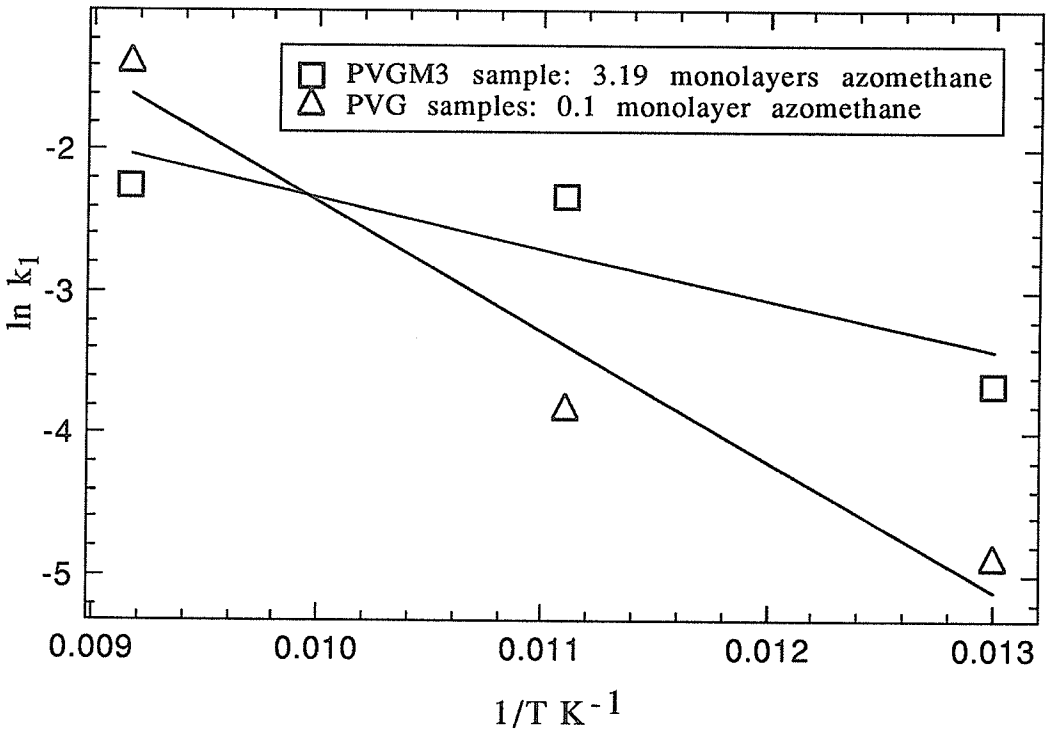

Figure AIII-10: Arrhenius plots for first-order decay of methyl radicals on PVG samples loaded with 0.1 and 3.19 monolayers azomethane.

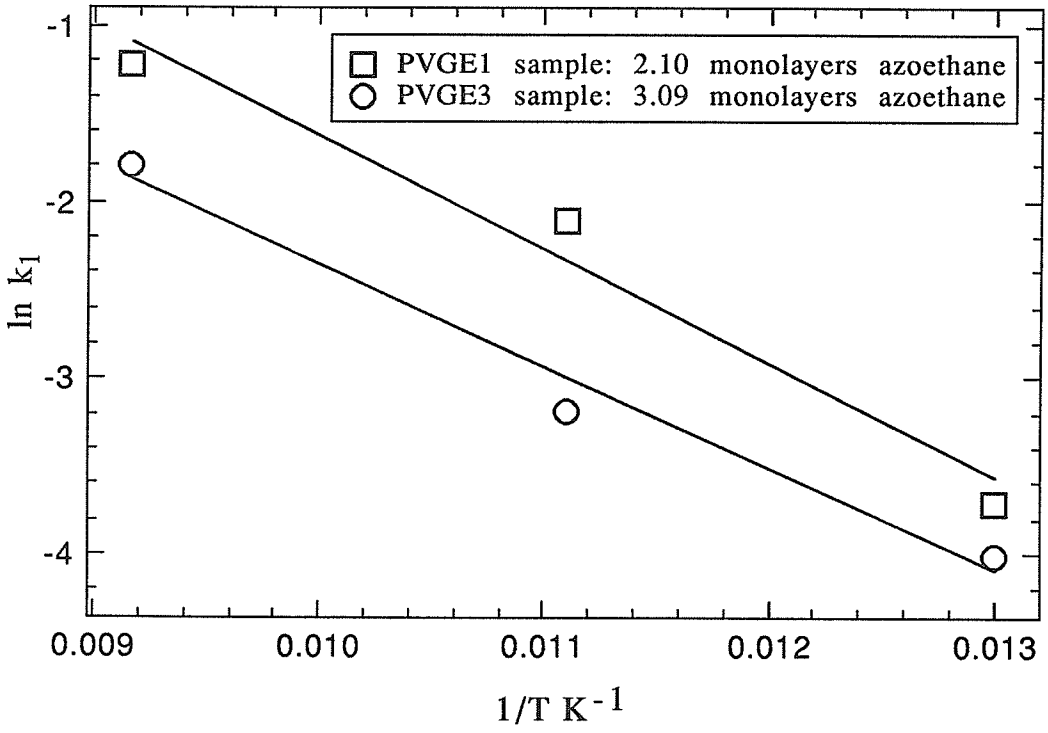

Figure AIII-11: Arrhenius plots for first-order decay of ethyl radicals on PVG samples loaded with 2.10 and 3.09 monolayers azoethane.

REFERENCES

1. H.D. Gesser; *Studies in Surface Science and Catalysis-Photochemistry on Solid Surfaces,* **47**, 168, (1989). [Editors: M. Anpo and T. Matsuura].
2. M. Fujimoto, H.D. Gesser, B. Garbutt and A. Cohen; *Science,* **154**, 381, (1966).
3. G.R. Joppien and J.E. Willard; *J. Phys. Chem.,* **78**, 1391, (1974).
4. G.B. Garbutt; Ph.D. Thesis, University of Manitoba (1968).
5. M.L. Hair; "Infrared Spectroscopy in Surface Chemistry," Marcel Dekker Inc., New York (1967).
6. G.M. Muha and D.J.C. Yates; *J. Phys. Chem.,* **70**, 1399, (1966).
7. I.D. Chapman and M.L. Hair; *Trans. Farad. Soc.,* **61**, 1507, (1965).
8. M.L. Hair and I.D. Chapman; *J. Amer. Ceram. Soc.,* **49**, 651, (1966).
9. M.J.D. Low and N. Ramasubramanian; (a) *J. Phys. Chem.,* **70**, 2740, (1966), (b) *J. Phys. Chem.,* **71**, 730, (1967), (c) *J. Phys. Chem.,* **71**, 3077, (1967).
10. L.H. Little; "Infrared Spectra of adsorbed species," Academic Press (1966).
11. P.B. Ayscough; "Electron Spin Resonance in Chemistry," Mathuen and Co. Ltd., London (1967).
12. J.E. Wertz and J.R. Bolton; "Electron Spin Resonance: Elementary Theory and Practical Applications," McGraw-Hill Inc., (1972).
13. M. Bersohn and J.C. Baird; "An introduction to Electron Spin Resonance," W.A. Benjamin, Inc., New York (1966).
14. A.J. Bard in "Standard Methods of Chemical Analysis," [Editor: F.J. Welcher] D. Van Nostrand Comp., Inc., Princeton, New Jersey 6th Ed., Vol. 3, Part A, Chapter 31, (1966).

15. G.G. Guilbault and L.R. Hargins; "Instrumental Analysis Manual," Marcel Dekker Inc., New York (1970).
16. J.H. Lunsford and J.P. Jayne; *J. Chem. Phys.*, **44**, 1487, (1966).
17. J.H. Lunsford; *J. Chem. Phys.*, **46**, 4347, (1967).
18. D.J. Driscoll, K.D. Campbell and J.H. Lunsford; *Adv. Catal.*, **35**, 139, (1987).
19. G.A. Ozin and A. Vander Voet; *Prog. Inorg. Chem.*, **19**, 105, (1975).
20. W. Martir and J.H. Lunsford; *J. Amer. Chem. Soc.*, **103**, 3728, (1981).
21. W. Gordy and C.G. McCormick; *J. Amer. Chem. Soc.*, **78**, 3243, (1956).
22. G.B. Pariiskii, G.M. Zhidomirov and V.B. Kazanskii; *Zhurnal Strukturnoi Khimmi* **4**, 364, (1963). English Translation. [*Chem. Abstr.*, **59**, 5967b, (1963)].
23. V.B. Kazanskii and G.B. Pariiskii; *Kinet. Katal.*, **2**, 507, (1961). English Translation. [*Chem. Abstr.*, **56**, 6810f, (1962)].
24. G.A. Noble, R.A. Serway, A. O'Donnell and E.S. Freeman; *J. Phys. Chem.*, **71**, 4326, (1967).
25. J. Turkevich and Y. Fujita; *Science*, **152**, 1619, (1966).
26. H.S. Taylor and J.P. Cunningham; *J. Chem. Phys.*, **6**, 359, (1938).
27. H.S. Taylor and J.O. Smith (Jr.); *J. Chem. Phys.*, **7**, 390, (1939).
28. P.J. Boddy and E.W.R. Steacie; *Can. J. Chem.*, **38**, 1576, (1960); *ibid.*, **39**, 13, (1961).
29. L. Mandelcorn and E.W.R. Steacie; *Can. J. Chem.*, **32**, 474, (1954).
30. D.G.L. James and E.W.R. Steacie; *Proc. Roy. Soc., (London)*, **A244**, 297, (1958).

31. S. Bywater and E.W.R. Steacie; *J. Chem. Phys.*, **19**, 326, (1951); *ibid.*, **19**, 319, (1951); *ibid.*, **19**, 172, (1951).

32. A.F. Trotman-Dickenson; "Gas Kinetics," Butterworths Scientific Publications, London, pgs. 299-308 (1955).

33. J.G. Stark and H.G. Wallace; "Chemistry Data Book," John Murray Publishers, London, pg. 32 (1975).

34. R. Gomer and G.B. Kistiakowsky; *J. Chem. Phys.*, **19**, 85, (1951).

35. D.L. Baulch and J. Duxbury; *Combust. Flame*, **37**, 313, (1980).

36. N.L. Arthur; *J. Chem. Soc., Farad. Trans. 2*, **82**, 331, (1986).

37. D.A. Parkes, D.M. Paul and C.P. Quinn; *J. Chem. Soc., Farad. Trans. 1*, **72**, 1935, (1976).

38. N.L. Arthur and J.C. Biordi; *Aust. J. Chem.*, **39**, 1257, (1986).

39. A. Shepp and K.O. Kutschke; *J. Chem. Phys.*, **26**, 1020, (1957).

40. K.J. Ivin and E.W.R. Steacie; *Proc. Roy. Soc. (London);* **A208**, 25, (1951).

41. P. Ausloos and E.W.R. Steacie; *Can. J. Chem.*, **33**, 1062, (1955).

42. N.L. Arthur; *J. Chem. Soc., Farad. Trans., 2*, **82**, 1057, (1986).

43. O. Dobis and S.W. Benson; *J. Amer. Chem. Soc.*, **113**, 6377, (1991).

44. F.E. Blacet and W.E. Bell; *Discuss. Farad. Soc.*, **14**, 70, (1953).

45. (a) J.N. Pitts (Jr.), R.S. Tolberg and T.W. Martin; *J. Amer. Chem. Soc.*, **79**, 6370, (1957), (b) J.N. Pitts (Jr.), D.D. Thompson and R.W. Woolfolk; *J. Amer. Chem. Soc.*, **80**, 66, (1958).

46. R.K. Brinton; *J.Amer. Chem. Soc.*, **83**, 1541, (1961).

47. K.J. Laidler; "Chemical Kinetics," 2nd Ed. McGraw-Hill, Inc., (1965).

48. M.H. Jones and E.W.R. Steacie; *J. Chem. Phys.*, **21**, 1018, (1953).

49. S. Toby; *J. Amer. Chem. Soc.*, **82**, 3822, (1960).

50. S. Toby and B.H. Weiss; *J. Phys. Chem.*, **68**, 2492, (1964).

51. E.D. Sprague and F. Williams; *J. Amer. Chem. Soc.*, **93**, 787, (1971).

52. J.-T Wang and F. Williams; *J. Amer. Chem. Soc.*, **94**, 2930, (1972).

53. M.H.J. Wijnen; *J. Chem. Phys.*, **22**, 1074, (1954).

54. R.J. LeRoy, E.D. Sprague and F. Williams; *J. Phys. Chem.*, **76**, 546, (1972).

55. A. Campion and F. Williams; *J. Amer. Chem. Soc.*, **94**, 7633, (1972).

56. A.F. Trotman-Dickenson and E.W.R. Steacie; *J. Chem. Phys.*, **19**, 329, (1951).

57. D.A. Oduwole and B. Wiseall; *Appl. Surf. Sci.*, **8**, 260, (1981).

58. Y. Tong, M.P. Rosynek and J.H. Lunsford; *J. Phys. Chem.*, **93**, 2896, (1989).

59. H.F. Liu, R.S. Liu, K.Y. Liew, R.E. Johnson and J.H. Lunsford; *J. Amer. Chem. Soc.*, **106**, 4117, (1984).

60. Y. Tong and J.H. Lunsford; *J. Amer. Chem. Soc.*, **113**, 4741, (1991).

61. M. Anpo; *Studies in Surface Science and Catalysis-Photochemistry on Solid Surfaces*, **47**, 119, (1989). [Editors: M. Anpo and T. Matsuura].

62. M. Anpo, S. Hirohashi and Y. Kubokawa; *Bull. Chem. Soc. Japan*, **48**, 985, (1975).

63. L.W. Bader; Ph.D. Thesis, University of Manitoba (1969).

64. R. Renaud and L.C. Leitch; *Can. J. Chem.*, **32**, 545, (1954).

65. T.E. Huber and C.A. Huber; *J. Low Temp. Phys.*, **80**, 315, (1990).

66. D.M. Young and A.D. Crowell; "Physical Adsorption of Gases," Butterworths, London, pg. 226 (1962).

67. S.J. Wyard; *J. Sci. Instrum.*, **42**, 769, (1965).

68. G.R. Joppien and J.E. Willard; *J. Phys. Chem.*, **76**, 3158, (1972).

69. R.W. Fessenden and R.H. Schuler; *J. Chem. Phys.*, **39**, 2147, (1963).

70. T. Katsu, M. Yanagita and Y. Fujita; *J. Phys. Chem.*, **75**, 4064, (1971).

71. L.W. Bader and H.D. Gesser; *Can. J. Chem.*, **50**, 2305, (1972).

72. C.V. Cannon and O.K. Rice; *J. Amer. Chem. Soc.*, **63**, 2900, (1941).

73. P.C. Goswami and H.D. Gesser; Unpublished results.

74. J.L. Weininger and O.K. Rice; *J. Amer. Chem. Soc.*, **74**, 6216, (1952).

75. P.J. Kozak and H. Gesser; *J. Chem. Soc.*, 448, (1960).

76. H. Gesser, J.T. Mullhaupt and J.E. Griffiths; *J. Amer. Chem. Soc.*, **79**, 4834, (1957).

77. M. Dole; *J. Phys. Chem.*, **91**, 3117, (1987).

78. N. Grozdic, R. Basheer, M. Mehta and M. Dole; *J. Phys. Chem.*, **85**, 1563, (1981).

79 T.R. Waite; *Phys. Rev.*, **107**, 463, (1957).

80 B.B. Hasinoff; *J Phys. Chem.*, **82**, 2630, (1978).

81. J.B. Peri and A.L. Hensley, (Jr.); *J. Phys. Chem.*, **72**, 2926, (1968).

82. D.A. Oduwole and B. Wiseall; *Bull. Chem. Soc. Japan*, **53**, 3037, (1980).

83. T. Shiga and A. Lund; *J. Phys. Chem.*, **77**, 453, (1973).